ANALYSIS OF REACTORS FOR THE PRODUCTION OF

TITANIUM DIOXIDE THROUGH COMPUTATIONAL

FLUID DYNAMICS

By

BRANT L. AGGUS

Bachelor of Science

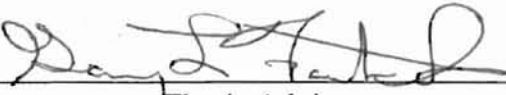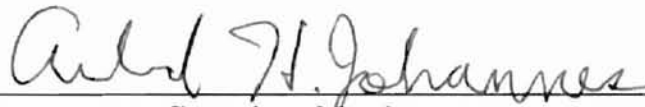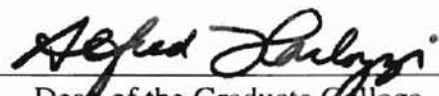University of Arkansas

Fayetteville, Arkansas

1996

ANALYSIS OF REACTORS FOR THE PRODUCTION OF

TITANIUM DIOXIDE THROUGH COMPUTATIONAL

FLUID DYNAMICS

Thesis Approved:

_____

Thesis Advisor

_____

Committee Member

_____

Committee Member

_____

Dean of the Graduate College

PREFACE

The purpose of this research was to examine a group of chloride-process titanium dioxide (TiO_2) reactors, and evaluate for their merits in eliminating deposition of solid TiO_2 product on the reactor walls. This is important to the industrial pigment industry, as a great deal of effort is put into reducing or elimating this deposition to control particle size, and reduce reactor down time for cleaning. Computational fluid dynamic (CFD) modeling was used to examine kinetic and thermodynamic phenomena within these reactors, while reactant nozzle configurations were altered to evaluate their effect on deposition.

Most of all I would like to thank my wife, Amy, for two years of patience, through thousands of miles of driving, thousands of dollars of long distance bills, and thousands of my "I wanna go home" whines. I could not have done it without her.

TABLE OF CONTENTS

LIST OF TABLES

LIST OF FIGURES

NOMENCLATURE

Symbols

A	Pre-exponential factor
C	Molar concentration, $kmol/m^3$
C_p	Heat capacity, J/kmol-K
D	Mass diffusivity, cm^2/s
d_p	Particle diameter, μm
E	Activation energy, kJ/mol
G_k	Energy generation term from velocity
G_b	Energy generation term from bouyancy
J	Diffusive flux, kg/m^2-s
k	Thermal conductivity, J/kmol-K
k	Turbulent kinetic energy, m
Le	Lewis Number, dimensionless
M	Molecular weight, kg/kmol
M	Mass fraction
N	Total number
p	Pressure, atm
R	Correlation coefficient
R	Reaction rate, kmol/s

Re	Reynolds Number, dimensionless
Sc	Schmidt Number, dimensionless
St	Stanton Number, dimensionless
T	Temperature, K
v_m	Specific volume, cm^3/mol
Y_M	Source term in turbulent kinetic energy equation from fluctuations in compressible turbulence

Greek Letters

ε	Eddy diffusivity
Φ	Arbitrary physical property
ν	Stoichiometric coefficient
η	Rate exponent
β	Temperature exponent
θ	Tapering angle of reactant inlet, degrees
Σ	Summation
Π	Multiplication
ρ	Density, kg/m^3
σ	Characteristic length of a molecule, Å
$\sigma_k, \sigma_\varepsilon$	Turbulent Prandtl Numbers for k or ε
Ω	Dimensionless Chapman-Engskog function
ε	Molecular energy parameter, J
μ	Viscosity, kg/m-s

Subscripts and Superscripts

AB	Between components A and B
c	At critical point
g	Of a gas
i'	Of component i
j'	Of component j
k	Of a given reaction k
m	At melting point
max	Highest value in system
o	At reference conditions
p	Of component p
r	Of component r
r	Reaction
w	Of the wall

Abbreviations

2D	Two-dimensional
3D	Three-dimensional
atm	atmosphere
CFD	Computational Fluid Dynamics
CVD	Chemical Vapor Deposition
kg	kilogram
KM	Kerr McGee Corporation
mol	mole

CHAPTER I

INTRODUCTION

Titanium Dioxide

This thesis focuses on chloride-process reactors for the production of titanium dioxide. Computational Fluid Dynamic (CFD) modeling is used to identify causes of, and solutions for, scale growth on the reactor walls. More specifically, to evaluate patented titanium dioxide reactor designs for their ability to control particle deposition, and to identify what factors are most instrumental in halting deposition.

Titanium dioxide (TiO_2) occurs naturally in three crystalline structures: anatase, rutile, and brookite. Anatase and rutile are both commercially produced. Both of these structures are tetragonal, though rutile has two atoms per unit cell and anatase has four. Rutile is harder, denser, and has a higher refractive index than anatase, scattering light about 20% more effectively (Braun, 1997).

TiO_2 rutile is a widely used pigment due to its high refracting index. In his article "Titanium Dioxide – A Review," Braun (1997) stated "among pigments, only TiO_2 and carbon black have essentially no competition." Combined with its usage as paper filler, catalyst support, paint opacifier, and in cosmetics, the world consumes over 3 million tons of TiO_2 yearly (Pratsinis and Spicer 1998). More than half this amount comes from aerosol synthesis, the 'chloride process,' and as of 1998, 8% of the total amount came from Kerr-McGee corporation (Thayer 1998).

Aerosol Synthesis

Synthesis of powders via gas-to-particle conversion is an increasingly important

process. The gaseous reactants form a supersaturated vapor of product, which, upon cooling, forms particles via nucleation, surface reaction, and coagulation. Product molecules can agglomerate to particles by two mechanisms: uninhibited collisions, or evaporation and condensation to and from clusters of molecules.

Advantages of gas-to-particle aerosol reactors are small particle sizes (nanometer to micrometer) with a narrow size distribution, the particles produced are nearly spherical, and the product tends to have high purity. On the down side, gas-to-particle conversion is impractical for multicomponent materials, like mixed ceramics. Different reaction rates and vapor pressures for the reactants tend to lead to non-uniform product composition (Powell et al. 1997).

In the chloride process, gaseous titanium tetrachloride ($TiCl_4$) produced from the chlorination of TiO_2 is oxidized within a flame to yield solid titanium dioxide and gaseous chlorine. The overall equation is:

$$TiCl_4 + O_2 \rightarrow TiO_2 + 2Cl_2$$
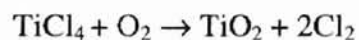
In most current production processes, preheated oxygen (about 1300-1800 °F) is introduced into the reactor within an axially directed flame. Cooler (about 600-800 °F) $TiCl_4$ is introduced downstream, and reacts with the oxygen to form TiO_2 monomer. Preheating both reactants serves to sustain the flame, as the reaction is only slightly exothermic ($\Delta H° = -22.50$ kJ/mol). Reaction temperature is typically in the range of 1291-2550 °F (Akhtar et al. 1991).

Directly downstream of the combustion chamber, the fluid enters a water-jacketed quench zone to control particle size. Through homogeneous nucleation, the monomer forms clusters of TiO_2 anatase. After this point, the particles grow by heterogeneous

2

condensation of TiO_2 vapor and by coagulation. The controlling mechanism is the subject of some controversy, as discussed in the Literature Review. A portion of these particles will remain anatase, the rest are transformed to rutile. The conditions that determine transformation rate are the subject of controversy, as well. The rutile crystalline structure is thermodynamically preferred, and is stable at all temperatures. The chloride process is a preferred production means because it produces particles that are typically all within the 0.1-0.2 particle size. After milling, the final pigment-quality particle size is typically in the 100-1000 micron range.

One of the major drawbacks of the chloride process is that reactors historically have issues with scaling, and eventually plugging, by TiO_2 on the reactor surface (Powell, 1968). A common problem is particle deposition on the wall of the initial section of reaction tube, immediately downstream from the $TiCl_4$ injection spool.
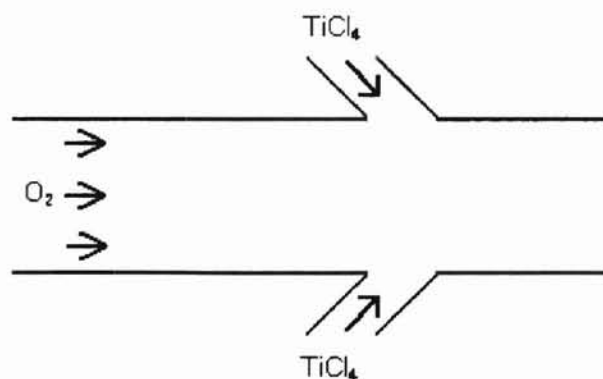
Figure I-1: Diagram of TiO_2 reaction zone

The ultimate aim of our research is to eliminate this deposition. This, in turn, would eliminate the costly process of scouring reactor tubes during TiO_2 production runs (Kronos 1988, du Pont 1993, du Pont 1994). Generally, our research has a twofold

3

purpose: cost reduction and increased production capability, and the study of deposition mechanisms in high temperature aerosol combustion reactors.

Many reactor designs, claiming to eliminate particle deposition, exist in patent literature, from the late 1960s to present day. Solutions to deposition range from knife edged $TiCl_4$ inlets that force the reaction to occur far downstream from the inlet (Montecatini Edison 1973), to reactors that have chlorine product recirculated to the reaction tube to cool the walls (Tioxide Group 1977). The validity of several of these patent claims are examined in this work, and their merit weighed against their feasibility of implementation.

The technique utilized to analyze reactor configurations was CFD modeling. This represents the physical structure within a CAD-type program, and then this model is "meshed" with a web of finite elements. The mesh is given boundary conditions, and the software then solves the energy, mass, and momentum balances simultaneously to give a two- or three-dimensional representation of conditions throughout the reactor including velocity, temperature, and species concentration profiles. The package used for the KM project was FLUENT 5, with GAMBIT as the geometry/mesh building software.

Objectives

This thesis is aimed toward understanding methods that eliminate deposition on the walls of TiO_2 aerosol reactors. The following tasks must be performed to reach this goal:

1. Find patent literature that details reactors designed with the purpose of eliminating product deposition in mind.

2. Evaluate these patents based on scientific merit and theoretical reproducibility.

3. Run simulations of these reactors in FLUENT 5 to authenticate the patents' claims.

4. Interpret these results and suggest variations or improvements to the designs that might further optimize reactor performance.

CHAPTER II

LITERATURE REVIEW

Introduction

This section begins with a review of the chloride process in general, with an explanation of the reaction kinetics and particle growth mechanism. (While there is an extensive library of information on chloride-process production of TiO_2, much of it contains conflicting theories on the particle growth mechanism. Several theories will be examined.) The next section is an examination of literature related to particle deposition in TiO_2 reactors, followed by a review of related CFD modeling techniques. While there are relatively few publications on CFD modeling of TiO_2 reactors, there are more on non-reacting flows, and a few on chemical vapor deposition (CVD) in aerosol processes, which will be presented as an analog. The final section is a review of patented reactor setups and their effect on the reduction of scale buildup.

The Chloride Process

Powell (1968) describes the four steps in the chloride process for TiO_2 production:

1. Solid TiO_2 ore is chlorinated, forming a mixture of gases. This is done in the presence of a reducing agent, typically coke. The reaction is as follows:

$$TiO_2 (s) + 2C (s) + 2Cl_2 (g) \rightarrow TiCl_4 (g) + 2CO (g)$$
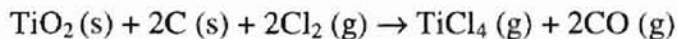
This is normally carried out in a shaft furnace at about 800° C and a pressure just slightly above atmospheric.

2. The solid product is separated from the $TiCl_4$. The most troubling of these are iron chlorides, which can condense from the reactor effluent onto condenser tubes and foul the system.

6

3. The crude $TiCl_4$ is purified. Even after the removal of iron, there are still impurities in the $TiCl_4$ stream. These typically include vanadium and silicon compounds. Purification techniques often involve reaction followed by distillation or filtration.

4. Gaseous titanium tetrachloride is reacted with oxygen at high-temperature (typically in the presence of a flame) to form solid titanium dioxide by the following reaction:

$$TiCl_4 \text{ (g)} + O_2 \text{ (g)} \rightarrow TiO_2 \text{ (s)} + Cl_2 \text{ (g)}$$
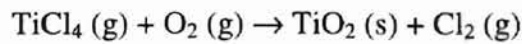
Reaction Kinetics and Particle Growth

Theoretical models of powder formation in tubular flow reactors conform to four general steps. First, monomer is formed by chemical reaction. Monomer concentration then increases as the gas flows down the reactor. Saturation is reached, at which point particles are produced by homogeneous nucleation. After this point, monomer is consumed by particle growth and diffusion to the reactor walls.

Many studies have been devoted to determining the kinetics of the oxidation of $TiCl_4$, and the particle growth mechanism following. Pratsinis and Spicer (1998) defined two pathways for this reaction to progress: the vapor phase reaction of $TiCl_4$ and O_2 to form titania or oxychloride particles at the rate R_g, and the reaction of $TiCl_4$ and O_2 on the surface of previously formed titania particles at the rate R_s. The overall oxidation rate is then:

$$\frac{dC}{dt} = -R = -(R_g + R_s) \tag{2-1}$$

where C is $TiCl_4$ vapor concentration (mole/cm^3). R is generally put into the form of a first order rate equation:

7

$$R = kC \qquad (2\text{-}2)$$

where k is calculated from the Arrhenius expression:

$$k = AT^{\beta} \exp(-E/RT) \qquad (2\text{-}3)$$

The values of A and E have been determined experimentally by Pratsinis et al. (1990) and Kobata et al. (1991). No exponential temperature effect was found in either study, so the value of β is zero in both.

Table 2-1: Arrhenius Constants

Author	A	E (kJ/mol)
Kobata et al.	25×10^4	1.020×10^7
Pratsinis et al.	8.26×10^4	8.88×10^7

Pratsinis (1990) created an experimental apparatus that bubbled argon (Ar) carrier gas through a $TiCl_4$ boiler, after which the mixture met an O_2 stream. The premixed reactants were then sent to an alumina tube that was externally heated by a furnace. A filter removed the TiO_2 product, and the gaseous effluent was sent through an FTIR spectrometer for measurement. These experiments were carried out at a $TiCl_4$ concentration of 2.5×10^{-5} mol/L, and with O_2 concentrations varying from 2.5×10^{-5} to 1.1×10^{-3} mol/L. The experimenters found that when oxygen concentration reached a 10:1 excess the reaction rate became half-order with respect to oxygen, with $A=1.4 \times 10^5$.

Pratsinis and his colleagues went on to propose a sequence of chemical reactions for oxidation of $TiCl_4$ and the formation of TiO_2 powder. The first step is the thermal decomposition of $TiCl_4$, followed by abstraction. The abstraction step produces $TiCl_3$ radicals, which go through the same decomposition/abstraction steps to produce $TiCl_2$,

and in turn TiCl, radicals. Radicals formed in these reactions can also abstract chlorine from $TiCl_4$ molecules

$$TiCl_4 + TiCl_x \rightarrow TiCl_3 + TiCl_{x+1}$$
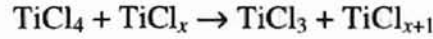
(where $x = 3,2,1,0$). The radicals can also undergo disproportionation reactions, where they exchange chlorine atoms. These radicals are oxidized to produce TiO_xCl_y oxides, which readily coalesce:

$$TiO_kCl_x + TiO_kCl_y \rightarrow (TiO_k)_2Cl_{x+y-n} + nCl$$

where $k = 0,1,2$, $y = 3,2,1,0$ and $n = 1,\ldots,x$. Coagulation reactions proceed as follows:

$$(TiO_k)_iCl_x + (TiO_k)_jCl_y \rightarrow (TiO_k)_{i+j}Cl_{x+y-n} + nCl$$
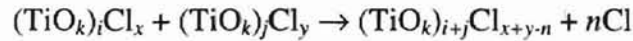
Chorine atoms are continuously removed from the growing particle, so the final growth step is the following:

$$(TiO_2)_i + (TiO_2)_j \rightarrow (TiO_2)_{i+j}$$
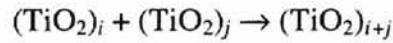
Kobata et al. (1991) developed an experimental setup consisting of a Mullite tube, heated externally by a furnace, with a concentrically sheathed nozzle at one end. Dried oxygen flowed down the reactor tube, and gaseous reagent grade $TiCl_4$ was introduced through the nozzle. Gaseous N_2 flowed through the sheath, blanketing the exiting $TiCl_4$. To determine the rate equation, 3 vol. % $TiCl_4$ was introduced with oxygen, and the chlorine product absorbed into a KI solution. Generated I_2 concentration was determined by titration, and the $TiCl_4/O_2$ reaction rate calculated (the constants are listed in Table 2-1).

Suyama et al. (1975) found that rutile formation increased at higher temperatures, and at low and high oxygen concentrations, but varied little by $TiCl_4$ concentration. The experimenters used two different setups to gather data: one introduced premixed dilute O_2

and $TiCl_4$ into the heated reaction tube via a single inlet, and the second introduced the reactants separately such that they mixed at the highest temperature zone in the reactor. The difference between the two methods of injection seemed slight, as curves of rutile content for both methods varied similarly with changes in O_2 content. The team went on to deduce that the product particle size decreased with decreasing $TiCl_4$ concentration, increasing reactor temperature, and increasing O_2 concentration.

Kodas and Friedlander (1988) derived a series of design equations for calculating the properties of an aerosol formed in a tubular flow reactor operated at steady state. While previous calculations were based on a growth model for $d_p \ll 0.065$ μm, many pigments and powders used for ceramic parts have a diameter of roughly 0.5 μm. Kodas and Friedlander extended the previous calculations to account for larger particle size (up to 10 μm). The set of equations they derived calculates product size based off of four controlling dimensionless parameters, Σ (a surface tension group), θ (the average residence time), E (a diffusion group), and R (the rate of monomer formation). In their conclusions they note that laboratory studies on nucleation rate are required to tune multipliers within the equations.

Akhtar, et al. (1991) studied oxidation of $TiCl_4$ in a tubular aerosol reactor. They found that increasing residence time, temperature, and $TiCl_4$ concentration all increased TiO_2 particle size. Rutile content was determined to increase with temperature, as well. The authors foreshadow the next work discussed here when they note that interparticle forces do not account for an increase of coagulation with temperature. Instead of investigating the surface growth mechanism, the researchers applied a coagulation enhancement factor to the calculation.

Pratsinis and Spicer (1998) attempted to reconcile the surface growth vs. agglomeration argument by developing a model that accounted for both. The model assumes TiO_2 monomer to be a perfect monodisperse aerosol, coalescing upon collision. The particle concentration and volume derivatives were solved via the following equations:

$$\frac{dN}{dt} = I - 0.5\beta N^2 \qquad (2\text{-}4)$$

$$\frac{dV}{dt} = Iv_1 + R_s N_A v_1 \qquad (2\text{-}5)$$

Where I is the nucleation rate, β is the collision frequency, N_A is Avagodro's number, and v_1 is the solid-state volume of the TiO_2 molecule. R_s is the surface reaction rate from equation 2-1. The first term on the right hand side of the equation is the nucleation term, while the second is the surface reaction term. The above equations were solved simultaneously with the equations for I, β, particle diameter, and surface area via the DGEAR routine, and the results plotted over a range of initial $TiCl_4$ concentrations and temperatures and compared to experimental data. The comparison was striking in that it showed that, very clearly, surface growth was the dominant mechanism at higher initial $TiCl_4$ mole fractions (ϕ), and the value of ϕ where the mechanism switched increased with temperature. The experimental data fit the graph reasonably. The authors concluded that the model reconciled and explained the conflicts in the literature on formation and growth of titania.

Deposition Mechanism

As the previous section illustrates, there have been several different theories on the particle growth mechanism in TiO_2 reactors. Accordingly, there are several different

theories on particle scaling on the reactor wall. The subject of controversy seems to be the means of transport of product to the wall. Some theories presented here cite thermophoresis as the mechanism, and others cite Brownian Diffusion. Thermophoresis is simply defined as "a term describing the fact that small particles suspended in a gas will acquire a velocity in the direction of decreasing temperature" (Montassier et al. 1990). Freitas (1998) sums up Brownian diffusion thusly: "....from time to time, a suspended particle receives a finite momentum of unpredictable direction and magnitude. The velocity vector of the particle changes continuously, resulting in an observable random zigzag motion, called Brownian movement."

Kim and Kim (1988) developed an apparatus to study deposition from a particulate high-temperature gas flow, and concluded that thermophoresis effect was the cause of deposition for small particle sizes ($d_p < 15$ μm), and particle inertia for larger particle sizes. The experiment was performed by flowing solid TiO_2 into a flat flame gas burner, and collecting the spherical TiO_2 particles on a cold Pt strip overhead. Optical intensity of a laser beam supplied incident to the strip measured deposition. The investigators determined a linear relationship to exist between deposition and wall temperature/bulk fluid temperature difference (for $d_p < 3$ μm), and developed a mathematical equation representing particle mass flux at the wall:

$$- j_w'' \cong - j_m'' = \rho_e U_e (\alpha_T Le)_w St_m [\frac{(T_g - T_w)}{T_w}] \omega_m \qquad (2\text{-}6)$$

The subscript w represents the wall value, m represents the value at the edge of the mass transfer boundary layer, and e is the outer edge of the convection boundary layer. Le is the Lewis number, α_T is the thermal diffusion factor of the particles, and U is the fluid

12

velocity parallel to the wall. The thermophoretic effect that is evident is the $(T_g-T_w)/T_w$ term (the thermophoretic "suction" parameter). St_m is the local Stanton number at the interface, and is augmented with a thermophoretic enhancement factor:

$$St_m = (\alpha_T Le)_w [\frac{T_{g-}T_w}{T_w}] \frac{\omega_m}{\omega_e} \tag{2-7}$$

Kim and his colleagues claim that this equation holds for particles of size such that Sc<<1. At larger particle sizes, the thermal terms drop out.

Montassier et al. (1990) investigated thermophoresis for particle sizes 0.05 µm to 8 µm by developing an experimental device that flowed uranin, a flourescent aerosol, down a deposition tube, which was then cut into segments and weighed. The study determined that for small particle sizes (0.1 µm< d_p < 1 µm) the deposition was consistent with a theoretical thermophoresis model, but at larger and smaller sizes, the relationship was merely qualitative. Chang et al. (1990) created a device that passed silicon dioxide (SiO_2) aerosol through a thermophoretic cell composed of a brass or porous stainless steel outer cylinder, and an inner cylinder of nichrome wire. They were able to induce thermophoretic deposition of greater than 50% through variations in temperature gradient between the inner and outer walls.

Okuyama, et al. (1992) attempted to develop a mathematical model of nucleation and growth of particles in a laminar-flow TiO_2 reactor. This did not evaluate thermophoresis as a cause of axial dispersion, and instead classified it as the result of Brownian diffusion. In turn, they developed separate mathematical models of mass and number concentrations of monomers and polymer that are irrespective of temperature. The reactor wall was treated as an adsorber, and the deposition fluxes calculated

simultaneously with the mass and number concentration equations, mass balance, and energy balance via the Crank Nicholson method. The results were compared with experimental data, and they agreed. This is quite different from to the previous studies of Montassier and Kim. Okuyama did note though, that deposition of reactant vapors, monomer, clusters, and particles on the reactor wall were enhanced by low temperatures, and interestingly, low feed concentration of the reactant, titanium tetraisopropoxide (TTIP). What is also curious is that the amount of deposition was dependent on the carrier gas, which was N_2 or He. Okuyama presents the theory that this is a result of the difference in diameter of the molecules of these gases. Because the helium molecule is roughly three times as large as the nitrogen molecule, the diffusivity of a particle in helium is about three times that of the particle in nitrogen. At a fast reaction rate, it is difficult to say whether this would have an effect in our case without experimentation, as the majority of particle growth occurs at the length of the reactor where deposition is occurring. Seto et al. (1995) examined the effect of changing carrier gas on the sintering rate of titania powder and determined that there was no effect. The only cases where Seto speculated there could be effect were in porous particles (i.e. ceramics) where diffusion into the vacancies was dependent on diffusivity of gases in the solid phase. Dekker, et al. (1993) investigated particle deposition, surface heterogeneous reaction, and the structure of deposited powder in a titanium nitride (TiN) reactor. They describe the mechanism of controlled deposition of particles on a substrate layer as PP-CVD: particle precipitation-aided chemical vapor deposition. An aerosol is formed at a high temperature, and then particles are deposited on a cooled substrate via thermophoresis. The PP-CVD process is further summed up in three steps: particle formation, deposition,

and finally sintering. The paper goes on to briefly discuss a possible mechanism of interest to this project, M-CVD, or modified chemical vapor deposition, where the substrate is the relatively cold reactor wall. This experiment differs from our system in two main aspects. The aim in their study was to induce PP-CVD and gain a desired deposition structure, and the substrate surface was a dead-end quartz tube, an idealized surface for deposition. The authors go on to conclude that the activation energy of the process indicates whether the deposition reaction is controlled by surface kinetics (approximately 100 kJ/mol or greater) or Brownian diffusion (typically 10-20 kJ/mol).

An important thing to remember is that while a heated reaction tube would appear to be a simple means to eliminate deposition, the wall must be cooled downstream to quench the reaction and control the particle size of the rutile product. Many of the studies mentioned previously searched for means to promote particle deposition, making them somewhat helpful to understanding the mechanism, but relatively bereft of development of ways to avoid it. Elimination of accretion within the reaction zone does away with the need of injecting scouring agent there, allowing it to be injected further downstream where it can act as a sink to cool the effluent.

CFD Modeling

CFD modeling is a technique of solving the energy, mass, and momentum balances for a finite-element representation of a system. While there has been considerable progress in the field within the last ten years, there has been precious little research into TiO_2 production through CFD modeling. Many of the sources cited here deal with related processes that are pertinent by analogy.

Jang et al. (1995) used a modified moment method to solve the Navier-Stokes,

15

continuity, vapor-conservation, and general dynamic (coagulation, diffusion, reaction, thermophoresis) equations for a TiO_2 reactor. While moment methods had been used previously to solve for particle properties (Kodas and Friedlander 1988), this newer solution accounted for a non-isothermal axial temperature profile within the reactor (a 2d model). Particle size and distribution were calculated for networks from 15,000 to 30,000 finite elements with TEACH and LSODE computation packages. These results were used to evaluate the effects of particle size and distribution on $TiCl_4$ and O_2 partial pressures and reaction temperatures. The model was compared with the experimental results of Jang and Jeong (1995) and good agreement determined.

Harris et al. (1996) used three examples to summarize the current state of CFD modeling of chemical reactors: a stirred-tank reactor, an extruder, and a tubular reactor with competing parallel and consecutive reactions. The third example consisted of two reactants, A and B, mixing in a nozzle to form products C and D. The reactants and products react selectively with each other to form products E, F, G, and H. The software package CFDS-FLOW3D was used to evaluate the mean value (MV), extended eddy breakup (EBU+), and probability density function (PDF) reaction models. Upon comparison with plant data (which show that the majority substance leaving the reactor should be D), the researchers determined that the EBU+ model is not adequate for parallel reactions, as it calculated similar rates for each parallel reaction. This is due to the fact that all reactions had very fast rate, so the model replaces the Arrhenius rate with a rate proportional to the frequency associated with turbulent eddies. (The eddy dissipation model in FLUENT 5 is used in the current research, and is valid as it is applied to a single reaction. It will be discussed further in Chapter III.) The researchers

16

went on to define the current limiting factor in CFD modeling of chemical reactors to be computer resources. They defined another current limitation as being the difficulty of modeling multiple phases. (FLUENT 5 is capable of handling multiple fluid phases, but does not have the ability to model a reaction that forms a discrete solid phase from fluid reactants.)

Stovall et al. (1997) used FLUENT, with the RG turbulence model, to examine a theoretical high velocity flow profile for a coolant (D_2O) through a narrow channel with an inlet blockage. The group also created an experimental setup whereby thermochromic crystals on a diagnostic heater measured wall temperature and laser Doppler velocimetry measured fluid velocity. The results were compared, and the group determined that FLUENT was accurate for determining the span-wise and axial velocity profiles, and provided a conservative estimate for heat transfer behind the inlet blockage.

The modeling of a creeping-flow zinc selenide aerosol reactor by Shay (1998) served to determine the flow regime in the reactor, and whether or not there was backflow present. Shay developed a 2d model of the reaction tube with nonreacting flow, supplied kinetic expressions and empirical mass transfer coefficients, and performed runs under a variety of flow conditions in FLUENT. Upon comparison with plant data for the reactor, he determined the FLUENT results to be reasonable and valid, as the model matched the plant data within the error limits of mass flow rate uncertainty. Shay went on to determine optimal flow rates and nozzle diameters for the reactants. Foster (1999) reached similar conclusions in his FLUENT modeling of the same reactor, and additionally ascertained optimal reactant and carrier gas flow rates and temperature for high yield.

17

Nami et al. (1997) investigated metalorganic chemical vapor deposition (MOCVD) using the FLUENT package. The investigators developed a 2d model of an inverted batch reactor for the growth of TiO_2 film, with TTIP and H_2O as precursors. The team modeled gas velocity, temperature profile, concentration of reactant gas, and most notably, deposition rate. The model included the effects of radiation, conductive walls, thermal diffusion, and surface temperature of the deposition surface. Deposition rate was modeled as a mass flux rate into the solid receptor surface, and not as a reaction. Theoretical results were compared with experimental data, and concentration profiles of reactants in the FLUENT model were relative to the film non-uniformity found in the experimental results. These results were used to back-calculate an Arrhenius rate constant for the surface reaction.

Warnecke et al. (1999) used CFD modeling to develop yield improvements for a proplylene chlorohydrin (a propylene oxide precursor) tube reactor. This is a complex process, as the reaction scheme involves multiple equilibrium, consecutive, and parallel reactions (all of different order), as well as multiple phases.

Both one and three-dimensional models were solved in the study. The 1d model was solved with the program SIMULSOLV, and the CFD package CFX was used to solve the 3d model. The group modified the CFX code with a FORTRAN subroutine to calculate compressible two-phase flow with mass transfer in between the phases. Because the reactor geometry in the study is relatively simple, the 1d model coincided with the more elaborate 3d model. When more complex reactor geometries were examined as alternatives to the tube shape, the 1d results were only qualitatively correct, and could be used as initial guesses for the 3d model.

Patented Reactor Designs

The basic theme for metal oxide reactor patents that claim to eliminate deposition is that they simply attempt to drive the reaction zone downstream from the $TiCl_4$ inlets, and away from the reactor wall. This deters both suspected mechanisms for scale growth, agglomeration or surface reaction at the wall. After searching through the patent literature, it appears the most common means for preventing deposition is flowing an inert gas, or chlorine, through or along the reactor wall. Some of the more well-defined examples of this will be described in detail.

Another repeated theme in the patents is the notion of "shielding" the $TiCl_4$ vapor from the O_2 stream when it initially enters the reactor. This is done by surrounding the $TiCl_4$ inlet with combustion gas, though some examples suggest an inert.

Researchers at American Cyanamid Company (1967) patented a configuration whereby $TiCl_4$ and O_2 reactants, either or both preheated with a plasma gun (3,000 to 12,000°C) and brought to turbulent flow, meet at a Y-angle from 25° to 160° in the reactor chamber. As the authors made the angle smaller (<50°), reactor plugging was minimized.

The back of the reaction chamber (Item 25, figure II-1) was a hemispherical dome, which, according to the authors, also served to eliminate deposition. The reactant inlets were flush with the reactor wall, and the absence of any sharp turns eliminated backflows and eddies that could lead to deposition. This claim is backed up by the fact that installation of the domed end led to 3% of the product not being suitable for pigmentation (particle size too large) vs. 8% with a flat-backed wall.
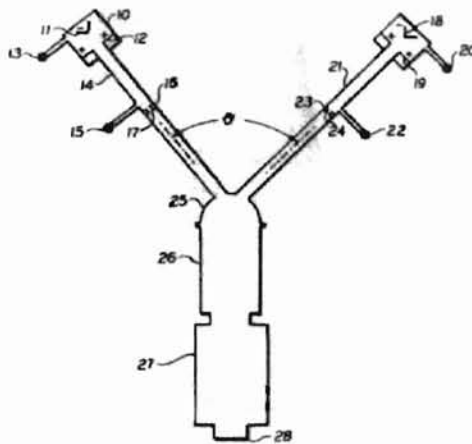
Figure II-1: American Cyanamid TiO$_2$ Reactor (from U.S. Patent # 3,328,126)

Cabot Corporation (1967) developed a reactor consisting of a series of concentric frusto-conical tubes, with reactants and combustion gas introduced via tangential, diametrically-opposed nozzles. Fuel gas flows through one of the conduits (Item 14, Figure II-2) into the outer annulus, while a mixture of O$_2$ and TiCl$_4$ flow through the second conduit (Item 16, Figure II-2) into the middle annulus. The flows meet in the reaction chamber (Item 12, Figure II-2) and mix, still spinning. The patent recommends an axial velocity between 75 and 350 ft/s. Above that range, the flame becomes extremely unstable.

The purpose of the tangential flow is simply to sweep the deposits off the side without the use of an inert. The authors reported that the apparatus "substantially eliminated" accretion.
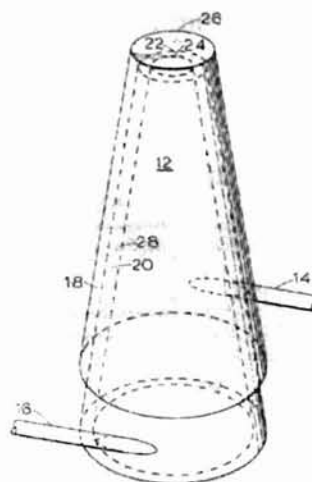
Figure II-2: Cabot Corporation TiO$_2$ Reactor (from U.S. Patent # 3,351,427)

British Titan Products, now part of Huntsman Corporation, created a design in 1969 (British Titan Products 1969) that consisted of oxygen at 170°C entering the reactor through an outer annulus (Item 56, Figure II-3), and TiCl$_4$ at 150°C introduced downstream through a second annulus (Item 57, Figure II-3). A wall separated the annuli. Both reactants flowed into the reaction tube through small holes tapped in its outer wall, and inside were met with the output of a plasma gun emitting argon at 11,000 K (directed through an orifice upstream, Item 51, Figure II-3), heating the mixture to about 2000°C. Additional TiCl$_4$ was fed in through axial inlets (Item 66, Figure II-3) facing the secondary reaction zone. The patent does not give a run time, but claims that all zones of the reactor were "substantially free" of TiO$_2$ accretion.

Though it is not used in any of the patent examples, there is an inlet to an additional concentric spool (Item 65, Figure II-3) where a "purge" gas can be introduced. The spool directs the gas along the wall of the reaction zone, where it acts as a sheath for the primary reactant stream. The authors list the purge gas possibilities to be one of the

reactants, an inert gas (argon or nitrogen), or most preferably a halogen (chlorine for a metal chloride reactant).
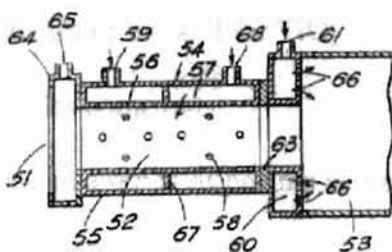
Figure II-3: British Titan Products TiO_2 reactor (from U.S. Patent # 3,464,792)

Researchers at Cabot Corporation (1971) developed a five-step process to eliminate deposition from $TiCl_4$ oxidizer walls. First, the reactor effluent stream met a recirculating stream of product gases, split off downstream from a baghouse filter, and upstream from the chlorine recovery unit. This stream cooled the reactor effluent from 2000°F to roughly 800-1400°F. The resulting suspension was then passed through a series of water-jacketed counterflow heat exchangers. At this point, the effluent temperature was roughly 600°F, and a small amount of water was injected into the stream. The patent makes it clear that the temperature must not be substantially greater than this, in order to avoid the formation of hydrogen chloride from H_2O and Cl_2. TiO_2 product was then removed in the baghouse, and the effluent gas recirculated to the first step. The patent claims that when a production run was started without water injection the efflux temperature from the two heat exchangers increased from 580°F to 800°F for the first, and 300°F to 500°F for the second over a period of four hours. After that point, water was injected, and the efflux temperature from the first heat exchanger initially dropped to 600°F, and then went to 590°F over the course of 16 hours. For the second

22

exchanger, the temperature initially dropped to 320°F, and then went to 290°F over the course of 16 hours. The patent does not make mention of product TiO_2 structure, but mentions that for an effluent stream of 5,000 lb/hr TiO_2, 45 lb/hr of titanium chlorides and 20 lb/hr of aluminum chlorides come out.

Swirling flow was utilized in a series of patents assigned to Montecatini Edison S.p.A. (1971, 1972). Premixed $TiCl_4$ and O_2 entered the reactor through an annulus where they meet an undisclosed "swirl device" (Item V1, Figure II-4). One would speculate that this device is a baffle or an irregular wall of some sort. A central axial inlet introduced O_2 for carbon monoxide (CO) combustion (Item T, Figure II-4), surrounded by a CO annulus, again with a swirl device (Item V2, Figure II-4). Item C3 in the diagram is O_2 flowing through an outermost annulus, which the patent claims "surrounds, like a film, the outer walls of the burner to prevent the formation of crusts on the outside of the terminal part of the burner." (Montecatini Edison 1971) The walls were also externally jacketed with a thermostatic liquid, presumably water. As the diagram shows, a recirculating reaction zone is formed (Item R, Figure II-4), which amounts to a common reaction zone for both CO combustion and $TiCl_4$ oxidation. The patent gives optimum dimensions and flow rates to maintain this recirculation in the "example" section.
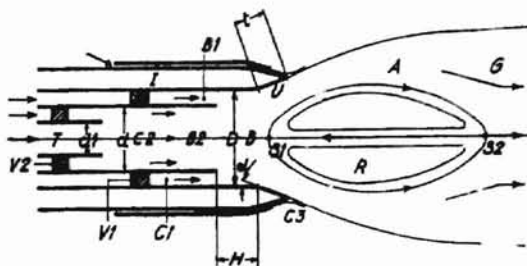
Figure II-4: Montecatini Edison TiO_2 reactor (from U.S. Patent # 3,552,920)

Titangesellschaft Corporation designed a reactor (Titangesellschaft 1972) that introduced all the oxygen for $TiCl_4$ reaction with combusting CO and oxygen, and brought in $TiCl_4$ via rotating jets sheathed with CO. The CO sheath ideally created a circular flame, which would force the reaction of $TiCl_4$ and O_2 downstream to a predetermined reaction zone. The deposition deterrents of the patent are the tangential injectors on the reaction chamber wall, which introduce cold inert gas tangentially to essentially "sweep" deposits off (See Item 27, Figure II-5). The example gas given in the patent was air at room temperature. The patent does not give the run time of the example, but claims that the chamber wall and gas-permeable plate were "largely free" of TiO_2 deposits after the run.
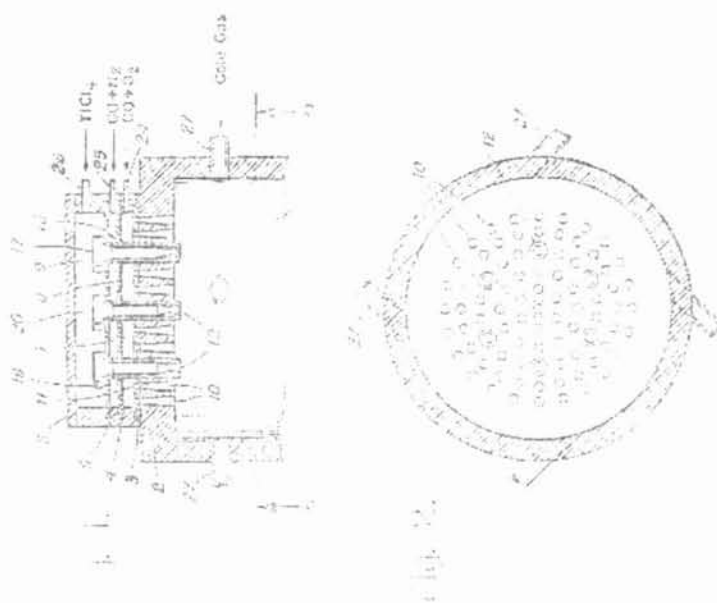
Figure II-5: Titangesellschaft TiO_2 reactor (from U.S. patent # 3,647,377)

Montecatini Edison S.p.A. designed a similar type of reactor (Montecatini Edison 1973) and stated that the arrangement of reactant inlets avoided premature reaction

24

between TiCl$_4$ and O$_2$, thereby eliminating deposition. The inventors discount one major aspect of earlier designs like the Titangesellschaft reactor: the introduction of TiCl$_4$ into the area where there is unburnt carbon monoxide. This is for two reasons, the first being that TiCl$_4$ is a strong combustion inhibitor, causing a lower mixing temperature and slower oxidation. Secondly, the uncombusted CO promotes rechlorination of TiO$_2$, giving decreased yield and poor particle size distribution. The solution proposed by the inventors was a tapered TiCl$_4$ inlet that extended past the combustion zone, downstream from the CO inlets surrounding it. The views in Figure II-6 are a cutaway side view, and an axial upstream view of the reactor, respectively.

a.   b.
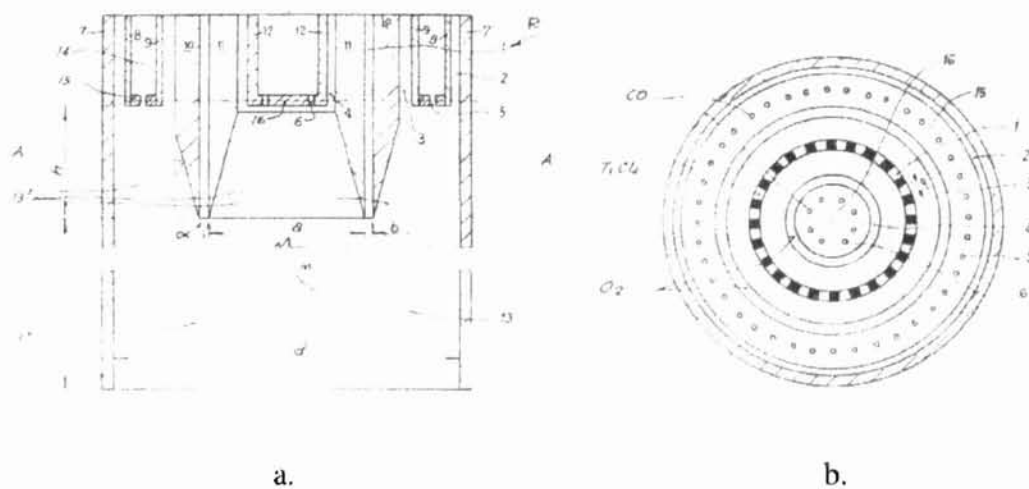
Figure II-6: Montecatini Edison TiO$_2$ reactor (from U.S. Patent # 3,764,667)

The TiCl$_4$ inlet is ringed with spacers, seemingly for the purpose of choking down the flow and pushing the reaction further downstream. These were added in the third of the three examples in the patent. Another embodiment mentioned by the inventors, but not given in an example, is the same configuration, but with a stream of nitrogen (N$_2$) interposed between the CO and TiCl$_4$ outlets. They mention that this could have major

drawbacks; most importantly it would contaminate the chlorine gas leaving the reactor, which is typically purified and recirculated to the TiO_2 chlorinator.

In the example, O_2 is heated to 750°C, CO to 400°C, and $TiCl_4$ to 500°C. The reaction temperature is stated to be about 1500°C. The patent claims of an 18-hour run time without plugging, but a 25-40% percent number coefficient of particle size, which is broad.

A simpler approach slowing the mixing of $TiCl_4$ and O_2 is the idea of a "turbulent wake" burner (American Cyanamid 1979). Oxygen flowed through a centerline inlet and through a diffuser screen (Item 6, Figure II-7) to force a flat velocity profile. $TiCl_4$ entered through a slotted conduit, (Item 4, Figure II-7) and mixed with O_2 in the turbulent wake from the oxygen flow over the conduit. (The patent specifies a Reynolds number of at least 50 for the oxygen flow, based off the conduit diameter.) The wake slows the contact of O_2 and $TiCl_4$, and presents flashback of product upstream. Oxygen is supplied in excess so an unreacted portion can sweep the reactor walls.

a. b.
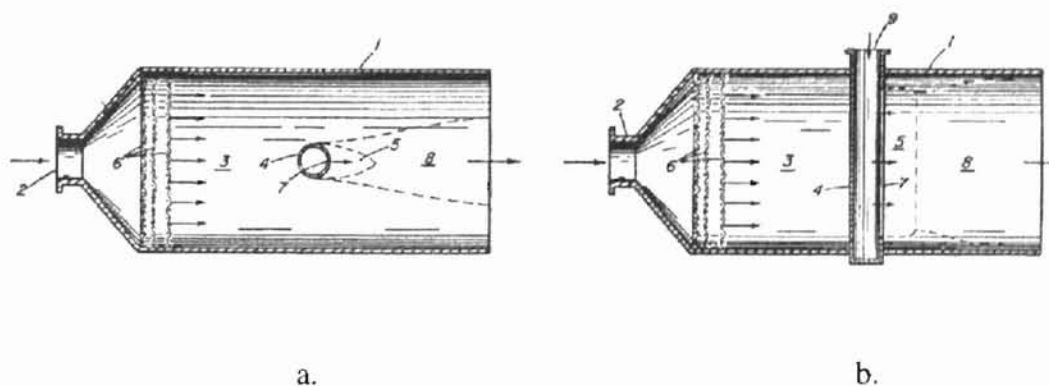
Figure II-7: American Cyanamid TiO_2 Reactor (from U.S. Patent # 4,170,630)

The patent does not have an example section, so some aspects of the reactor are not detailed. Most notably, there is no description of how the oxygen is heated and reaction zone temperature maintained. Sizing for any of the components is not supplied, either.

Tioxide Group, Ltd. designed a reactor (Tioxide Group 1977) that eliminates deposition by passing an inert gas (or oxygen) through an outer annulus around the reaction-completion tube and making the wall of the reaction-completion tube porous (Item 22, Figure II-8), so the gas can transpire through it. This serves a two-fold purpose, as it eliminates accretion and at the same time cools the reactor wall. In the example, a mixture of argon arc-heated to 10,000 K and oxygen were introduced through the porous wall of the preconditioning zone (Item 7, Figure II-8). Premixed aluminum chloride (a rutilization agent), O_2, and $TiCl_4$ at 175°C were introduced through the outer perforated jacket of the reaction zone (Item 11, Figure II-8. Items 12-17 in the figure are crimped disks which distribute the flow). Oxygen flowed through the reaction-completion tube's porous wall and maintained a wall temperature below 500°C throughout the run. After 25 minutes of operation, the experimenters found "little accretion" in any zone of the reactor.
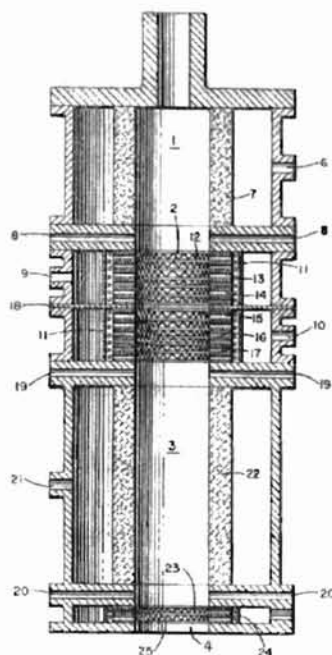
Figure II-8: Tioxide Group TiO$_2$ reactor (from U.S. patent # 4,013,782)

Another theme that runs through several recent patents is the scrubbing of the cooling tube wall by recirculating larger (above 150 μ) TiO$_2$ particles (Kronos 1988, du Pont 1993, du Pont 1994). The advantage of this is that TiO$_2$ particles do not contaminate the raw pigment, and no low melting eutetics are formed. This technique is costly, and with tighter particle size distributions there are not an appreciable amount of large TiO$_2$ particles present with which to scrub. This, along with flexing the reactor wall to break up the accretion (Cabot 1965), and sonication of reactant gases (Cabot 1970) amount to "brute force" methods of removal will not be examined here.

28

CHAPTER III

ANALYSIS OF PATENTED REACTOR CONFIGURATIONS AND MODELING TECHNIQUES

Introduction: Selection of Patents

The patents chosen for analysis in were the following: Cabot Corporation's reactor with tangential reactant and combustion gas injection (Cabot 1967), and Montecatini Edison's reactor with a knife-edged $TiCl_4$ spool (Montecatini Edison 1973), both discussed in Chapter II. The main reason for selecting these reactors is that they both claim to eliminate deposition without the presence of an inert gas. This is important, as the presence of inert in the effluent stream would require larger equipment to obtain undiluted chlorine for recirculation (Montecatini 1971).

In addition to examining the deposition reducing effect of these configurations, a patent from Kronos USA Inc. (Kronos 1993) will be examined. This patent was chosen because it is a good general example of an industrial scale apparatus.

Analysis of the Kronos TiO_2 Preheater from U.S. Patent #5,196,181: A "Trial Run"

a. (side view)   b. (back view)
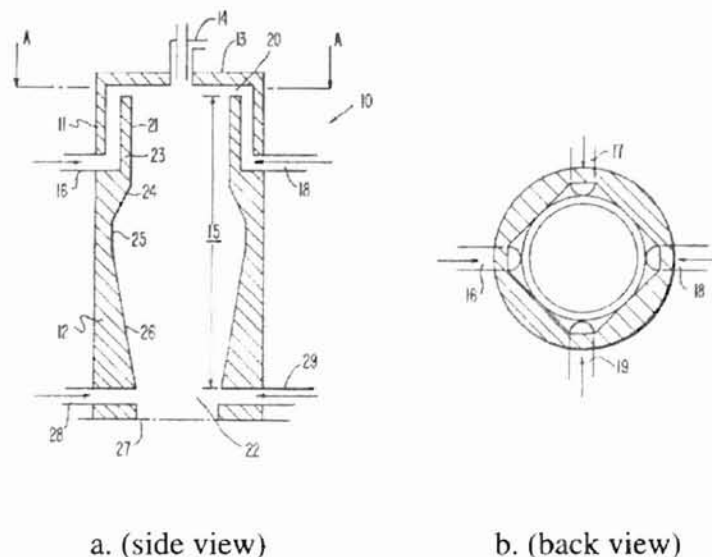
Figure III-1: Kronos Reactor (from U.S. Patent #5,196,181)

29

While this patent does not directly claim to reduce deposition, it serves as a good model to test physical property calculation schemes. The conditions supplied in the patent also put the flow in the turbulent regime, the only example of turbulent flow in this work.

In this setup, oxygen flows into an annulus through four semi-circular inlets (Items 16-19, Figure III-1), and then into the preheat section with an axially directed toluene (C_7H_8) burner (Item 14, Figure III-1). The patent goes into detail describing the shape of the preheat section and the oxygen annulus, as it claims the oxygen forms a protective "film" on the surface of the refractory lined preheat section. The inventors purport that this film enhances the life span of the refractory material.

Items 28 and 29 in the drawing are $TiCl_4$ inlets. While a two-dimensional representation is supplied in the "Drawings" section of the patent and a mass flow rate is supplied in the "Examples" section, the number of inlets is not given. This leaves the parameter open to experimentation to determine the likely optimum number of inlets to provide the best mixing scenario, and at the same time attempt to eliminate backflow. The patent does not describe the geometry downstream from these inlets, so a reaction tube in the shape of an inverted cone was added. This is a common shape for downstream section from the TiCl4 inlets in much of patent literature. Cabot Patent # 3,351,427 (1967), Cabot Patent # 3,322,499 (1967), and Pittsburgh Plate Glass Patent # 3,356,456 (1967) are good examples. The following diagram shows the initial reactor geometry used for the FLUENT simulation.
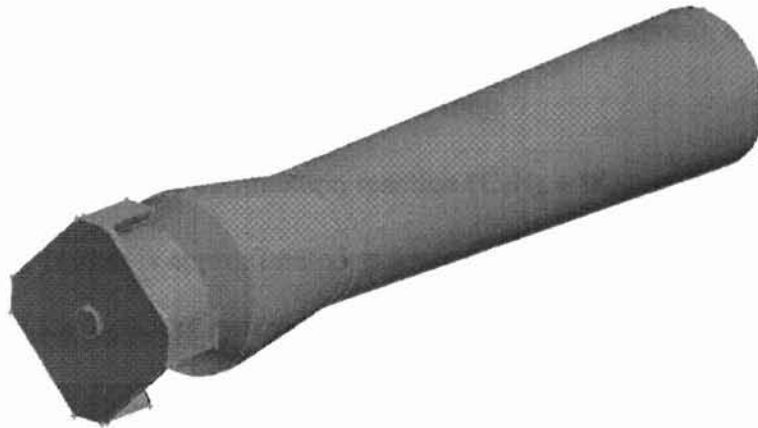
Figure III-2: Initial GAMBIT Geometry of Kronos Reactor with 4 TiCl₄ Inlets (from U.S. Patent #5,196,181)

To accelerate the iteration process, and to address issues of asymmetry within the calculated results, this geometry was cut into a quarter, and each cut treated as a centerline in the FLUENT. The following figure shows the final geometry used for calculation.
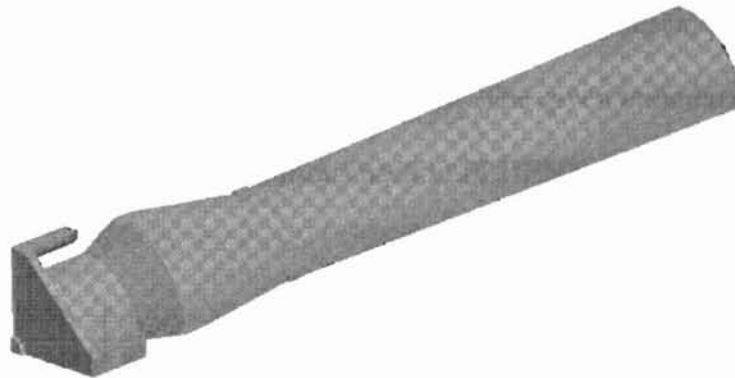
Figure III-3: GAMBIT Geometry of Kronos Reactor with 4 TiCl₄ Inlets (from U.S. Patent #5,196,181) Used for Calculations

Several assumptions and simplifications were made to implement this model:

1. As mentioned previously, a reverse-frustum reaction chamber was added, with a small-side diameter of 480 mm (same as the $TiCl_4$ spool), and a large side diameter of 560 mm. The tube is 2 m long.

2. In lieu of a toluene combustion reaction ($C_7H_8 + 9O_2 \rightarrow 7CO_2 + 4H_2O$), the toluene burner is approximated as a velocity inlet, emitting carbon dioxide (CO_2) and water (H_2O). This shortens the time per iteration, as there are not two reactions with O_2 as a reactant, one rate dependent on O_2 concentration.

3. The reactor is approximated as adiabatic. This is only an assumption for the reaction chamber, as the patent states that the entire preheat zone is lined with refractory material, and insulated with 180 mm total thickness of insulating bricks.

4. H_2O and Cl_2 in the effluent do not react to form HCl. This reaction is not really of interest to this work, and would just complicate the calculations.

The patent contains two separate examples, the first is for a constant-diameter preheat chamber, and the second, the one used in this work, gives the dimensions and boundary conditions for a variable-diameter preheat chamber. The given boundary conditions are in Table III-1, and the boundary conditions used in FLUENT are in Table III-2.

	Flow Rate	Temperature
C_7H_8	90 L/hr (liquid) with 170 Nm^3/hr O_2	STP
O_2	101 m/s	1223 K
$TiCl_4$	12.5 t/hr (99% pure)	723 K

Table III-1: Boundary Conditions Given in Kronos Patent 5,196,181, Example 2

32

	Boundary Type	Value	Temperature	Turb. Intensity	Length Scale
C_7H_8 burner	Mass Flow Inlet	80.28 kg/h	2873 K	1%	3.675 mm
O_2 inlets	Velocity Inlet	101 m/s	1223 K	5%	4.2 mm
$TiCl_4$ inlets	Velocity Inlet	85.84 m/s / # of inlets	723 K	5%	4.2 mm

(Toluene burner is 81% CO_2, 19% H_2O by mass)

Table III-2: Boundary Conditions Used with FLUENT Simulation of Kronos Patent 5,196,181

Length scale (ℓ) is calculated for this system and for all following systems by

$$\ell = 0.07L \qquad (III-1)$$

from a heuristic provided in the FLUENT User's Guide (1998). L is the relevant inlet dimension, either width or diameter, depending on the shape of the duct. The intensity value of 5% represents full turbulence development at the boundary, which is reasonable in this case, as the Reynolds number in the O_2 ducts and the $TiCl_4$ ducts are calculated to be 50,000 and 190,000, respectively.

The patent is relatively detailed in its description of the preheat zone, giving the diameters of every part of the chamber. These are tabulated in Table III-3. The adjustable parameter for this case was chosen to be the number of $TiCl_4$ inlets, which is not specified in the patent. The only supplied parameters are the mass flow rate of $TiCl_4$ (see Table III-2), and the inlet diameter.

Section	Diameter	Length
16 and 18	60 mm (cylinder halved axially)	214 mm*
20	30 mm	118 mm*
21	480 mm	300 mm
22	480 mm	60 mm
24	480 to 640 mm	128 mm**
25	640 mm	72 mm**
26	640 to 480 mm	475 mm
28 and 29	60 mm	1 mm

(* = Length measured from schematic, ** =Length for both is 200 mm, length of each measured from schematic.)

Table III-3: Section Diameters for Items in Figure III-1 and Corresponding Length

Three different numbers of $TiCl_4$ inlets are used to determine the optimum arrangement to eliminate backflow: 2, 4, and 8. Total mass flow rate was converted to velocity based on the density at the $TiCl_4$ inlet temperature, giving a total calculated velocity of 85.84 m/s for a single, 60 mm × 60 mm square duct inlet. This was simply divided by the number of inlets to give the boundary condition for the simulation.

Analysis of Montecatini Edison Patent # 3,764,667

The Montecatini reactor, previously discussed in chapter II, has multiple oxygen inlets, with the outermost inlet flowing O_2 along the outer reactor wall (see Figure II-5). As will be shown in the results, this oxygen remains mostly unreacted, shielded by a stream of hot CO_2 from the combustion of CO gas. This is a benefit that is not disclosed in the patent, but likely plays a large role in the prevention of deposition.

The adjustable parameter chosen for this case is the tapering angle θ of the inner and outer walls of the $TiCl_4$ annulus (see Figure III-4). The patent specifies a range of 4-20°, and values over that range were examined in this work. The patent also specifies that the inlets protrude in a range of 0.3 to 0.6 times the reactor width beyond the CO jets. In this work, this length is exceeded for the 4° taper. This is purposely done to examine the significance of this ratio.
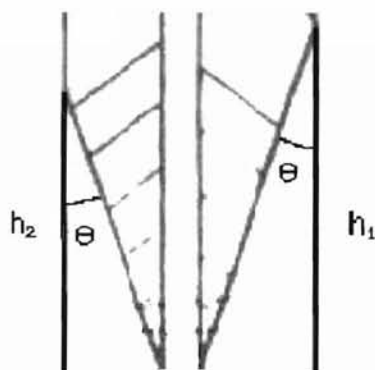
Figure III-4: Detail of TiCl$_4$ Annulus for Montecatini Patent 3,764,667, Side View

Several assumptions were made to model the reactor geometry given in the patent. They are as follows:

1. The tapering angle of the inner side of the TiCl$_4$ annulus was assumed to begin at the same axial coordinate as the opening of the CO annulus into the reaction chamber.

2. The width of the inner wall of the TiCl$_4$ annulus was based off triangulation of the given θ and length values for the wall. The width of the outer wall was gained by measuring the inner/outer widths off the schematic, and scaling to the triangulated inner wall value.

3. CO annulus openings were assumed to be 0.1 mm "pinholes".

4. There is no aluminum chloride (AlCl$_3$) included in the TiCl$_4$ injection. (The patent lists a 1% composition of AlCl$_3$, but it is injected solely as a rutilizing agent. This work does not encompass particle growth, making it meaningless to include.)

The third of three examples given in the patent lists the following known parameters:

1. Inside diameter of the TiCl$_4$ inlet ring is 32 mm.

35

2. Reactor length is 800 mm.

3. Reactor diameter is 61 mm.

4. Axial distance from the bottom of the CO spool to the bottom of the $TiCl_4$
   spool is 27 mm.

5. The $TiCl_4$ inlet is 2 mm wide.

6. Each $TiCl_4$ ring spacer is separated by 2.5 mm OD.

7. There are 25 $TiCl_4$ jets created by the spacers.

8. There are 8 jets on the inner CO tube, and 40 jets on the outer CO annulus.

Using this information, a 3D model of the reactor was created in GAMBIT, the

geometry-building software bundled with the FLUENT package.
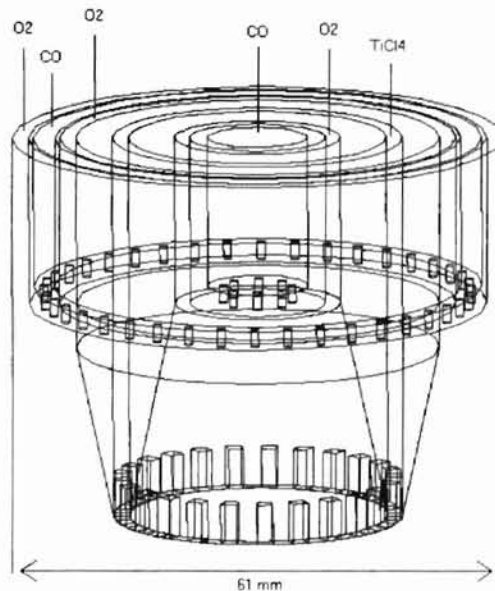
Figure III-5: Side view of GAMBIT geometry for Montecatini Patent 3,764,667

Progress with this model did not extend beyond creation of the geometry, as creating grid

interfaces between the CO jets and the open reactor zone proved infeasible. This is

because FLUENT cannot form a grid interface between one face and more than one opposing face, an issue that will likely be addressed in future versions of the software. While using the current version, further investigation into the 3D model of this reactor should involve attempting to formulate a system of subvolumes to allow this model to function.

To continue forward, a 2D model of the reactor was created, and was used to carry out all FLUENT runs. The following figure illustrates the geometry created in GAMBIT:
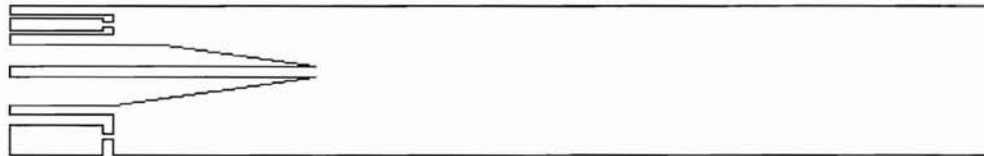
Figure III-6: 2D GAMBIT Geometry of Montecatini Patent 3,764,667 (θ=8°)

The bottom of the diagram represents the centerline of the reactor. 2D reactor models were made for five separate θ values: 4, 8, 12, 16, and 20 degrees. The table below gives the values for h_1 and h_2, as shown in Figure III-4, calculated for each θ. The width of each annulus wall was held constant.

θ	h_1 (mm)	h_2 (mm)
4°	82.1	62.2
8°	40.8	31.0
12°	27.0	20.5
16°	20.2	15.2
20°	15.8	12.0

Table III-4: TiCl$_4$ Inlet Geometry for Each Montecatini Patent 3,764,667 Reactor Model

All geometries were analyzed using the same boundary conditions. Velocity values were calculated from volumetric and mass flow rates given for each inlet in the third example of the patent, using density values for each inlet temperature (see Table A-1).

	Total flow rate	Temperature
CO	7.5 Nm^3/hr	400 °C
O$_2$	15 Nm^3/hr	750 °C
TiCl$_4$	87 kg/hr	500 °C

Table III-5: Boundary Conditions Given in Montecatini Patent 3,764,667, Example 3

	Boundary Type	Value	Temperature	Turb. Intensity	Length Scale
Inner CO Inlet	Velocity Inlet	8.41 m/s	673 K	5%	0.87 mm
Outer CO Inlet	Velocity Inlet	8.41 m/s	673 K	5%	0.19 mm
Inner O$_2$ Inlet	Velocity Inlet	20.51 m/s	1023 K	5%	0.13 mm
Middle O$_2$ Inlet	Velocity Inlet	20.51 m/s	1024 K	5%	0.19 mm
Outer O$_2$ Inlet	Velocity Inlet	20.51 m/s	1025 K	5%	0.14 mm
TiCl$_4$ Inlet	Velocity Inlet	37.27 m/s	773 K	5%	0.14 mm

Table III-6: Boundary Conditions Used with FLUENT Simulations of Montecatini Patent 3,764,667

The patent does not specify a TiCl$_4$ supply ratio, but does specify a velocity range of 10-40 m/s for O$_2$ and 20-120 m/s for TiCl$_4$. Stoichiometric ratio is 2.762:1, inlet velocity of TiCl$_4$ vs. inlet velocity of O$_2$. Assuming complete CO combustion, the required TiCl$_4$ vs. O$_2$ velocity ratio for stoichiometric reaction is 1.81:1. The boundary conditions given in the example are almost exactly stoichiometric (1.84:1).

All the reactor walls were assumed to be adiabatic. This is done for simplification purposes, and also because the reactor material and cooling methods are not specified in the patent. The reactor model was given a length of 200 mm for the 12-20° tapers, 250

mm for the 8° taper, and 300 mm for the 4° taper. These are all shorter than the 800 mm specified in the patent, because trial runs showed that the great majority of the $TiCl_4$ oxidation occurs immediately downstream from the $TiCl_4$ inlet. This makes the region a great distance downstream of little interest, as this is a region designated for particle growth, which is not modeled in this work.

In addition to claims on configuration and flow rate ranges within the patent, it is also claimed that the $TiCl_4$ inlet protrudes into a zone of the reaction chamber where "only oxygen and carbon dioxide are present" (Montecatini 1973). This claim is investigated in this work, though only for validation of the combustion model.

Analysis of Cabot Patent # 3,351,427

This patent, previously discussed in chapter II, was selected for primarily the same reason as the Montecatini patent. It also does not employ any inert gas, rather using tangential flow of the product mixture through the reaction chamber to sweep the walls of deposit. This reactor operates under an excess of oxygen (ideal outlet mole fraction for example in the patent: 15.2%), the significance of which will be examined in chapter IV. The GAMBIT geometry for the reactor is shown in Figures III-7. CO enters through the outer frustum, the $TiCl_4/O_2$ mixture enters through the middle frustum, and they meet at the top of the apparatus. (The multiple rings at the top of the geometry in Figure III-7 are the edges of individual volume elements, created to allow a high node density at the top of the reactor. This is for better visualization at that zone, where the reactants meet.) This is very different from the Montecatini patent, as the combustion and oxidation reactions are intentionally occurring in the same space. The inner cone is the reaction tube.
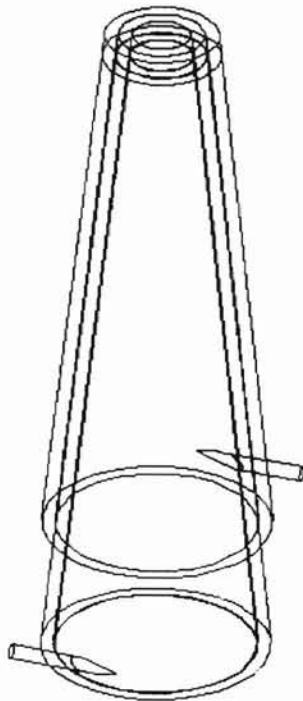
39

Figure III-7: GAMBIT Geometry of Cabot Patent 3,351,427

To develop the geometry and perform the simulations, several assumptions were made:

1. The reactor is adiabatic. This is a large simplification, and was done for two reasons. First, the addition of a heat transfer calculation for the reactor wall led to divergence in the iteration process. Second, temperatures above ~500 K tend to trigger the reaction of $TiCl_4$ and O_2. Allowing heat transfer would initiate the reaction before the mixture reached the flame front.

2. The inlet temperature of the mixture was set to 400 K. This was done for the reason mentioned in assumption one, and also because it was found that, because of the large amount of CO present, non-preheated reactants do not

extinguish the flame. A temperature of 400 K is an approximation based off mixing of O_2 at 298K and reboiled $TiCl_4$ at 588 K (600 °F), at a 0.27:1 molar ratio of $TiCl_4$ to O_2.

3. The walls are approximated as near-zero width. (Width = 0.01 in.)

4. For simplification, the tangential inlets are set to 1/16" in diameter, same as the width of the annuli.

5. The gap between the top of the inner cone and the enclosed top of the outer cone is set to 0.1". This is an estimate based off the schematic included in the patent (Figure II-2).

6. Inflowing CO is at standard temperature and pressure.

The patent's only variable parameter is the claim that the linear velocity of the reacting mixture as it enters the reaction zone is between 75 and 350 ft/s (Cabot 1963). The reason given for this requirement is that below 75 ft/s, deposition of TiO_2 on the reactor wall was found to occur, and above 350 ft/s, the flame became unstable. As will be shown in chapter IV, the patent's sole example gives a velocity of 184.4 ft/s.

To observe the effects of increased reactant flow rate on tangential velocities within the reactor chamber, the flow rate of $TiCl_4$ was doubled and then tripled in separate simulations. Accordingly, the oxygen flow rate was increased to a value that would double and triple the excess amount, while still retaining the necessary stoichiometric amount for CO combustion. Conversely, to examine the lower limits of the recommended flow rate, the $TiCl_4$ flow rate of the example was cut fivefold and tenfold. The boundary conditions from the patent's example are shown in Table III-7; the boundary conditions used in the simulations are shown in Table III-8.

41

	TiCl$_4$	O$_2$	CO
Flow Rate (s.c.f.h.)	25	100	100
Temperature	Unspecified	Unspecified	Unspecified

Table III-7: Boundary Conditions Given in Cabot Patent 3,351,427 Example

0.1x TiCl$_4$ Flow in Example	Rate/Composition	Temp.	Turb. Int.	Length Scale
Reactant Inlet	0.592 kg/h TiCl$_4$, 2.004 kg/h O$_2$	400 K	5%	0.004375 in.
Comb. Gas Inlet	3.181 kg/h CO	298 K	5%	0.004375 in.
0.2x TiCl$_4$ Flow in Example				
Reactant Inlet	1.184 kg/h TiCl$_4$, 2.19 kg/h O$_2$	400 K	5%	0.004375 in.
Comb. Gas Inlet	3.181 kg/h CO	298 K	5%	0.004375 in.
1x TiCl$_4$ Flow in Example				
Reactant Inlet	5.91 kg/h TiCl$_4$, 3.689 kg/h O$_2$	400 K	5%	0.004375 in.
Comb. Gas Inlet	3.181 kg/h CO	298 K	5%	0.004375 in.
2x TiCl$_4$ Flow in Example				
Reactant Inlet	11.84 kg/h TiCl$_4$, 5.542 kg/h O$_2$	400 K	5%	0.004375 in.
Comb. Gas Inlet	3.181 kg/h CO	298 K	5%	0.004375 in.
3x TiCl$_4$ Flow in Example				
Reactant Inlet	17.76 kg/h TiCl$_4$, 7.405 kg/h O$_2$	400 K	5%	0.004375 in.
Comb. Gas Inlet	3.181 kg/h CO	298 K	5%	0.004375 in.

Table III-8: Boundary Conditions Used in FLUENT Simulations of Cabot Patent
3,351,427

As for all examples, physical properties and calculation techniques are detailed in

appendix A. Initial runs using kinetic theory to calculate viscosity and thermal

conductivity with Lennard-Jones parameters did not converge, so constant values were

calculated for these, based off inlet temperatures for reactants, and reaction temperatures

for products. (They are tabulated in Table A-5.) This is a reasonable assumption, as the

eddy dissipation reaction model assumes that mixed reactants react immediately.

CHAPTER IV:

RESULTS OF CFD MODELING

Introduction

This chapter contains information gained from computational fluid dynamic (CFD) modeling of three separate patented titanium dioxide (TiO_2) reactors from Cabot Corporation (1967), Kronos Corporation (1993), and Montecatini Edison (1973). The data are analyzed to first evaluate whether the CFD results agree with the claims of the patent. The effect of variable parameters on the performance of the reactors is examined, and the optimum value for each is determined.

While data taken from FLUENT simulation that is directly pertinent to analysis of variable parameters is included in this chapter, there is additional data located in appendix B that illustrate various factors in the reactors' performance.

Analysis of CFD Data for the Kronos Reactor

For each of the three sets of reactant inlets analyzed, the following criteria were used, upon which the strength of each configuration was based:

1. Does the inlet configuration eliminate backflow, specifically the backflow of TiO_2 product?

2. Does the inlet configuration provide adequate and even mixing to give 100% reactant conversion and consistent particle size?

3. In the O_2 annulus, is the Reynolds number (Re) between 15,000 and 20,000 as the patent states (Kronos 1993)? (For all configurations.)

The first criterion was the easiest to determine, as evaluation of contours of TiO_2 mole fraction tell the story best.

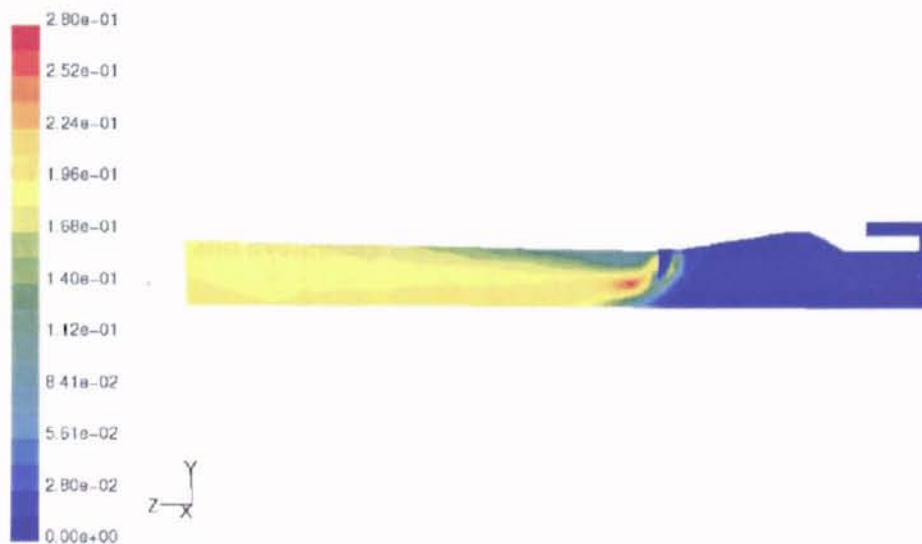Figure IV-1: TiO_2 Mole Fraction Contour for 2 Symmetric $TiCl_4$ Inlets

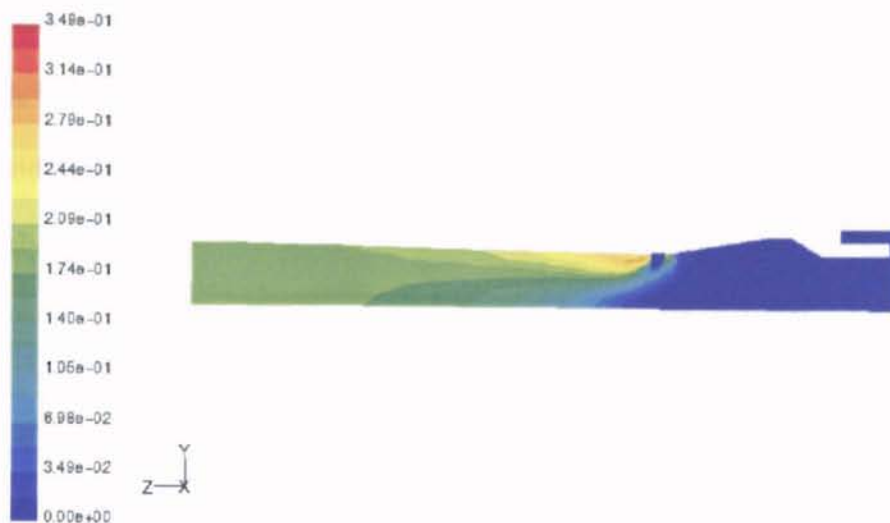Figure IV-2: TiO_2 Mole Fraction Contour for 4 Symmetric $TiCl_4$ Inlets

44

Figure IV-3: TiO$_2$ Mole Fraction Contour for 8 Symmetric TiCl$_4$ Inlets

As the previous figures and the following table (Table IV-1) illustrate, the optimum

number of inlets appears to be two, for two reasons. First, the higher velocity of the

TiCl$_4$ exiting the duct results in a collision and eddying of the two streams at the middle

of the reaction tube. This channels oxygen towards this high-shear area, allowing for

more controlled mixing, and flatter downstream concentration profile. (Compare Figure

IV-1 to Figures IV-2 and IV-3). Secondly, the high velocity pushes the TiCl$_4$ away from

the area of the reactor wall immediately downstream from the inlet. This lowers the

possibility of crusting and eventually blockage of the inlet. Figures B-12 through B-20,

in Appendix B, detail the radial TiO$_2$ concentration profiles immediately upstream and

downstream from the TiCl$_4$ inlets.

In terms of the first criterion, what Table IV-1 shows is that due to the high

velocity of the TiCl$_4$ exiting the two inlets, there is little diffusional transport or mixing,

so the bulk of the reaction occurs farther downstream. Figure IV-7, when compared to

Figures IV-8 and IV-9 also indicates this very clearly. When examining these, note that

the upstream end of the TiCl$_4$ spool is located at $z = 1.025$ m. Number if inlets, and in turn, TiCl$_4$ boundary velocity, are directly proportional to the highest downstream mole fraction and the radial location of the highest mole fraction. (R^2=0.9703 and R^2=0.9934, respectively.)

Number of Inlets	Downstream Radial Coordinate	Upstream Radial Coordinate	Downstream High Mole Fraction	Upstream High Mole Fraction
2	0 mm	172.0 mm	0.123	0.017
4	96.9 mm	189.5 mm	0.238	0.112
8	239.0 mm	241.4 mm	0.360	0.288

Table IV-1: Radial Coordinates of Highest TiO$_2$ Mole Fractions Upstream/Dowstream from TiCl$_4$ Inlets

The second criterion is determined from two separate values: the location and value of the highest reaction rate (Figures IV-4 through IV-6), and the outlet mole fraction of TiO$_2$ monomer (Figures IV-7 through IV-9). Ideal outlet mole fractions at 100% conversion should be the following: 14.7% TiO$_2$, 29.4% Cl$_2$, 53.5% O$_2$, 0.9% H$_2$O, 1.5% CO$_2$.
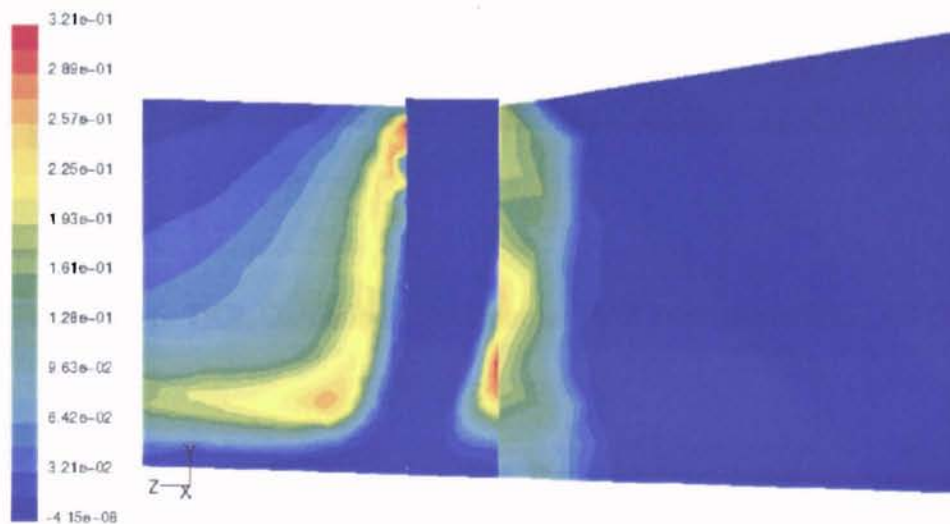
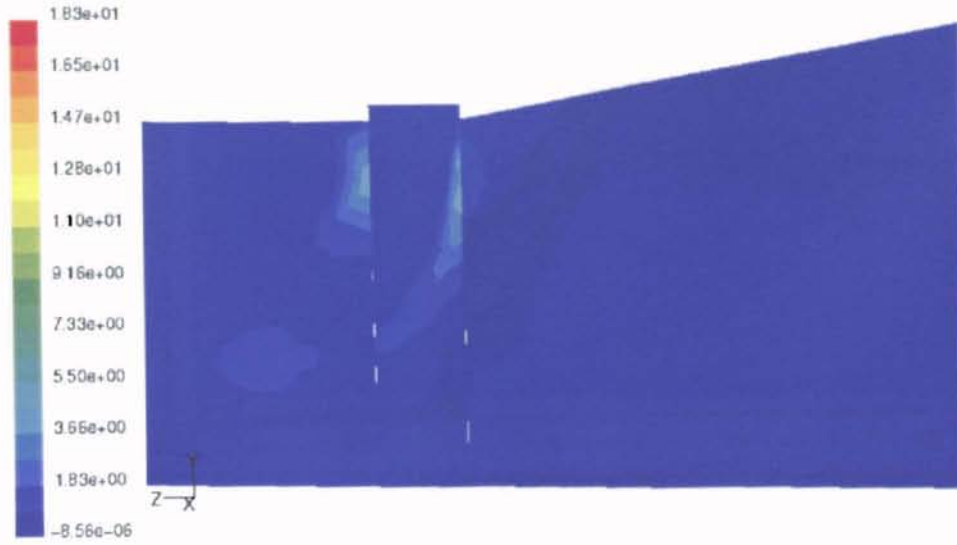Figure IV-4: TiCl$_4$ Oxidation Rate Contour for 2 Symmetric TiCl$_4$ Inlets

Figure IV-5: TiCl$_4$ Oxidation Rate Contour for 4 Symmetric TiCl$_4$ Inlets

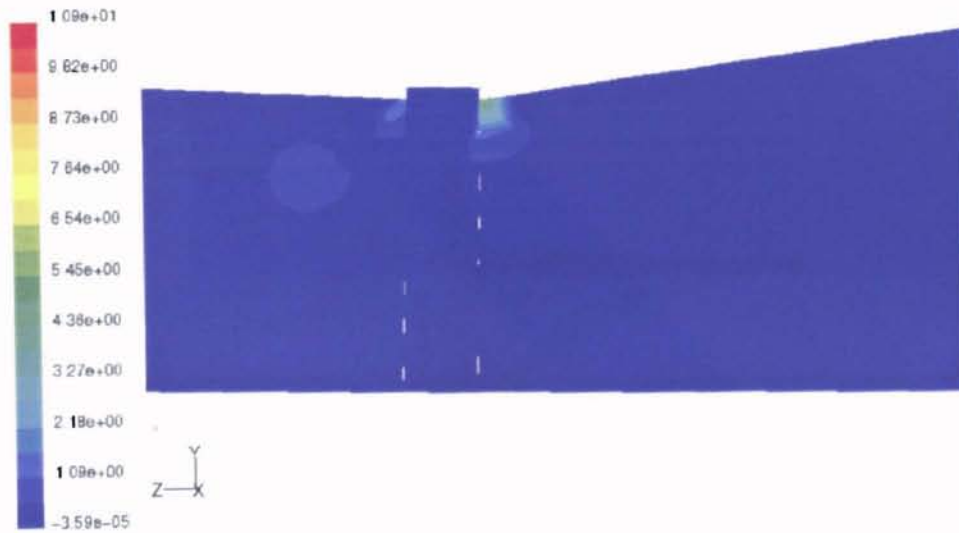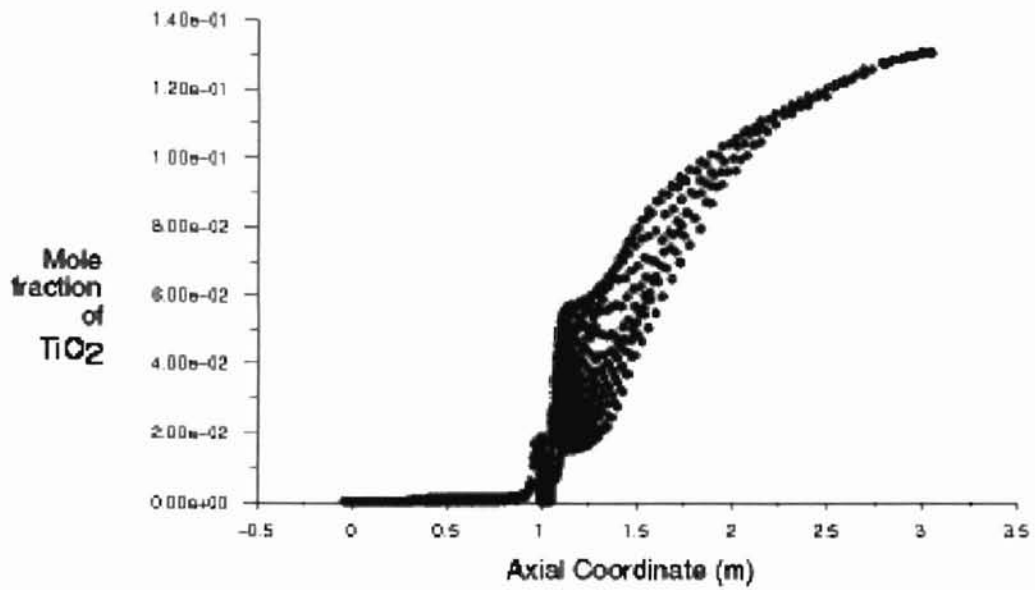Figure IV-6: TiCl$_4$ Oxidation Rate Contour for 8 Symmetric TiCl$_4$ Inlets

Figure IV-7: TiO_2 Mole Fraction vs. Axial Coordinate for 2 Symmetric $TiCl_4$ Inlets
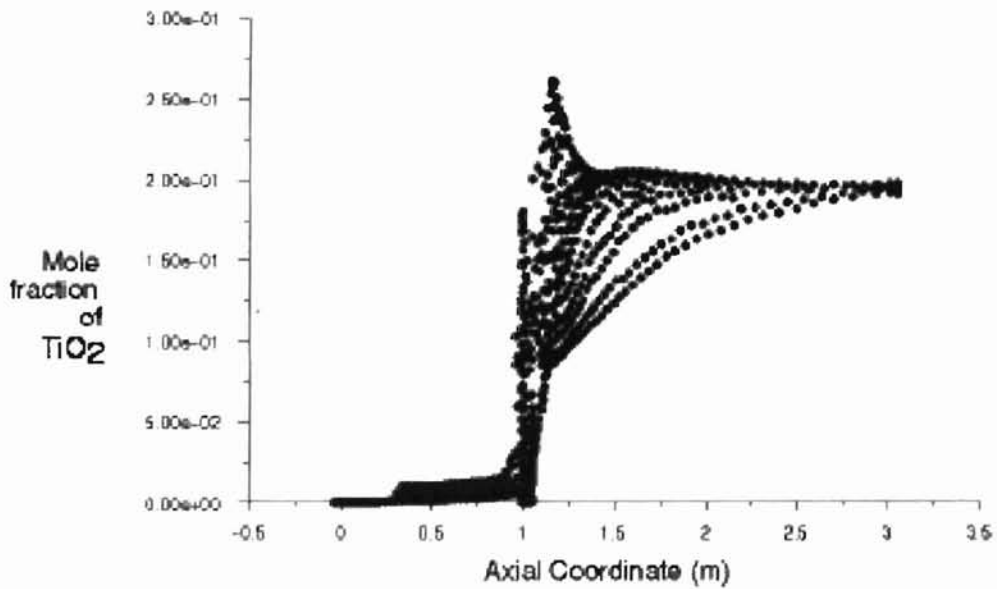
Figure IV-8: TiO_2 Mole Fraction vs. Axial Coordinate for 4 Symmetric $TiCl_4$ Inlets
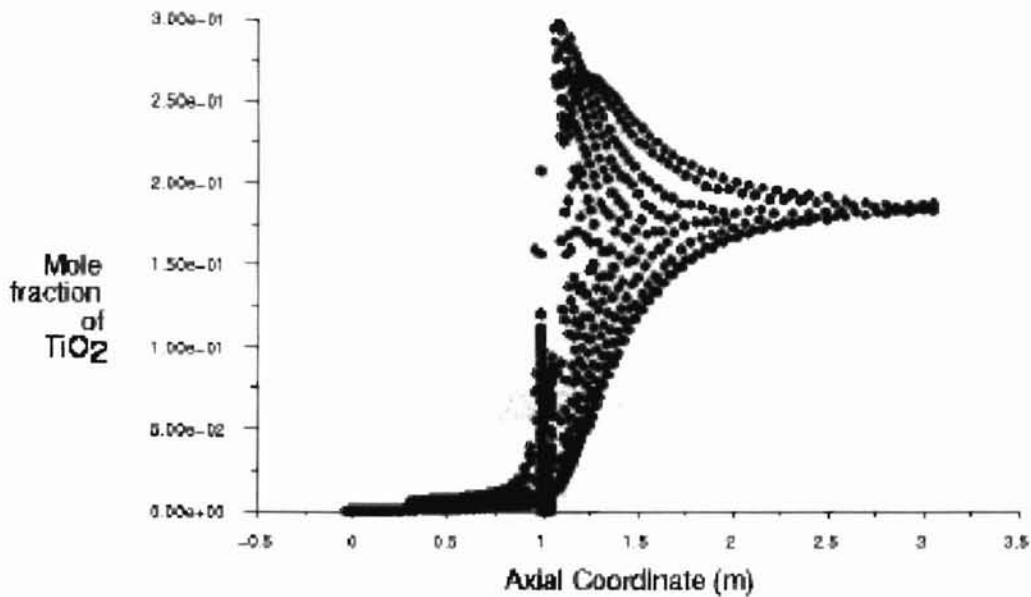
48

Figure IV-9: TiO₂ Mole Fraction vs. Axial Coordinate for 8 Symmetric TiCl₄ Inlets

Again, the two inlet configuration appears to give the optimum results. The radial mole fraction profile of TiO_2 is tight throughout the distance of the reactor, which translates to consistent particle size. The reason the 4 and 8 inlet configurations do not perform to this standard relates to the great density gap between $TiCl_4$ and O_2 (see appendix A, Table A-2). Figures IV-8 and IV-9 also show a mole fraction higher than ideal for TiO_2. This is because a large part of the completely reacted mixture is made up of Cl_2, at a 1.8:1 mass ratio to TiO_2, a mole fraction of TiO_2 higher than 14.7% says the $TiCl_4$ has not completely reacted. The high inlet velocity of the $TiCl_4$ in the 2 inlet reactor results in contact between the opposing $TiCl_4$ streams, whereby they are dispersed radially, perpendicular to their inlet direction. The dispersed $TiCl_4$ reacts quickly, as is evidenced by the high reaction rate behind the inlets at the centerline (Figure IV-4). The 4 and 8 inlet cases do not have a $TiCl_4$ inlet velocity sufficient for the streams to collide. Figures IV-10 through IV-12 below illustrate this, as well.
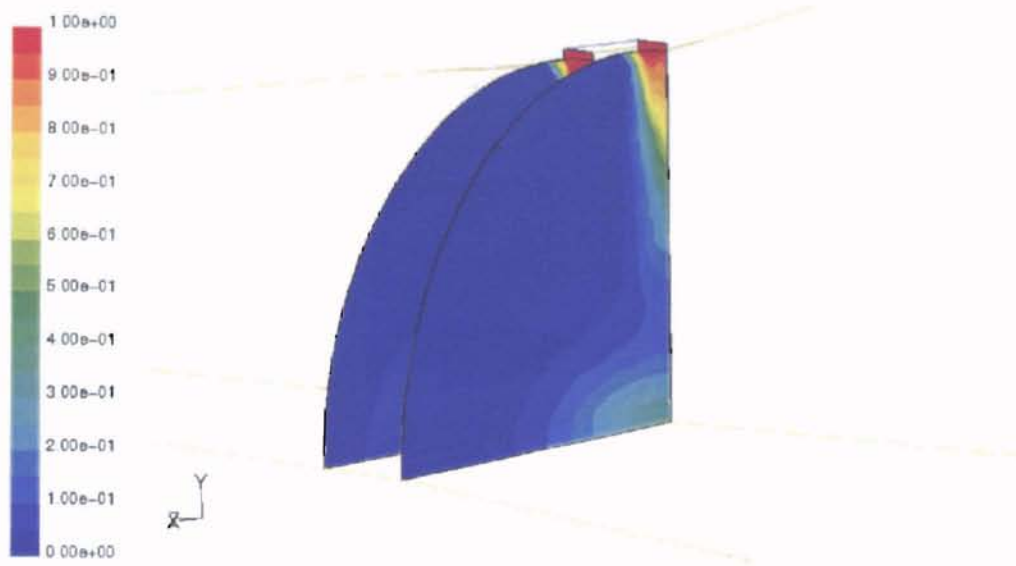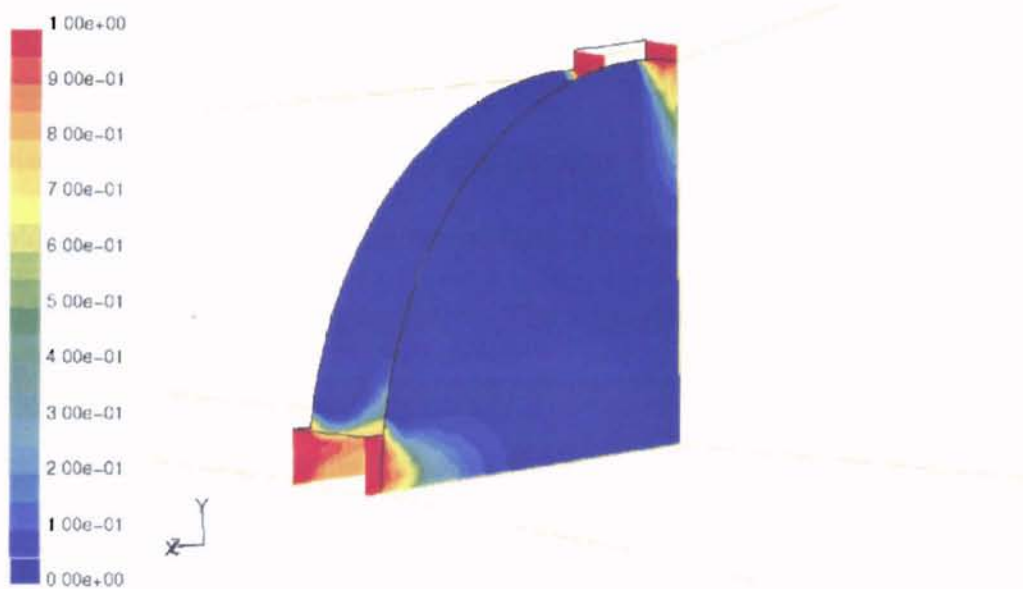
49

Figure IV-10: TiCl$_4$ Mole Fraction Contours at the Front and Back of the Inlet Spool for 2 Symmetric Inlets

Figure IV-11: TiCl$_4$ Mole Fraction Contours at the Front and Back of the Inlet Spool for 4 Symmetric Inlets
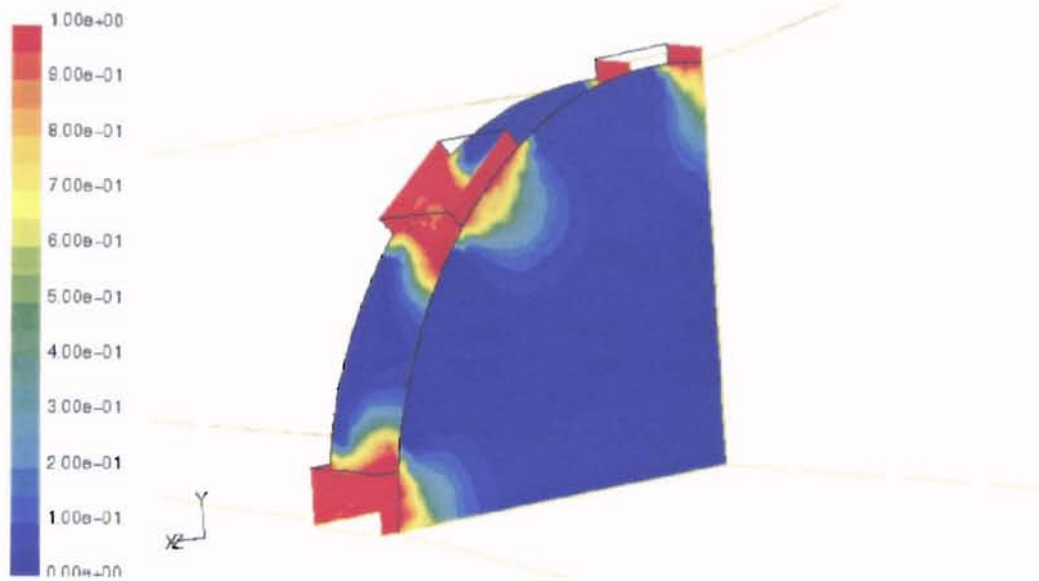
50

Figure IV-12: TiCl₄ Mole Fraction Contours at the Front and Back of the Inlet Spool for 8 Symmetric Inlets

To answer the third question, whether the Reynolds number is between 15,000-20,000 in the O_2 annulus, the boundary conditions (V=101 m/s, T=1223 K) were used to calculate ρ and μ. Density was calculated via linear interpolation from the data in Table B-2; viscosity was calculated via Chapman-Engskog method. (See appendix A.) The Reynolds number was calculated as $Re=\rho VD/\mu$. The result was an extremely high value, more than 5x the value given in the patent. The Reynolds number at the point where the O_2 annulus meets the reaction chamber was calculated using simulation values for physical properties, to determine if an error was made in the patent. Because of turbulent backmixing at that point, the number ranged from $0-10^7$. All three values (in the O_2 annulus, high value at the end of the annulus, and low value at the end of the annulus) are shown in Table IV-2. The properties used to calculate Re at the annulus are shown in Figures IV-13 through IV-15, which are all views looking upstream toward the O_2

annulus. All three inlet configurations should have identical velocity profiles at the back

of the reactor, so the 2 inlet case is used here.

	D (m)	ρ (kg/m^3)	μ (kg/m-s)	V (m/s)	Re
In O$_2$ Annulus	0.06	1	2.17E-05	1.01E+02	279263
At Back of Preheat Zone (High V)	0.48	0.885	2.17E-05	56.7	1109961
At Back of Preheat Zone (Low V)	0.48	0.885	2.17E-05	0	0

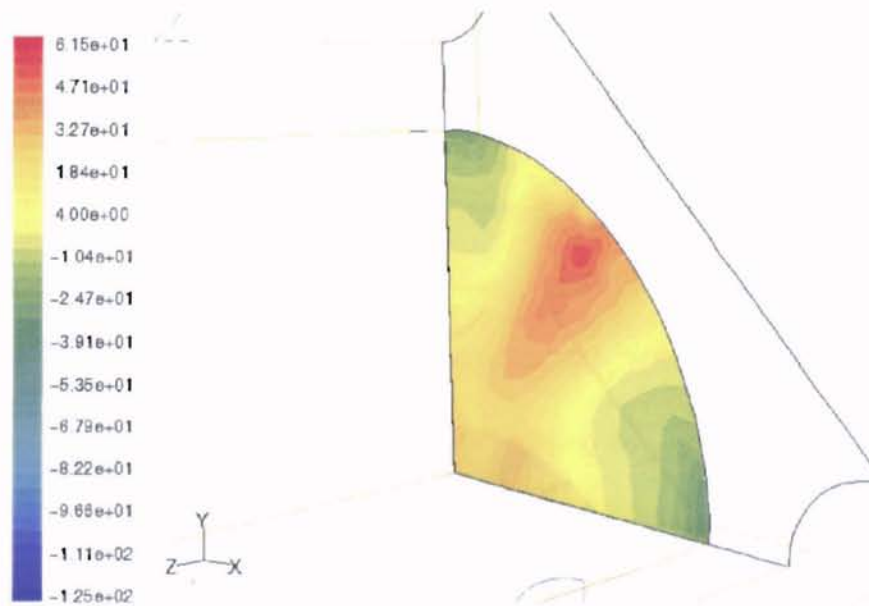Table IV-2: *Re* for Different Zones of the O$_2$ Annulus (2 Inlet Case)

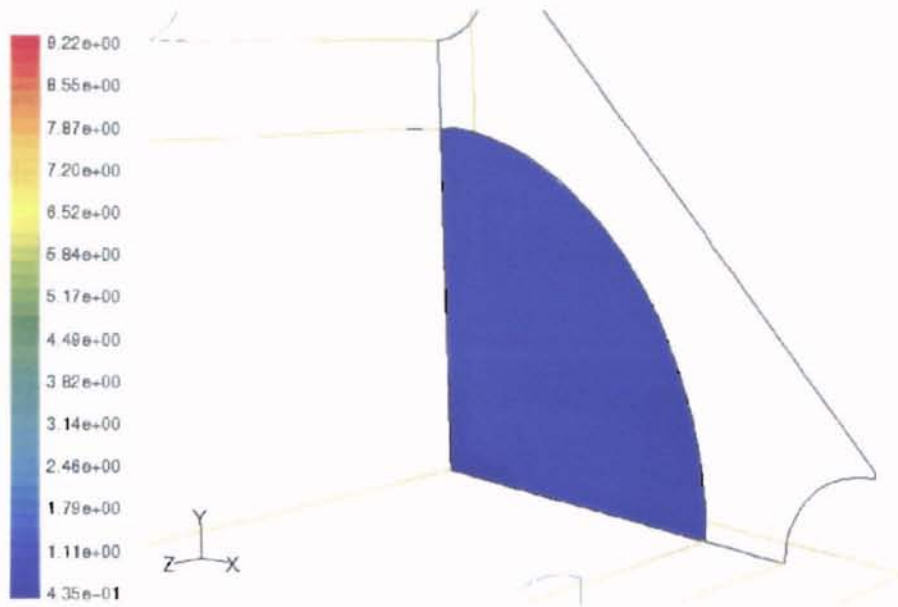Figure IV-13: Axial Velocity Contours at the Front End of the O$_2$ Annulus (2 Inlet Case)

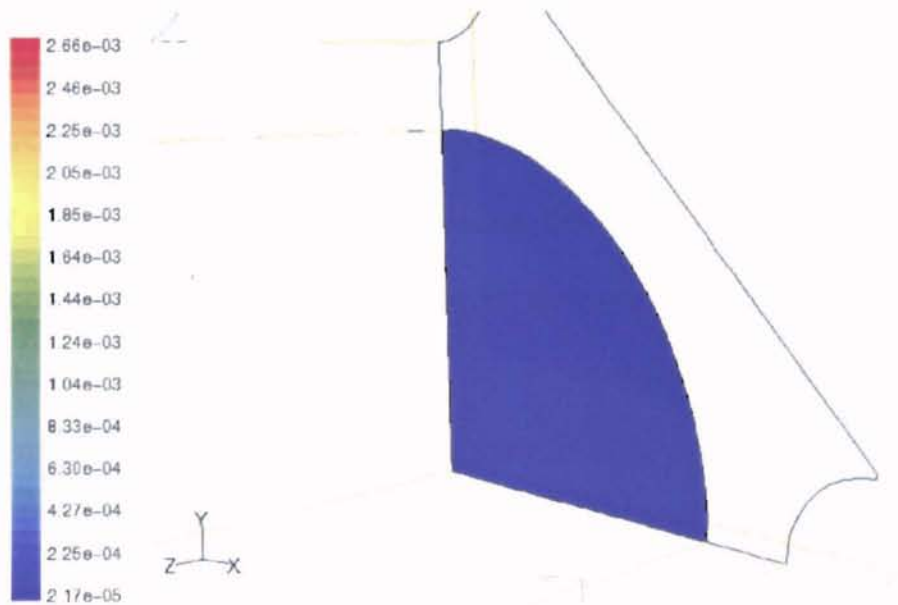Figure IV-14: Density Contours at the Front End of the O_2 Annulus (2 Inlet Case)

Figure IV-15: Axial Velocity Contours at the Front End of the O_2 Annulus (2 Inlet Case)

Analysis of CFD Data for the Montecatini Reactor

For the five different titanium chloride ($TiCl_4$) inlet geometries of the dimensions in Table III-4, three questions were asked:

1. Does the oxidation reaction occur far enough downstream to feasibly avoid crusting on the $TiCl_4$ inlet?

2. Does the reaction occur far enough away from the outer reactor wall to avoid surface reaction or coagulation there?

3. Do the reactants mix well enough, and evenly enough, to ensure 100% conversion and consistent particle size?

After performing FLUENT runs with each configuration, contours of $TiCl_4$ oxidation rate for each were examined. Figures IV-16 through IV-20 are close-ups of these contours. The patent's merits are immediately apparent, as the reaction zone is removed from the $TiCl_4$ entrance by a small distance that grows visibly larger by the $\theta=8°$ configuration. Conversely, the distance between the reaction zone and the reactor's outer wall (the left side of the figure) grows smaller as θ gets smaller. What is not apparent here is how large a distance must be between the reaction zone and a growth surface to avoid deposition. The one certainty is that having the zone of highest reaction rate immediately on the nozzle or wall will lead to surface reaction on it.
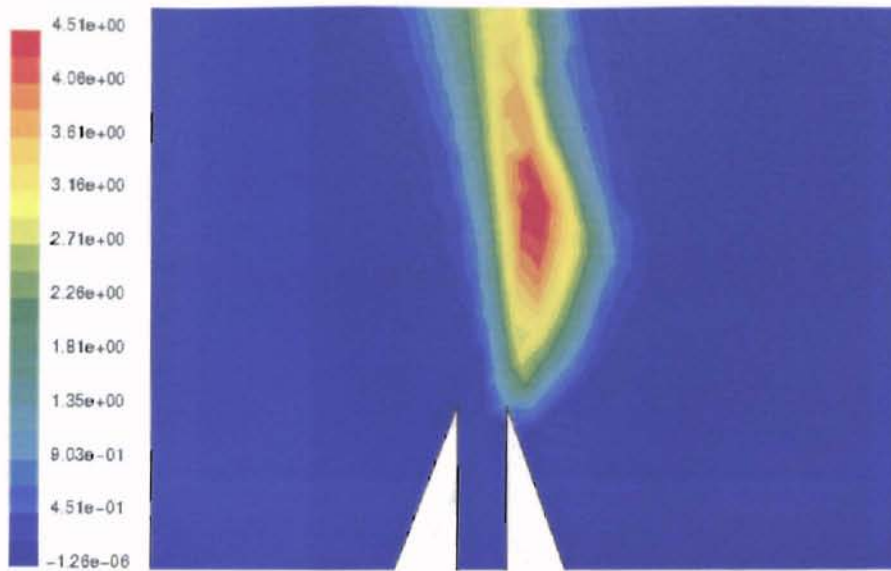
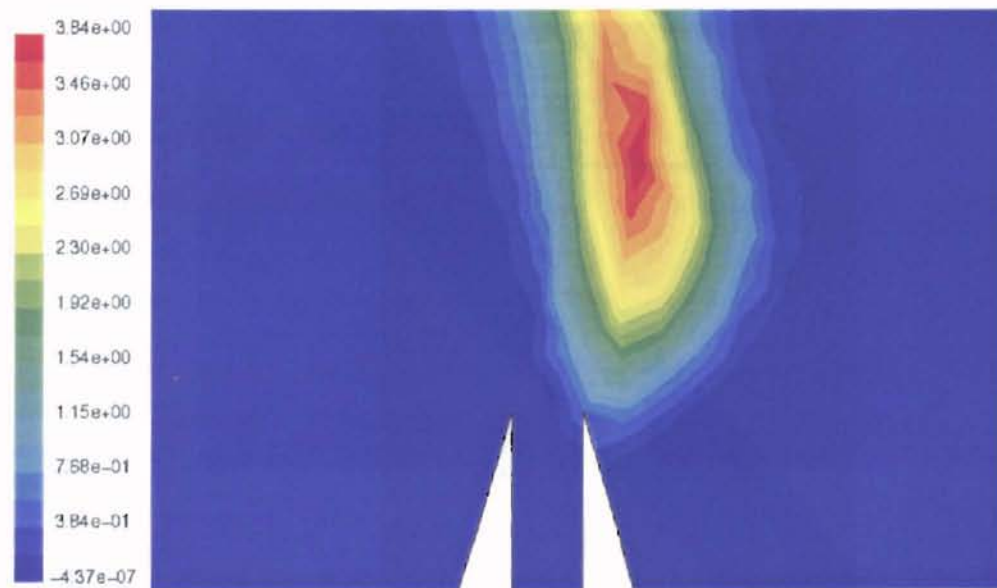Figure IV-16: Reaction Rate Contour for $\theta = 20°$ (kgmol/s)

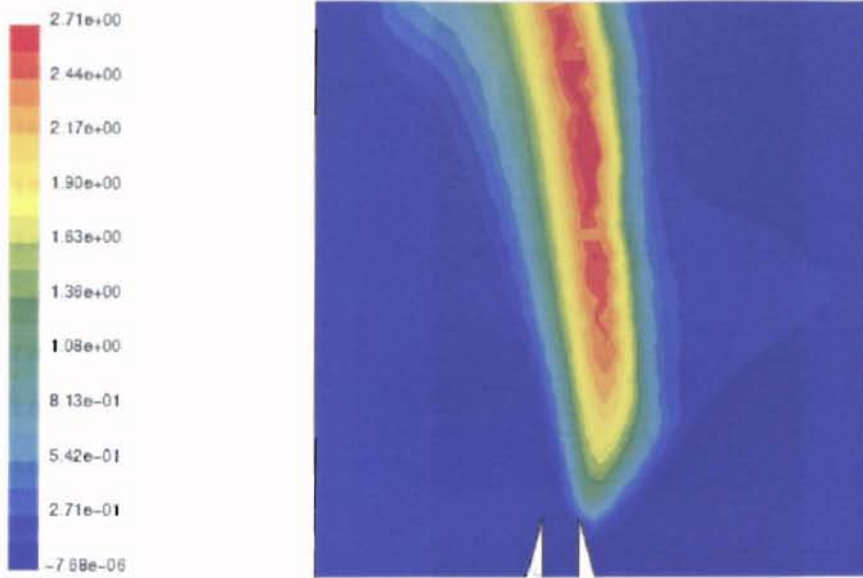Figure IV-17: Reaction Rate Contour for $\theta = 16°$ (kgmol/s)

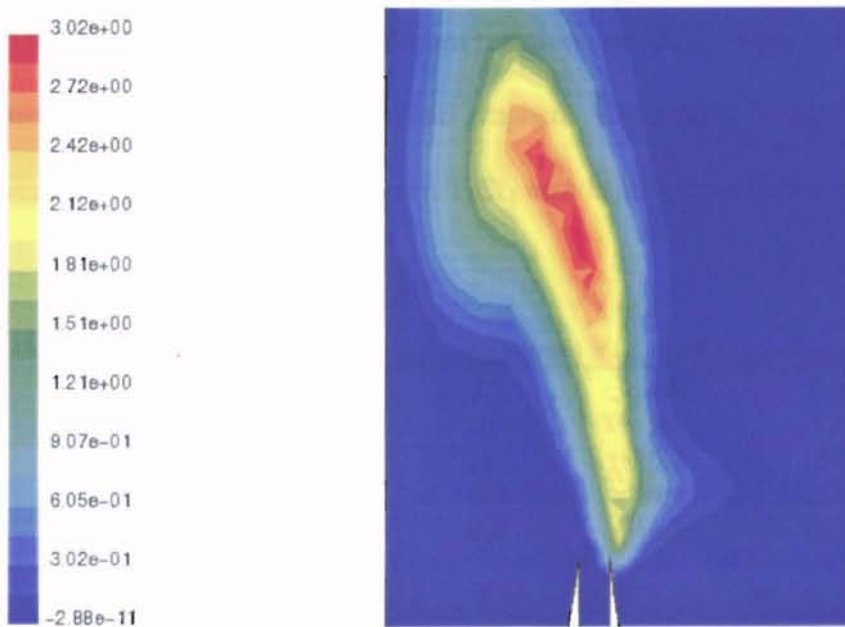Figure IV-18: Reaction Rate Contour for $\theta = 12°$ (kgmol/s)

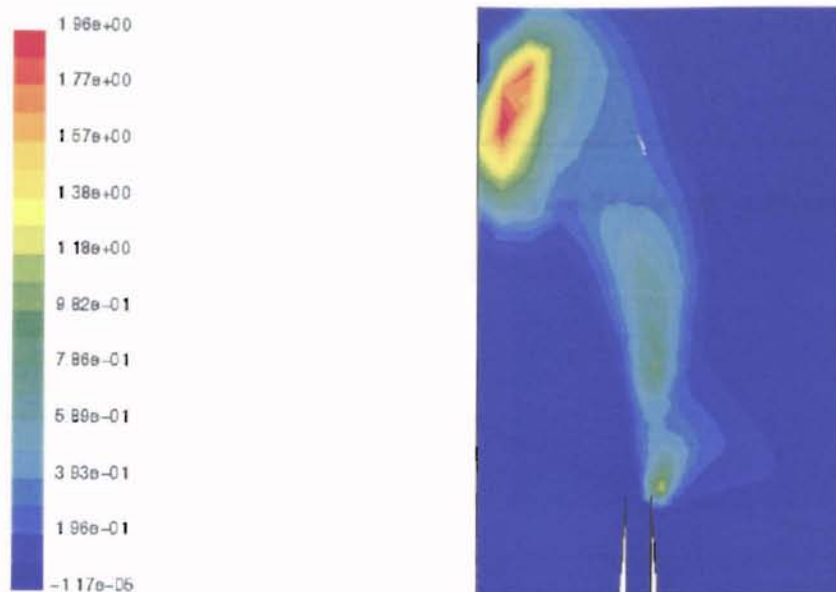Figure IV-19: Reaction Rate Contour for $\theta = 8°$ (kgmol/s)

56

Figure IV-20: Reaction Rate Contour for $\theta = 4°$ (kgmol/s)

The r and z values of the maximum reaction rate (R_{max}) were determined for each configuration, and the data tabulated and graphed. The graphs (Figure IV-21 through IV-23) reveal a direct relationship between $TiCl_4$ nozzle length and reaction "hot spot".

θ (degrees)	z_{inlet} (mm)	z_{Rmax}-z_{inlet} (mm)	r_{Rmax} (mm)	r_{wall} - r_{Rmax} (mm)
4	103.2	31	28.2	2.8
8	61.9	20.8	18	13
12	48.1	14.9	15.7	15.3
16	41.3	6.8	14.5	16.5
20	36.9	7.8	14.9	16.1

Table IV-3: Location of R_{max} Within Each Reactor Configuration

57

$$z = 5.74 \, (\sin (\theta))^{-1} + 21.1 \text{ mm}$$
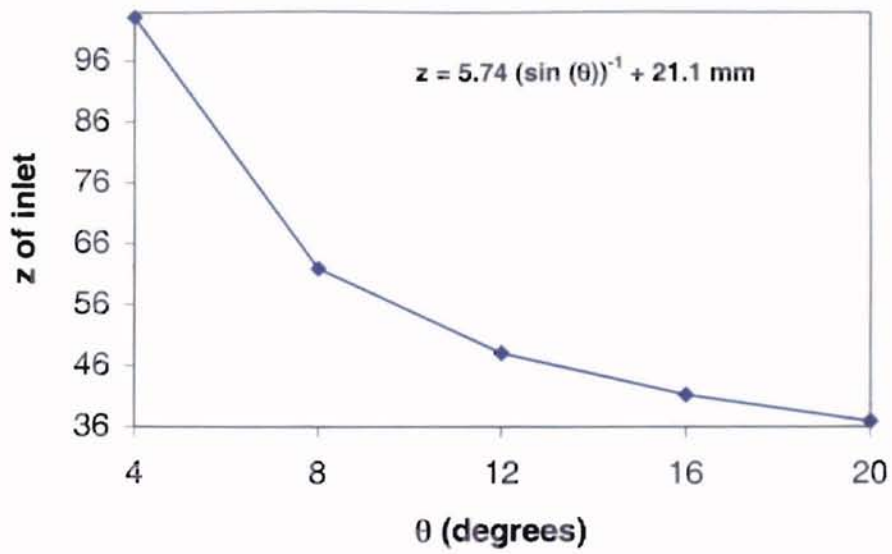
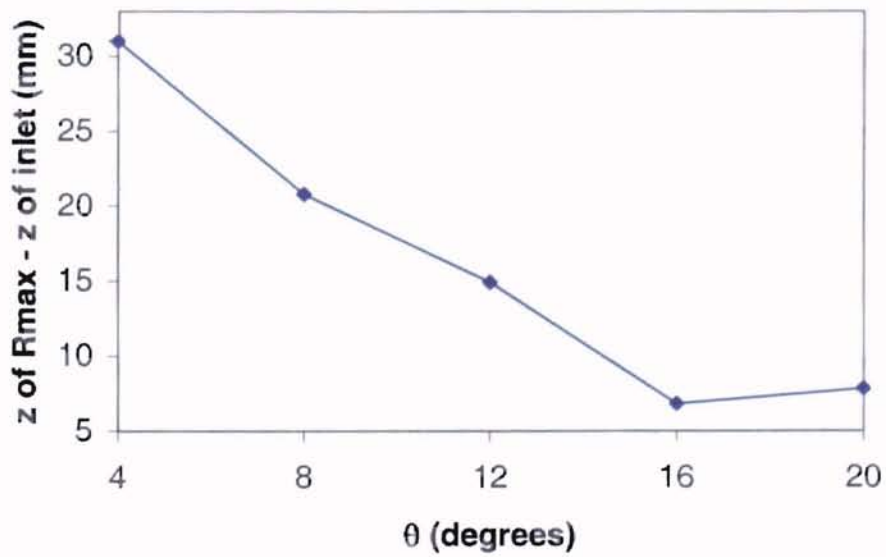Figure IV-21: Total length of $TiCl_4$ inlet vs. θ (with formula)

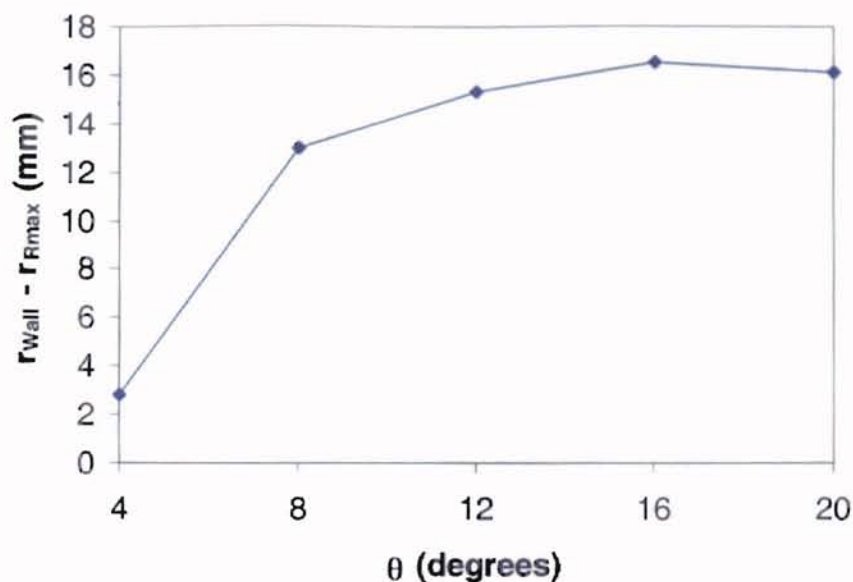Figure IV-22: Axial Distance from End of $TiCl_4$ Inlet to R_{max} Zone

Figure IV-23: Radial Distance from the Wall to R_{max} Zone
(r_{wall}=30.5 mm)

The data shows that the optimum value for θ is near 8°, within the 4-20° range

recommended in the patent. As Figures IV-22 and IV-23 show, the reaction zone is

definitely away from both the $TiCl_4$ inlet and the reactor wall. The authors' assertion that

the $TiCl_4$ inlet must not protrude more than 0.6 times the reactor diameter beyond the CO

jets seems valid, as well, as the reaction takes place very near to the outer wall for the

θ=4° degree example in this work ($TiCl_4$ annulus protrusion = $1.35 \times$ reactor diameter).

The answer to the first two questions asked at the beginning of this section appears to

be "yes" for some $TiCl_4$ inlet shapes, and "no" for others. To answer the third question,

whether a uniform particle diameter can be achieved, the axial coordinate at which O_2

appeared fully, or as near to fully as achievable, consumed ($Z_{O2=0}$) was first determined.

This value was left to the author's discretion after examining diagrams of O_2 mole

fraction contours (Figures IV-24 through IV-28). The values are also tabulated and

graphed for each θ (Table IV-4 and Figure IV-29). Upon comparison with Figure IV-21,

59

what becomes obvious first is the direct relationship between θ and product mixing. This is due to the longer residence time of the oxygen before encountering the $TiCl_4$ stream, so it develops a flatter concentration profile.
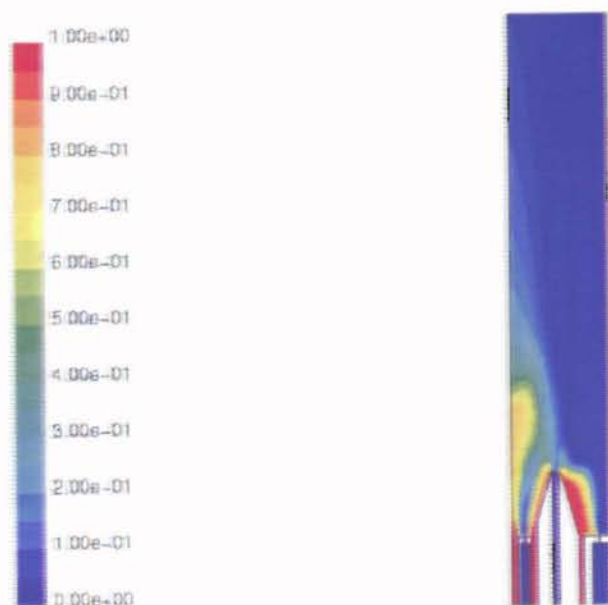

Figure IV-24: Mole Fraction of O_2 for $\theta=20°$
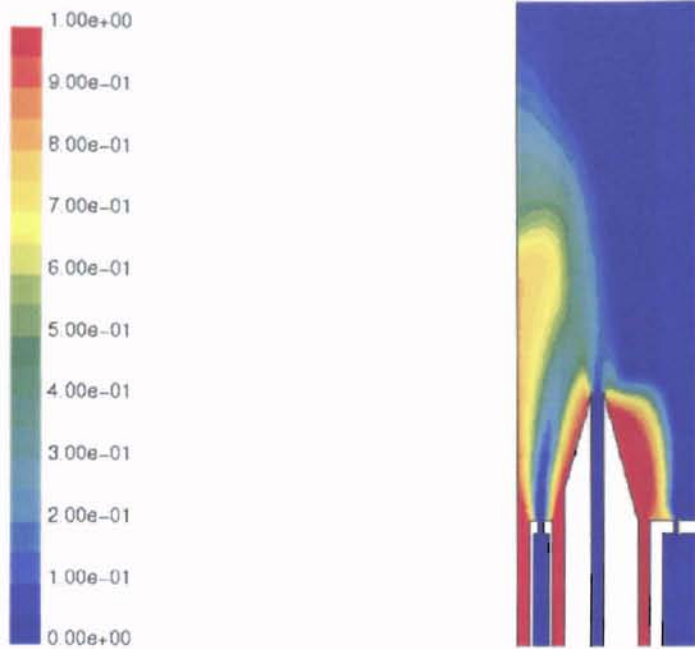

Figure IV-25: Mole Fraction of O_2 for $\theta=16°$

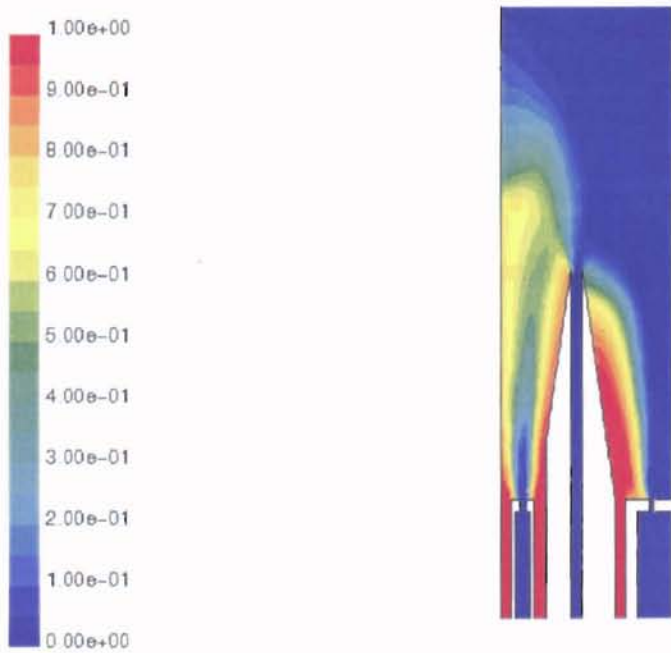Figure IV-26: Mole Fraction of O_2 for $\theta=12°$

Figure IV-27: Mole Fraction of O_2 for $\theta=8°$
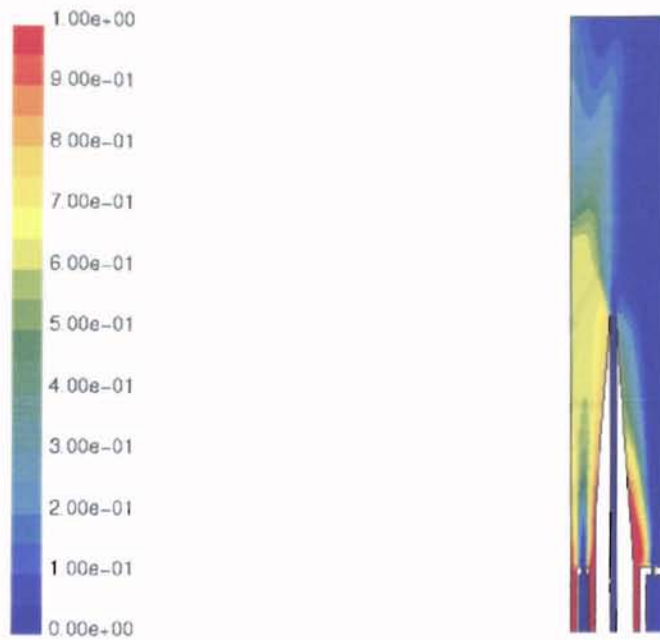
Figure IV-28: Mole Fraction of O_2 for $\theta=4°$

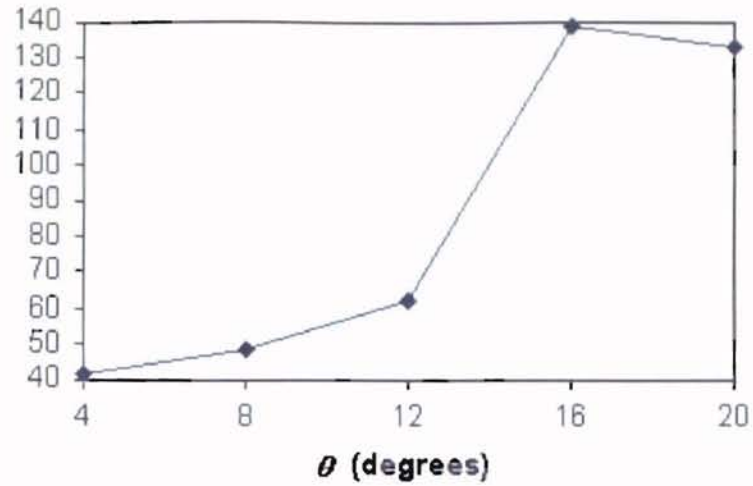| θ (degrees)	z_{inlet} (mm)	$z_{O2=0}$ (mm) - z_{inlet}
4	103.2	41.8
8	61.9	48.1
12	48.1	61.9
16	41.3	138.7
20	36.9	133.1

Table IV-4: Axial Coordinates of O_2 Exhaustion

Figure IV-29: Axial Distance from End of $TiCl_4$ Inlet to Point of O_2 Exhaustion

The following charts (Figure IV-30 through Figure IV-34) show the TiO_2 mole faction profile along $z_{O2=0}$. (NOTE: for these charts, calculated directly from FLUENT node values, "Position" corresponds to distance away from the reactor wall, with the centerline at 0.0305 m.)
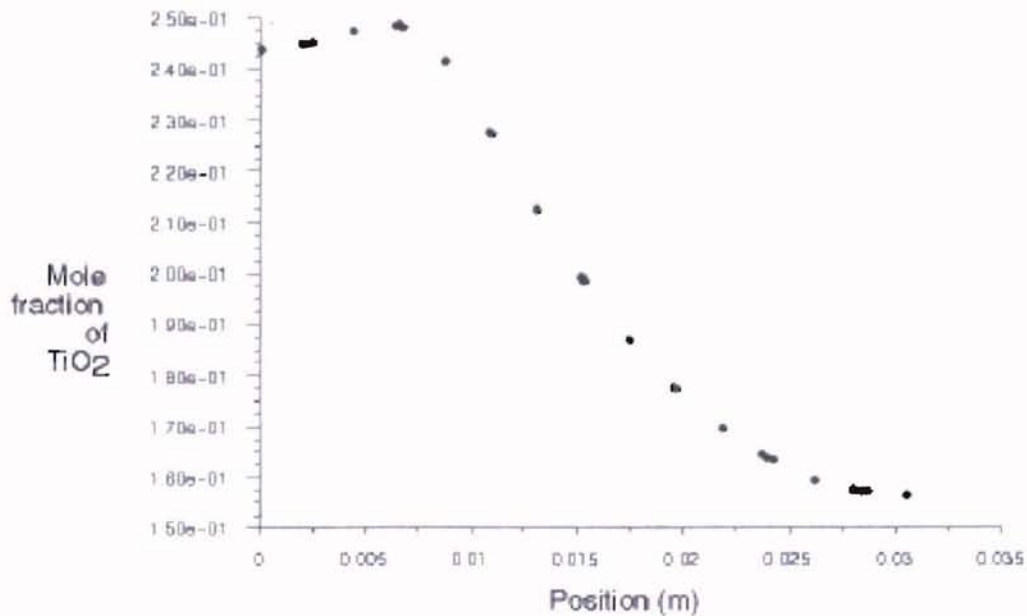

Figure IV-30: TiO_2 Mole Fraction at $z_{O2=0}$ for $\theta = 20°$

Figure IV-31: TiO$_2$ Mole Fraction at $z_{O2=0}$ for $\theta = 16°$

Figure IV-32: TiO$_2$ Mole Fraction at $z_{O2=0}$ for $\theta = 12°$
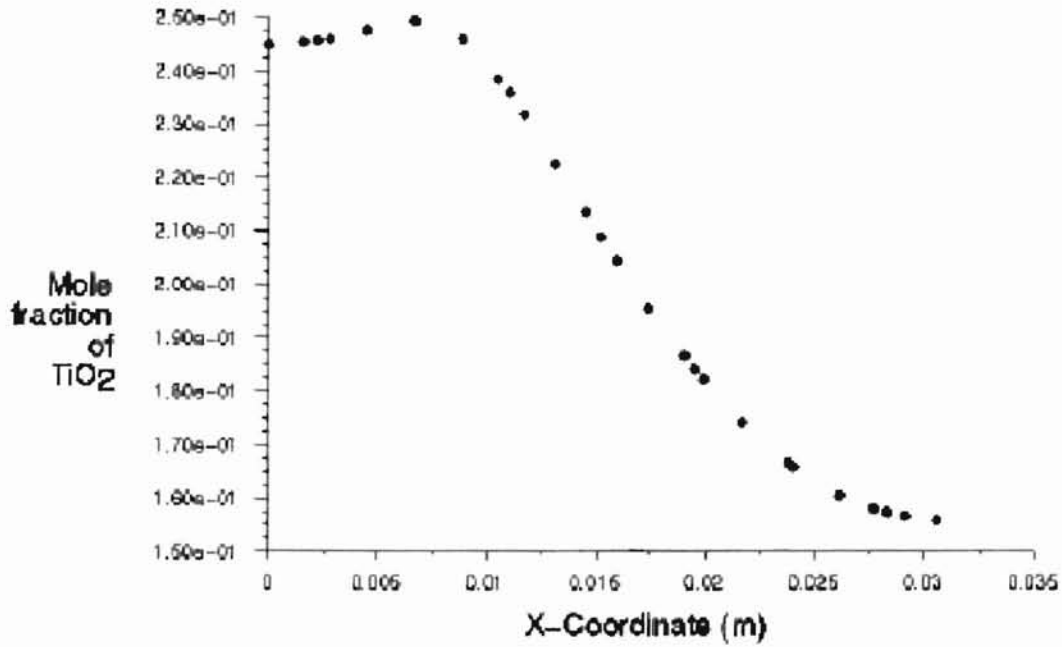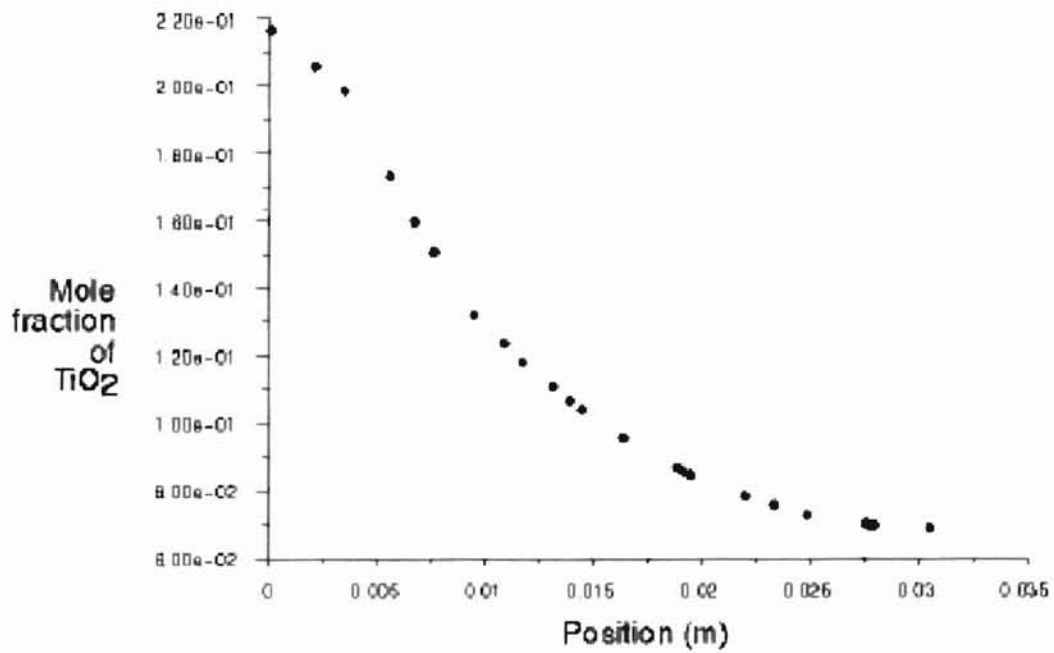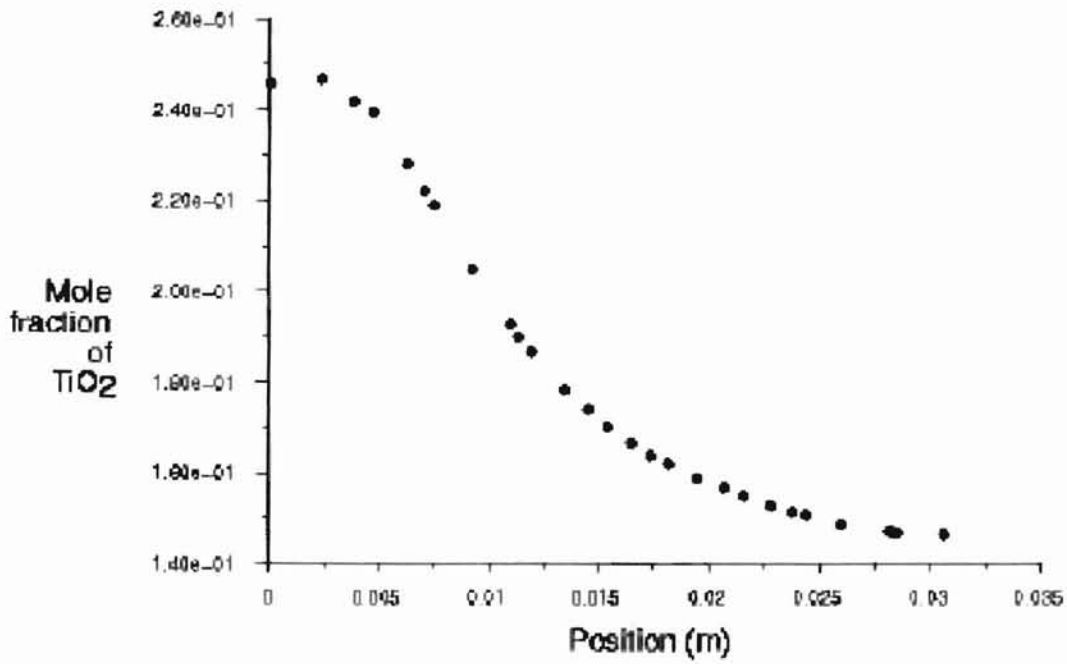
Figure IV-33: TiO_2 Mole Fraction at $z_{O2=0}$ for $\theta=8°$
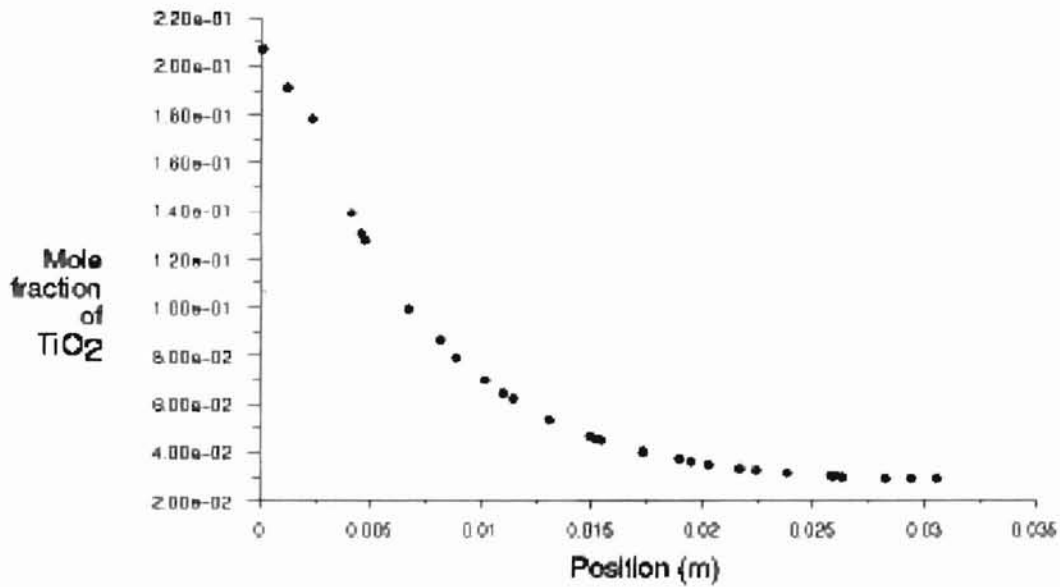
Figure IV-34: TiO_2 Mole Fraction at $z_{O2=0}$ for $\theta=4°$

The mole fractions of reactant and product for an ideal plug flow reactor with 100% conversion using the given boundary conditions are the following: 26.0% TiO_2, 52.0% Cl_2, 17.9% CO_2, and 4.1% O_2. It becomes apparent from examination of Figures

IV-30 through IV-34 that there is an inequity of reactants on the interior side of the

reactor. This is better clarified by diagrams of $TiCl_4$ mole fraction contours for each of

the configurations (Figures IV-35 through IV-39)

Figure IV-35: Mole Fraction of $TiCl_4$ for $\theta=20°$

Figure IV-36: Mole Fraction of $TiCl_4$ for $\theta=16°$

Figure IV-37: Mole Fraction of TiCl$_4$ for θ=12°
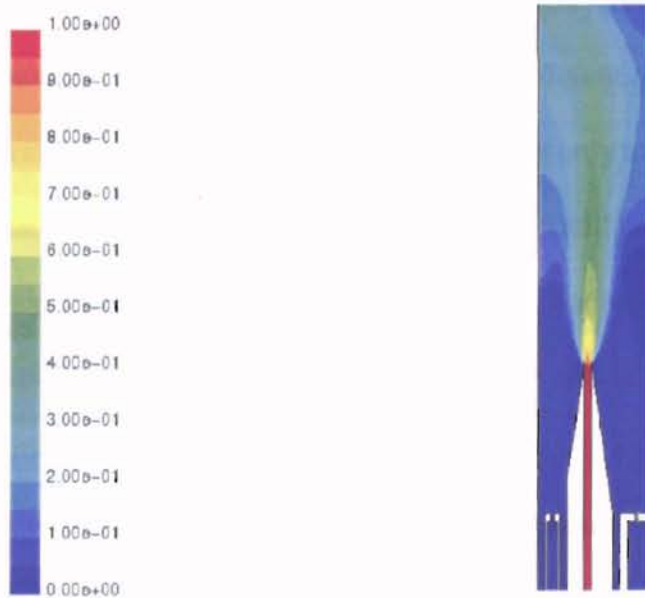
Figure IV-38: Mole Fraction of TiCl$_4$ for θ=8°

67
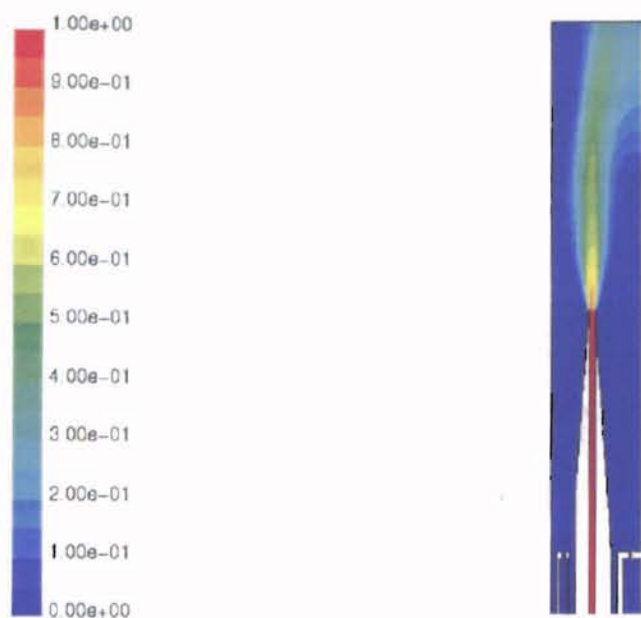
Figure IV-39: Mole Fraction of $TiCl_4$ for $\theta=4°$

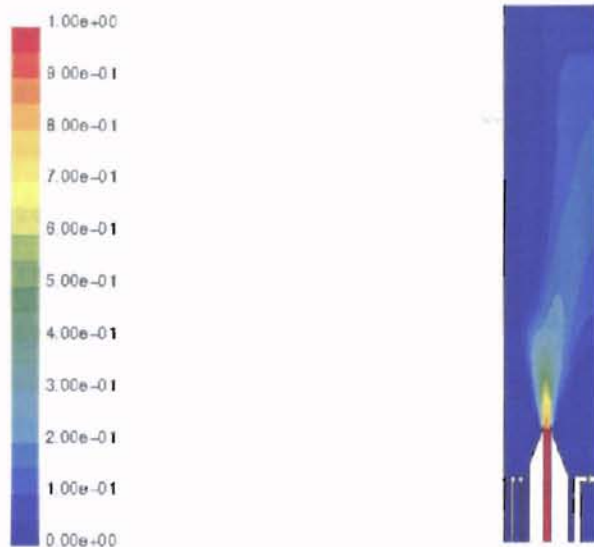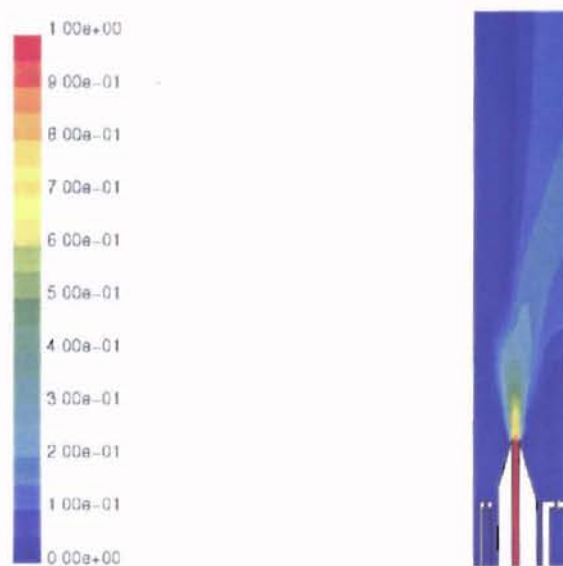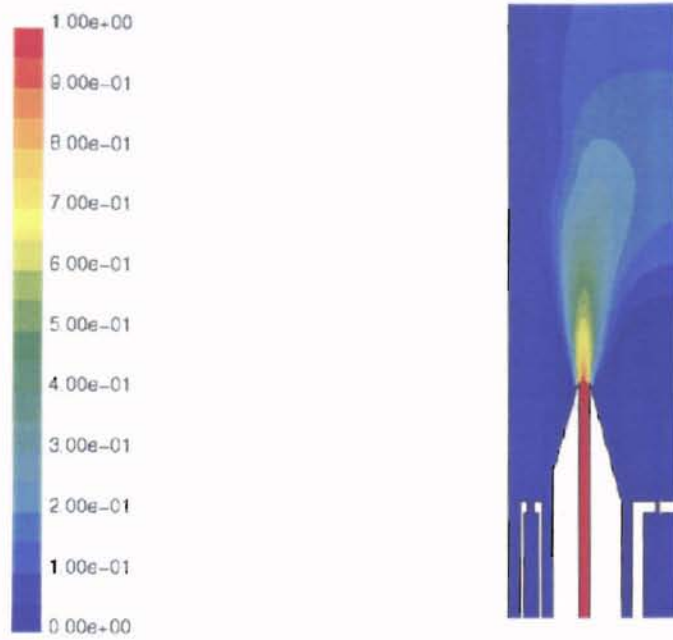Because of the arrangement of oxygen spools, the outer side of the $TiCl_4$ inlet is an oxygen rich environment, while the inner side oxygen is predominantly consumed in CO combustion. In reality, these spools have a different oxygen source, supplying a different flow rate. The patent is unclear on this, giving only a total volumetric flow rate of O_2 to the reactor. (See Table III-5.) In summary, it could be possible to get an even product size range and reaction profile for this reactor, but it would require different velocities for each individual O_2 inlet. A good place to start would be to halve the outer and middle O_2 velocities while doubling the inner O_2 velocity.

As was mentioned in Chapter 3, the patent claims to have complete combustion of carbon monoxide by the time the reactant mixture reaches the $TiCl_4$ inlet. A diagram of CO reaction rate contours (Figure IV-40) compared with a corresponding diagram of CO concentration at $z_{O2=0}$ (Figure IV-41) for the shortest inlet ($\theta=20°$) show that it is not necessarily true that there is no combustion occurring beyond the $TiCl_4$ nozzle, and the

CO is not exhausted. This reaction terminates prematurely on the interior side of the TiCl$_4$ nozzle, due to the same oxygen deficiency that terminates the TiO$_2$ reaction. The fact that combustion is occuring beyond the nozzle is not an important issue as it is still not in a zone where TiCl$_4$ is present.

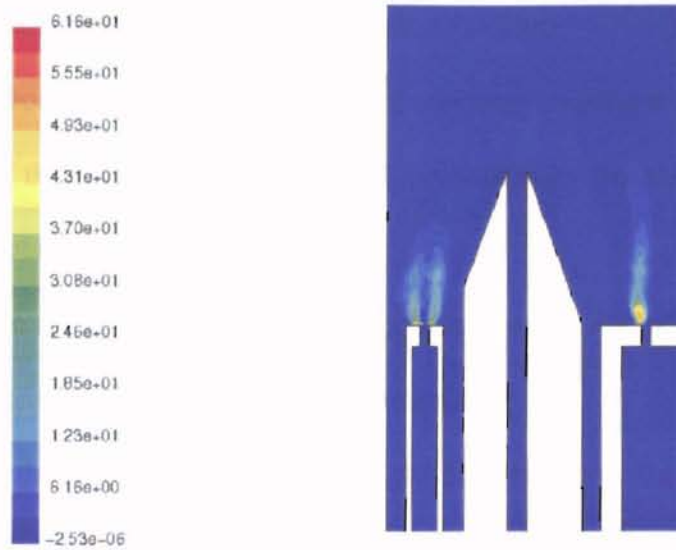Figure IV-40: Contours of CO Combustion Rate for θ=20° (kgmol/s)
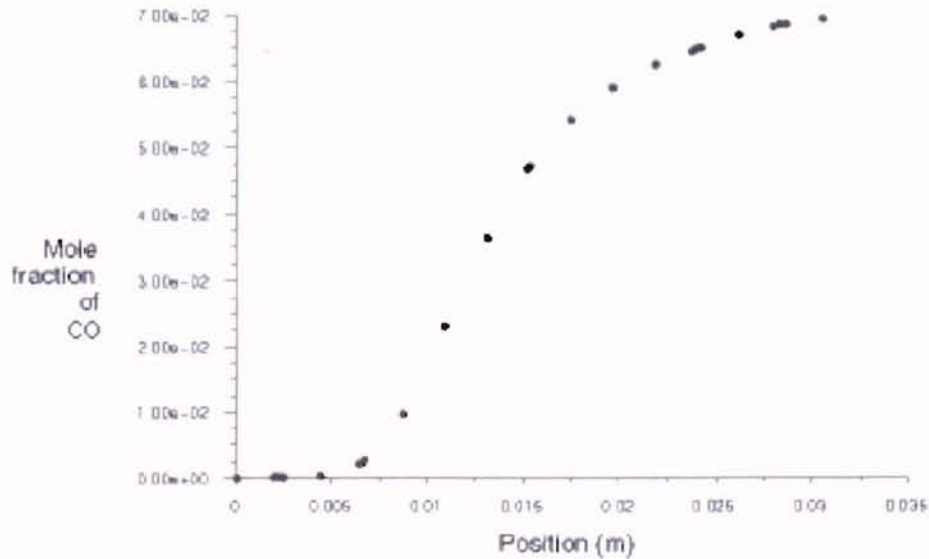
Figure IV-41: Mole Fraction of CO at $z_{O2=0}$ for θ=20°

Analysis of CFD Data for the Cabot Reactor

The inventors' claims for the Cabot reactor are direct, stating that if the linear velocity as the mixture enters the reactor tube is above 75 ft/s (22.9 m/s), deposition does not occur in the reactor tube. The evaluation criteria are similar to the previous reactor, with one change to accommodate the patent's claim:

1. Does the tangential injection of reactants creating a velocity > 75 ft/s at the top of the reaction tube sweep TiO_2 product away from the reactor walls, most notably in the reaction zone?

2. Do the reactants mix well enough, and evenly enough, to ensure 100% conversion and consistent particle size?

For the five runs outlined in Chapter III, velocity at the mouth of the reaction tube ranged from about 308 ft/s to just underneath the 75 ft/s minimum. This is shown in Table IV-5, with Figures IV-42 through IV-46 giving views of the inside of the reactors and the velocity vectors.

	Velocity
0.1x Example	22.5 m/s (74.0 ft/s)
0.2x Example	22.5 m/s (74.0 ft/s)
1x Example	56.2 m/s (184.4 ft/s)
2x Example	67.9 m/s (222.7 ft/s)
3x Example	93.8 m/s (307.6 ft/s)

Table IV-5: Average Linear Velocity at Reaction Tube Mouth for Multiples of Example $TiCl_4$ Flow Rate
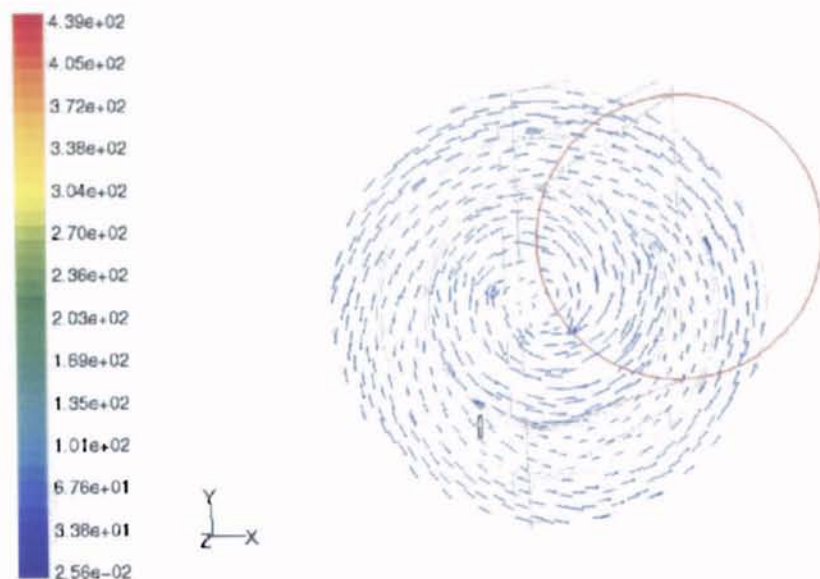
Figure IV-42: Velocity Vectors at Mouth of Reaction Tube For 0.1x TiCl$_4$ Flow of Example
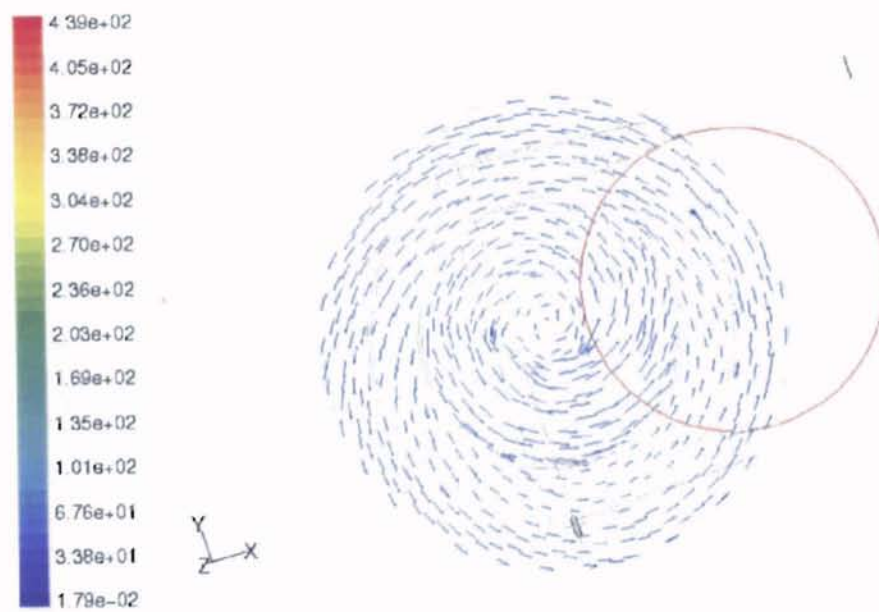
Figure IV-43: Velocity Vectors at Mouth of Reaction Tube For 0.2x TiCl$_4$ Flow of Example
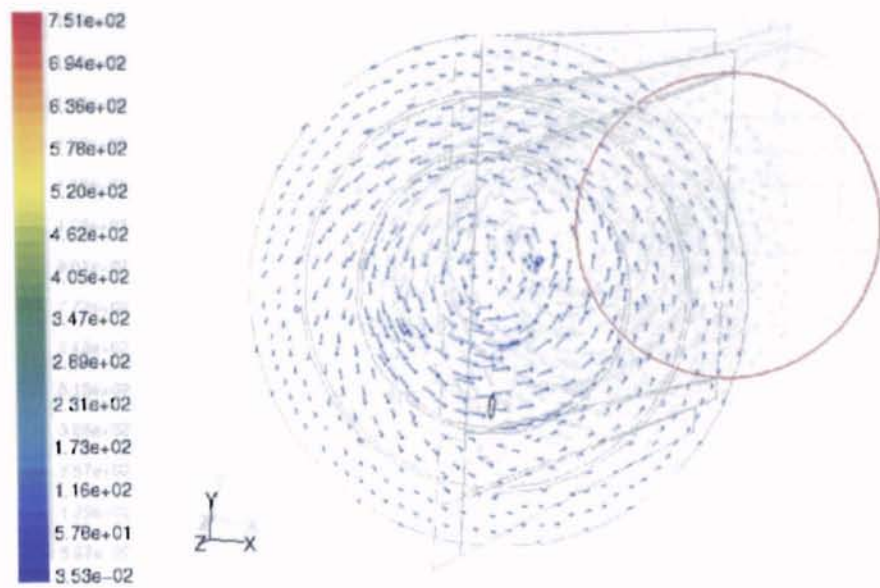
Figure IV-44: Velocity Vectors at Mouth of Reaction Tube For 1x TiCl$_4$ Flow of Example

Figure IV-45: Velocity Vectors at Mouth of Reaction Tube For 2x TiCl$_4$ Flow of Example
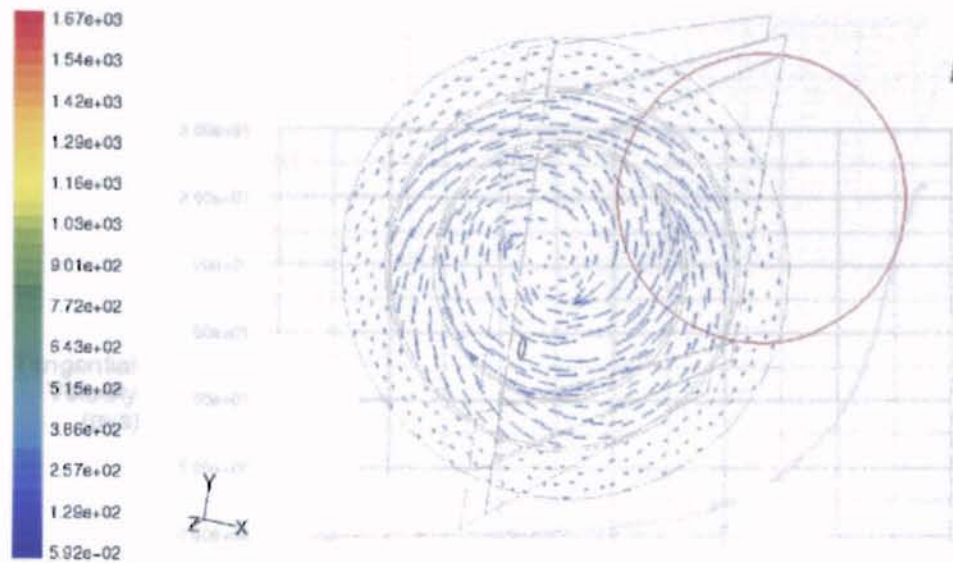
Figure IV-46: Velocity Vectors at Mouth of Reaction Tube For 3x TiCl₄ Flow of Example

At the reactor tube's mouth, the direction of velocity is almost entirely tangential

for all configurations. There is a point, however, in all these reactors where the flow

ceases to spin and becomes solely axial. Plots of tangential velocity vs. downstream

distance are shown in Figures IV-47 through IV-51. (z=2.9 is the upstream end of the

reaction tube, z=0 is the reactor exit.)
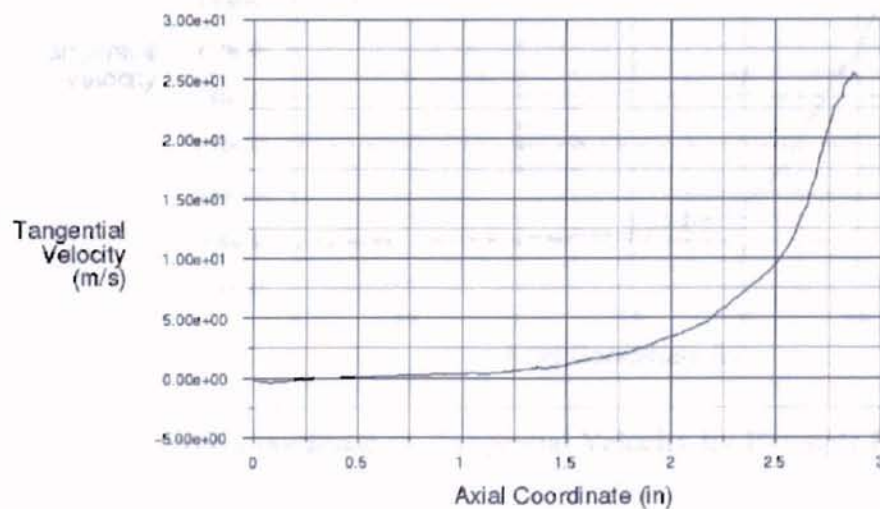
Figure IV-47: Axial Coordinate vs. Tangential Velocity for 0.1x Example Production Rate
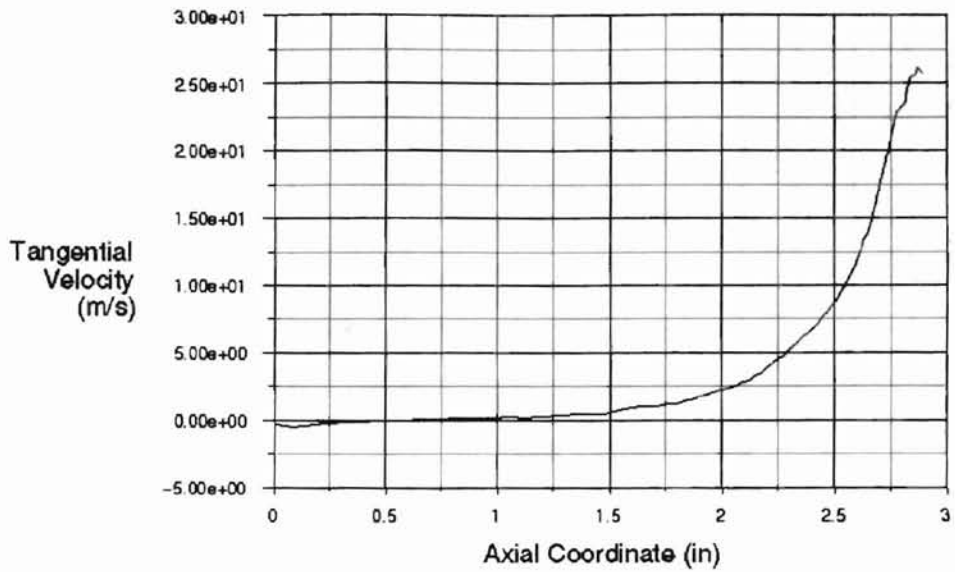
Figure IV-48: Axial Coordinate vs. Tangential Velocity for 0.2x Example Production Rate
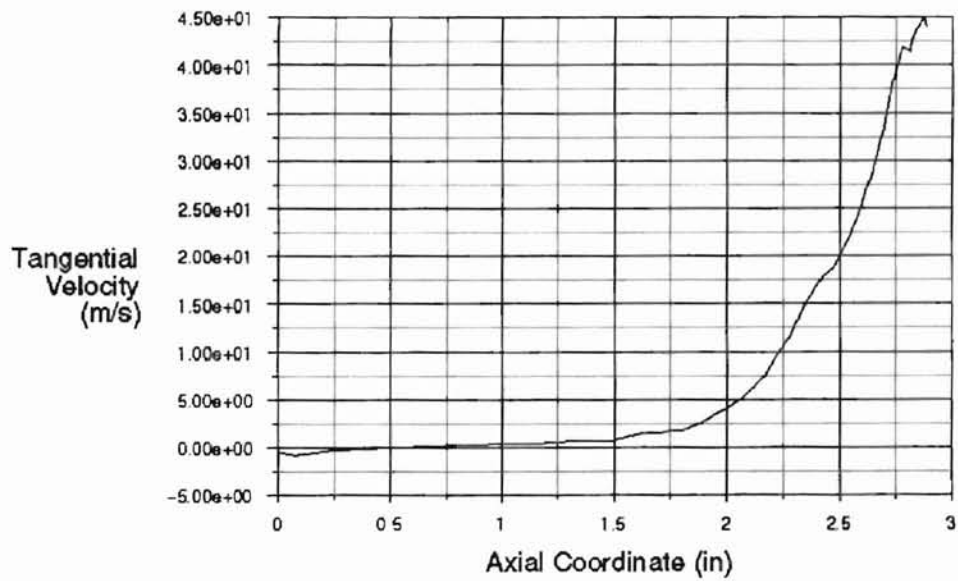
Figure IV-49: Axial Coordinate vs. Tangential Velocity for Example Production Rate

74
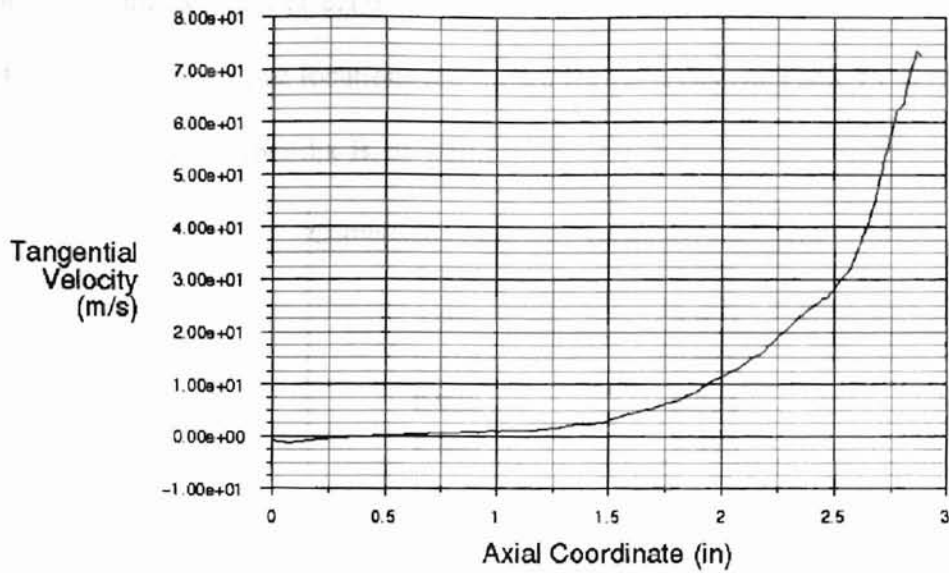
Figure IV-50: Axial Coordinate vs. Tangential Velocity for 2x Example Production Rate
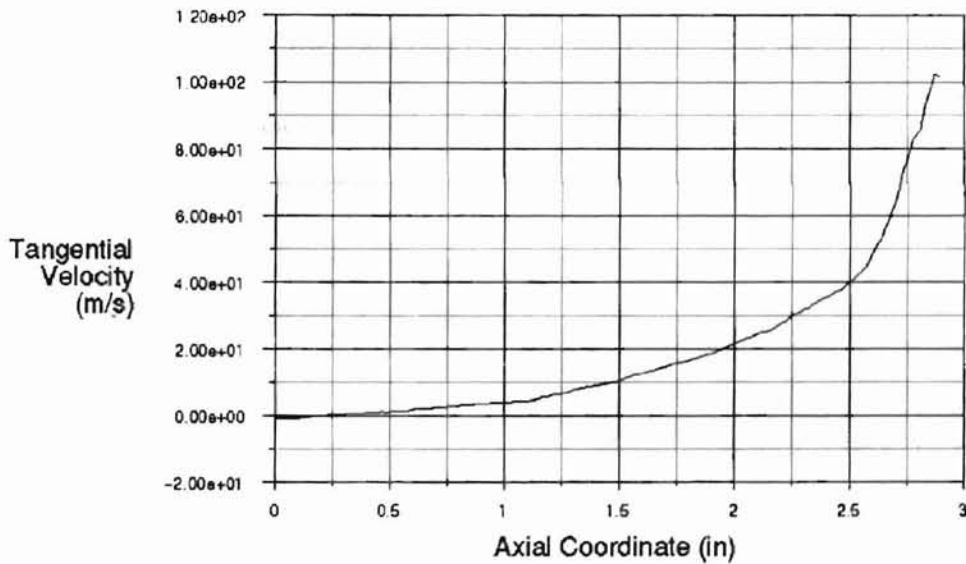
Figure IV-51: Axial Coordinate vs. Tangential Velocity for 3x Example Production Rate

From the charts, it appears that there is only a slight difference in the axial location at which the spin ceases for each production rate. The real indicator of the significance of the importance of the 75 ft/s velocity limit would appear to be the axial location of the

75

reaction zone, and its direct effect on TiO_2 mole fraction along the wall downstream. The highest rate-of-reaction zone locations are shown for each case in Table IV-6. (Figures of each are included in appendix B, as well.)

	Combustion z_{Rmax} (in.)	Oxidation z_{Rmax} (in.)
0.1x	2.904	2.922
0.2x	2.904	2.922
1x	2.712	2.311
2x	2.905	2.894
3x	2.998	2.915

Table IV-6: Axial Location of Reactions for Each Multiple of Production Rate

Note that the oxidation reaction begins to occur behind the most intense point of the flame front for the first two cases, where V at the mouth of the reaction tube is < 75 ft/s. In actuality, the flame front for these two cases is most intense at the end of the $TiCl_4/O_2$ annulus, as Figure IV-52 shows.
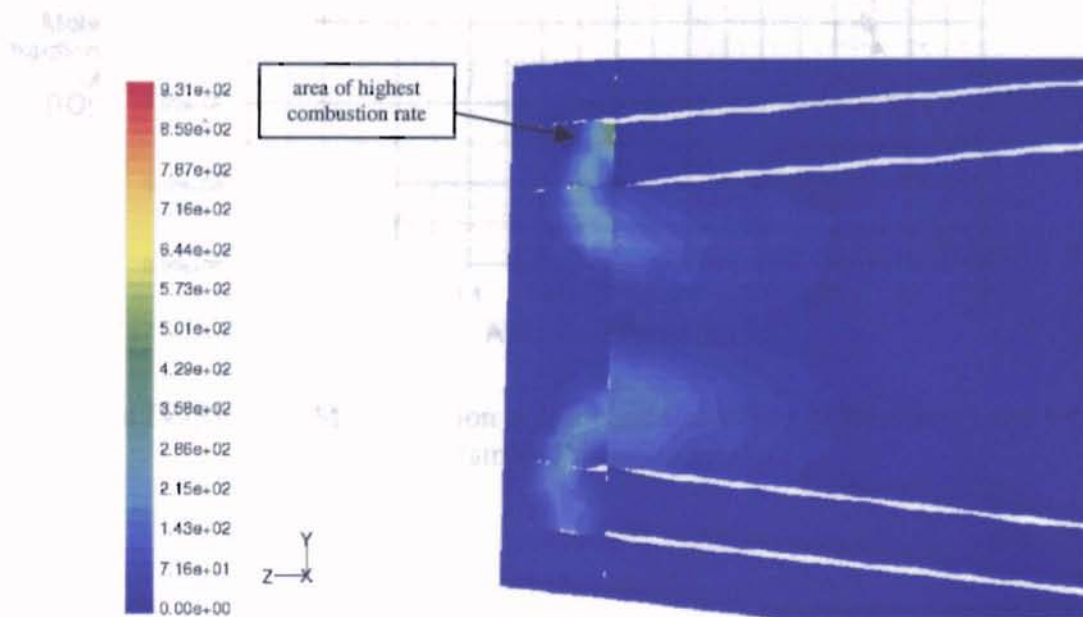
Figure IV-52: Contours of Combustion Rate (kmol/s) for 0.1x Example Production Rate

This is again an issue of density and its effect on diffusivity. As show in Tables A-10 through A-12, diffusivity of CO through oxygen is roughly twice that of CO through TiCl$_4$, at any temperature. As the inlet mass fraction of TiCl$_4$ becomes smaller (see Table III-8), the CO diffuses more quickly, and moves back the flame front. Because the reactants and combustion gas are on a concurrent tangential path in the top of the reactor, convective mass transfer does not become an issue until the entrance to the reaction tube, where the choking down of the vessel's diameter forces the streams to mix. With this in mind, the following charts show TiO$_2$ mole fraction along the reactor wall and TiO$_2$ mole fraction along the centerline of the tube for each case.

Figure IV-53: TiO$_2$ Mole Fraction at Wall and Centerline of Reaction Tube for 0.1x
Example Production Rate

77
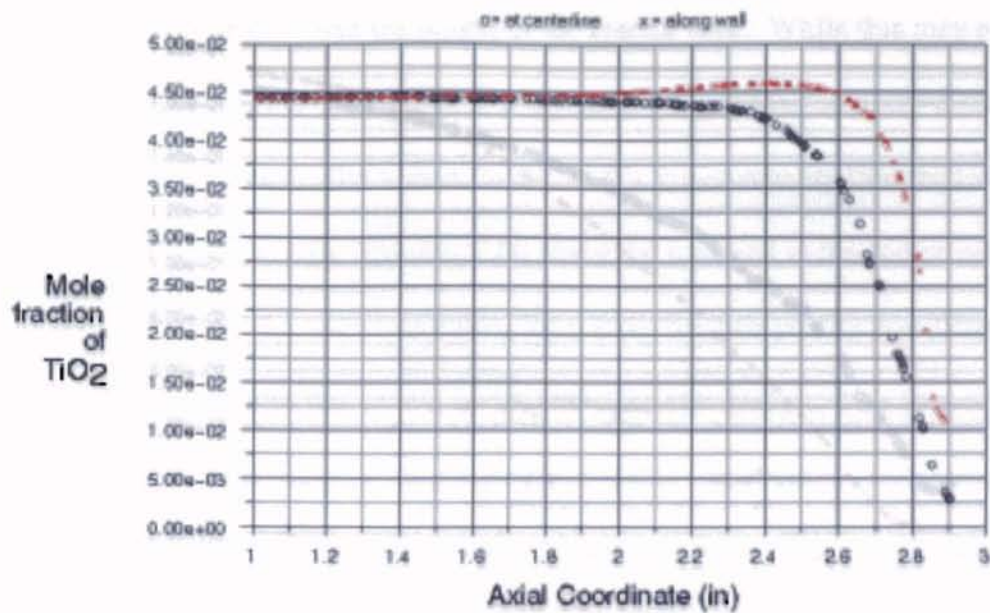
Figure IV-54: TiO$_2$ Mole Fraction at Wall and Centerline of Reaction Tube for 0.2x Example Production Rate
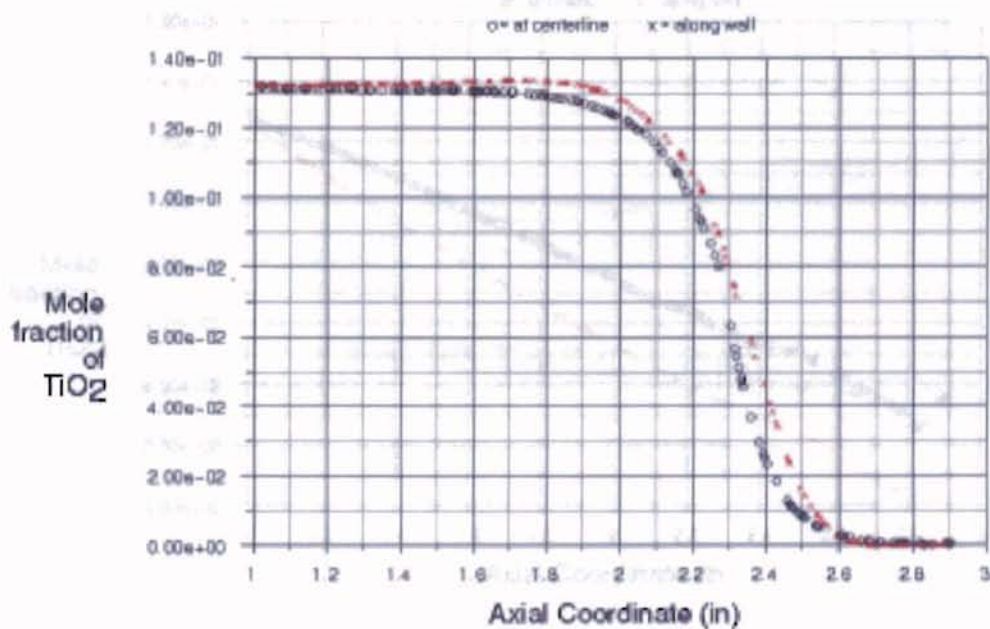
Figure IV-55: TiO$_2$ Mole Fraction at Wall and Centerline of Reaction Tube at Example Production Rate

Mole fraction of TiO₂

Axial Coordinate (in)
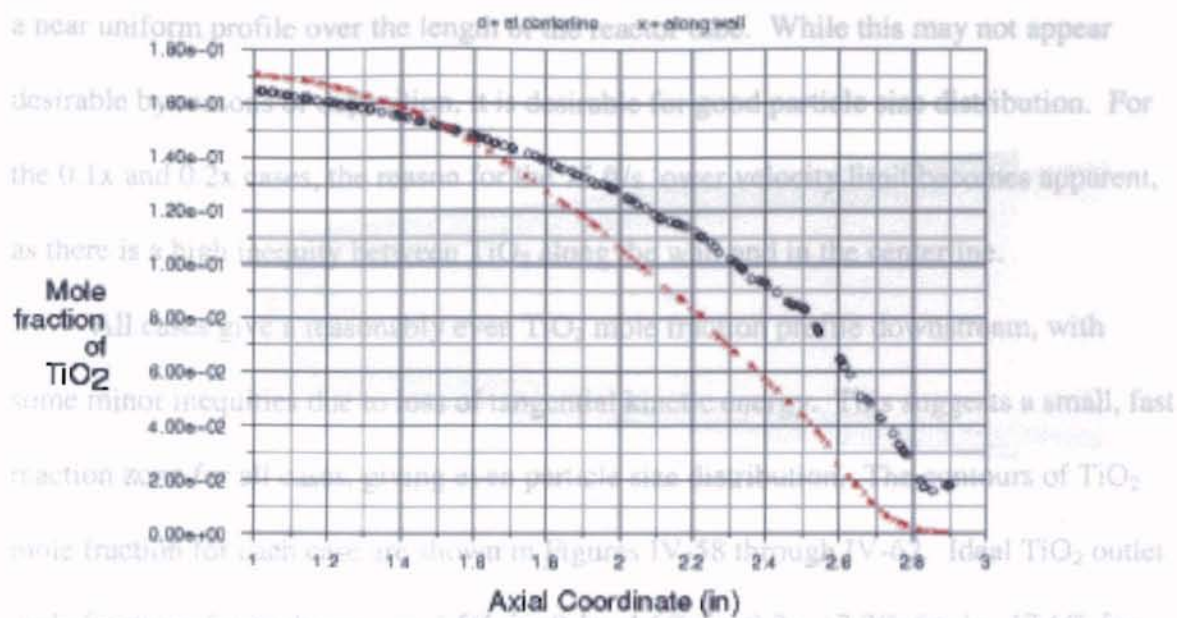
Figure IV-56: TiO₂ Mole Fraction at Wall and Centerline of Reaction Tube for 2x
Example Production Rate

Mole fraction of TiO₂

Axial Coordinate (in)
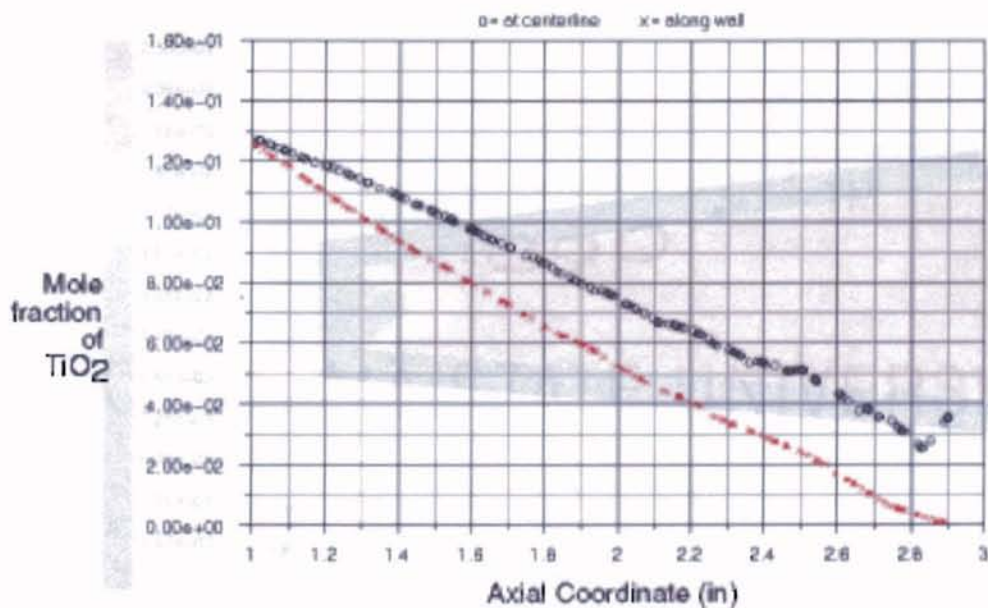
Figure IV-57: TiO₂ Mole Fraction at Wall and Centerline of Reaction Tube for 3x
Example Production Rate

The 2x and 3x rate cases show a higher mole fraction of TiO₂ in the centerline of

the reactor than the wall along the reaction zone (z = 2.6-2.9 in). The 1x rate case shows

79

a near uniform profile over the length of the reactor tube. While this may not appear desirable by reasons of deposition, it is desirable for good particle size distribution. For the 0.1x and 0.2x cases, the reason for the 75 ft/s lower velocity limit becomes apparent, as there is a high inequity between TiO_2 along the wall and in the centerline.

All cases give a reasonably even TiO_2 mole fraction profile downstream, with some minor inequities due to loss of tangential kinetic energy. This suggests a small, fast reaction zone for all cases, giving even particle size distribution. The contours of TiO_2 mole fraction for each case are shown in Figures IV-58 through IV-62. Ideal TiO_2 outlet mole fractions for each case are 2.5% for 0.1x, 4.5% for 0.2x, 13.3% for 1x, 17.6% for 2x, and 19.7% for 3x.
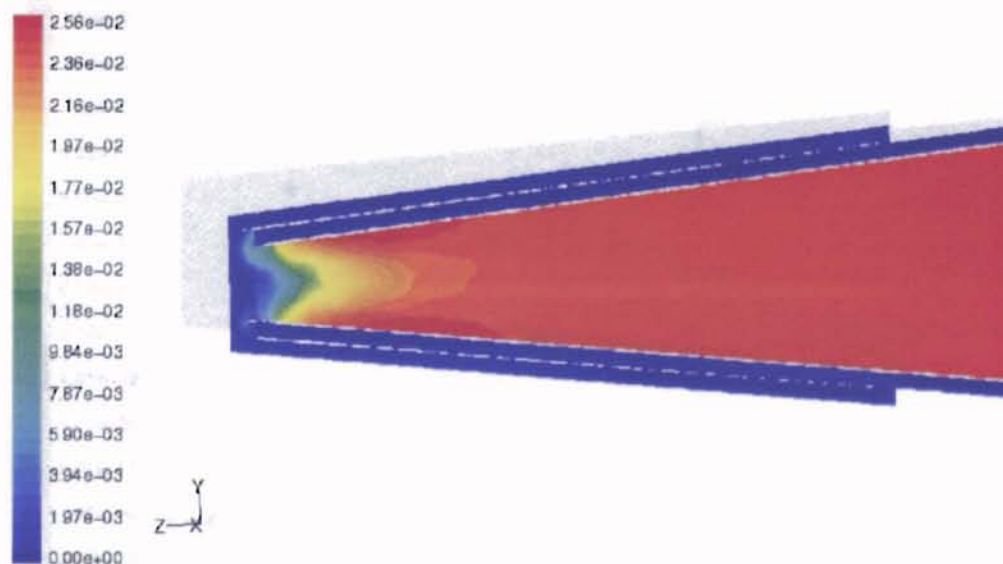
Figure IV-58: Contours of TiO_2 Mole Fraction for 0.1x Example Production Rate
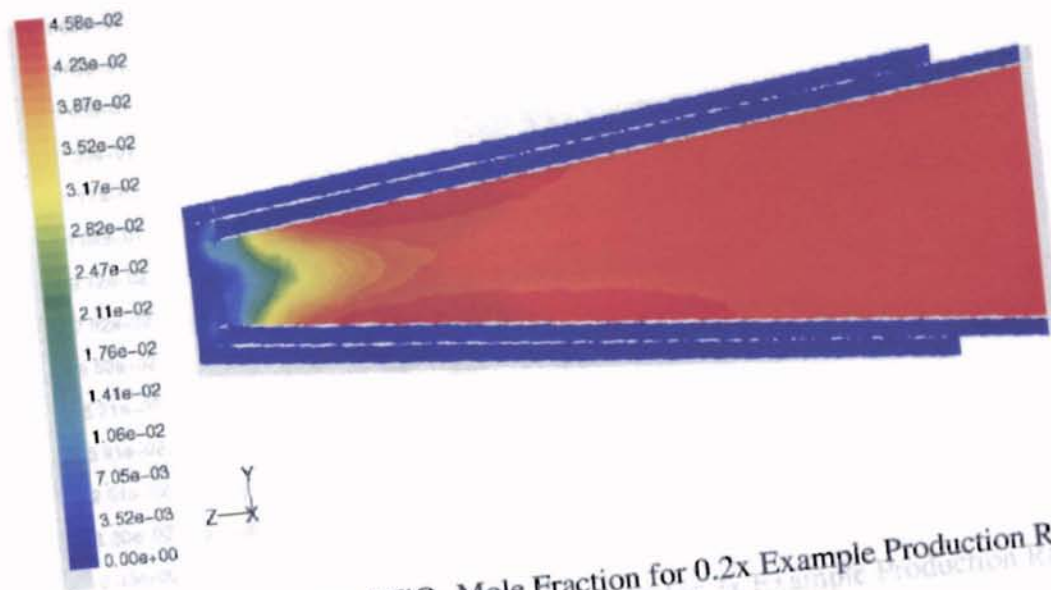
Figure IV-59: Contours of TiO$_2$ Mole Fraction for 0.2x Example Production Rate
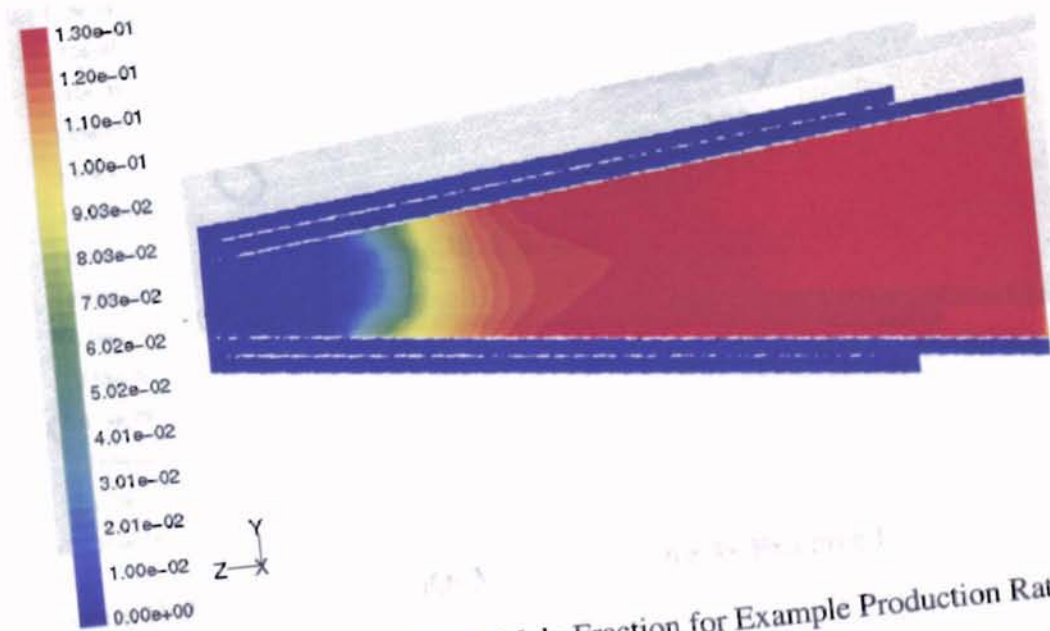
Figure IV-60: Contours of TiO$_2$ Mole Fraction for Example Production Rate
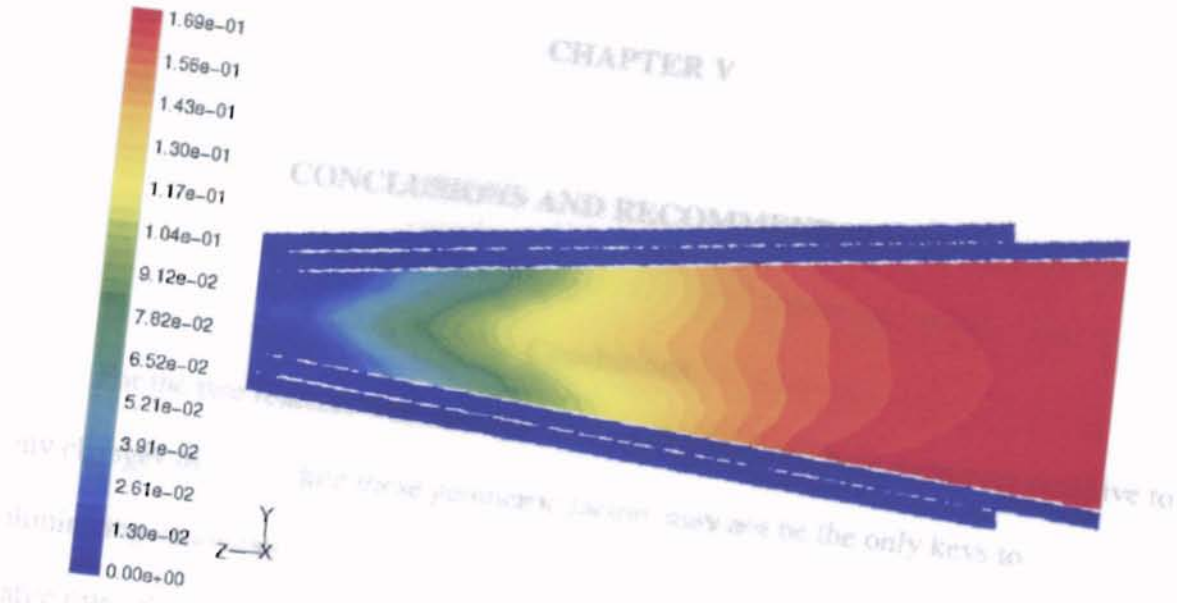
Figure IV-61: Contours of TiO_2 Mole Fraction for 2x Example Production Rate
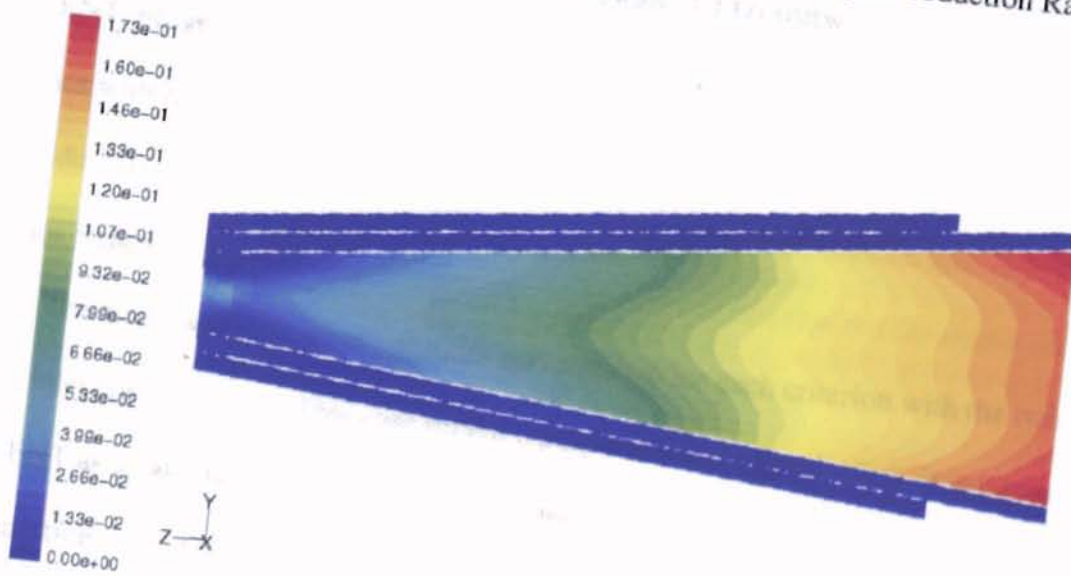
Figure IV-62: Contours of TiO_2 Mole Fraction for 3x Example Production Rate

CHAPTER V

CONCLUSIONS AND RECOMMENDATIONS

Conclusions

For the two reactors with variable TiCl$_4$ inlet geometry, both were very sensitive to any changes made. While these geometric factors may not be the only keys to eliminating deposition in chloride-process titanium dioxide reactors, it certainly plays a large role. Simulations of each of the patents did not verify many of their claims, but did give credible results. Computational fluid dynamic (CFD) software packages, in this case FLUENT, prove to be an efficient method of analyzing flow regimes and reaction kinetics within each of these reactors. The following sections give conclusions for each individual design.

Kronos Reactor

The Kronos reactor gave optimum performance for each criterion with the two TiCl$_4$ inlet configuration. This case served a purpose in two regards: first, it validated FLUENT as a calculation tool, second, it evaluated the claims of the patent. In regards to the questions asked in chapter IV, the answers are as follows:

	2 Inlets	4 Inlets	8 Inlets
Does the inlet configuration eliminate backflow?	Yes	No	No
Does the inlet configuration provide even mixing?	Yes	No	No
Is the Reynolds number 15,000-20,000 in the O$_2$ inlet?	No	No	No

Table V-1: Evaluation Criteria for Kronos Reactor Models

The device described in the patent likely utilizes a single pair of $TiCl_4$ ducts. One can only speculate about the Reynolds number issue, but in the high velocity, highly turbulent flow within this reactor it is likely that the positioning of a bare-wire thermocouple or other velocimeter would greatly affect measured velocity. This is evidenced in the diagrams included in appendix B.

In addition to satisfying the purposes stated at the beginning of this study, this model served as a means to examine the deposition effects of $TiCl_4$ flowed radially into a plug flow of O_2 in a tube.

Montecatini Reactor

Optimum performance for this reactor was achieved when θ is equal to 8°. All nozzle configurations still had the same single problem in the end: with uniform oxygen flow rates through each individual annulus, neither full $TiCl_4$ conversion nor uniform reaction rate can be achieved, and in turn, the reactor gives poor particle size distribution. The claim that CO combustion is complete before the mixture reaches the mouth of the $TiCl_4$ nozzle falls to the same issue of O_2 inequity.

These are issues that should be addressed in future work. Otherwise, the reactor lives up to the patent's claim; the reaction zone is away from the reactor wall and away from the $TiCl_4$ nozzle. This is a compelling and simple solution to the problem of deposition. Assuming a 5 mm distance allowance for the wall, and a 10 mm allowance for the inlet, the following table shows the results.

84

$\theta =$	4	8	12	16	20
Does the reaction occur far enough downstream from the TiCl$_4$ nozzle to avoid deposition there?	Yes	Yes	Yes	No	No
Does the reaction occur far enough away from the wall to avoid deposition there?	No	Yes	Yes	Yes	Yes
Does the reaction occur completely and evenly?	No	No	No	No	No

Table V-2: Evaluation Criteria for Montecatini Reactor Models

Cabot Reactor

It is difficult to develop criteria for success of this reactor, as none of the simulated production rates maintained tangential flow over the course of the reaction tube. However, the deposition described in the patent at low velocities occurs in a zone where it can cause "non-uniform mixing of the reactants through deflection or disturbance of flow patterns of non-mixed reactants." (Cabot 1967). This would suggest that deposition tends to occur near the mouth of the reaction tube, before the bulk of the oxidation can occur. If this is the case, then the patent's claim of a 75 ft/s velocity requirement at the top of the reaction tube holds true. A single tangential injection of reactants also has the benefit of giving an even residence time and, in turn, particle size distribution for all of the examined cases. Assuming an even radial TiO$_2$ mole fraction profile as the criterion for lack of deposition, the following table shows the results of the evaluation.

Velocity at Top of Reaction Tube	0.1	0.2	1	2	3
Does the tangential injection of reactants sweep TiO$_2$ product away from the reactor walls?	No	No	Yes	Yes	Yes
Do the reactants mix well enough to ensure consistent particle size?	Yes	Yes	Yes	Yes	Yes

Table V-3: Evaluation Criteria for Cabot Reactor Models

Recommendations

One primary, universal goal should be the main point of future investigation for all these reactors: the modeling of TiO_2 particle growth. FLUENT allows the addition of user-defined functions (UDFs) to the set of equations it solves for each cell. A good growth model to use would be the work of Pratsinis and Spicer (1998) discussed in chapter II. Their work addresses both vapor phase and surface reaction based on temperature and reactant concentrations, and consists a relatively simple set of moment equations for particle size.

Additionally, some effort should be invested into getting a converged solution while applying multicomponent diffusivities to the mixture. It would be interesting to compare those results with the approximations used in this work. (Discussed in appendix A.)

As these works are all patents, and at one time or another proprietary information, it is unfortunate that no recent experimental work on large scale TiO_2 production has been performed that is public domain. It would be very useful to see more works performed on the kinetics of $TiCl_4$ oxidation in large-scale turbulent flow.

Kronos Reactor

Additional work on this reactor should include the addition of toluene combustion. This was bypassed in this work by treating the toluene burner as a high-temperature carbon dioxide and water inlet, which is a safe assumption. Some comparison should be made between the combusting and non-combusting systems to determine how accurate this approximation is.

Kronos also has patented a cooling tube configuration that consists of a series of modular conical tubes (Kronos 1986). The inventors claim a one-third reduction from a cylindrical tube in the amount of scrub solids needed to prevent deposition. It would be a good idea to couple this reaction tube with the preheating section studied in this work and examine the results. Additionally, calculation of heat flux across the reaction tube wall to a water jacket should be approximated. The data from this work could be used in conjunction with tabular data for water from any source, such as Incropera and DeWitt (1996) to approximate the jacket as a counterflow heat exchanger and get a flux estimate.

Montecatini Reactor

Clearly, the most important work to be done on this model is to unequalize the oxygen flow rate. While this is a small scale, laminar flow reactor, it has the potential to be extremely useful if a set of proper boundary conditions may be determined.

This leads to the next step for the reactor, which should be the process of scaling it up to a production-size model, and applying turbulent flow conditions to it.

Cabot Reactor

This patent meets its claims in the cases tested. Like the Montecatini reactor, it should be scaled up to a turbulent flow condition. Because of the success of tangential flow, it would be a good idea to seek out further patents with a similar configuration.

The model should be augmented to include heat transfer between the walls. This creates additional preheating of the reactants. It would be useful to understand at exactly what inlet temperature the reactants would combust in their entrance annulus, and the effect that a particle formation UDF would have on heat transfer.

BIBLIOGRAPHY

Akhtar, K. M., Y. Xiong, and S. E. Pratsinis, "Vapor Synthesis of Titania Powder by Titanium Tetrachloride Oxidation," *AIChE Journal* 37, 1561-1570 (1991).

American Cyanamid Company, "Pigment via Plasma Jet-Improved Preheather Configuration," U.S. Patent, US3328126 (1967).

American Cyanamid Company, "Method for Producing Particulate Solids in a Turbulent Wake Burner," U.S. Patent, US4170630 (1979).

Aspen Plus® V.10, Aspen Technology, Inc., Cambridge, Massachusetts (1999).

Bird, R.B., W.E. Stewart, E.N. Lightfoot, Transport Phenomena, John Wiley and Sons, New York (1960).

Braun, J. H., "Titanium Dioxide – A Review," *Journal of Coating Technology* 69, 59-72 (1997).

British Titan Products Company Ltd., "Method for the Production of Metal Oxide Particles by Vapor Phase Oxidation," U.S. Patent, US3464792 (1969).

Cabot Corporation, "Apparatus and Process for the Production of Titanium Dioxide," U.S. Patent, US3203762 (1962).

Cabot Corporation, "Apparatus for the Production of Metal Oxides," U.S. Patent, US3322499 (1967).

Cabot Corporation, "Vapor Phase Process for Producing Metal Oxides," U.S. Patent, US3351427 (1967).

Cabot Corporation, "Method for Preventing Product Deposition on Reaction Zone Surfaces," U.S. Patent, US3488148 (1970).

Cabot Corporation, "Cooling of Pyrogenic Titanium Dioxide Pigment Containing Gas Streams," U.S. Patent, US3607049 (1971).

Chang, Y.C., M.B. Ranade, and J.W. Gentry, "Thermophoretic Deposition of Aerosol Particles on Transport Tubes," *Journal of Aerosol Science* 21, 581-584 (1990).

Dekker, J.P., P.J. van der Put, H.J. Veringa, and J. Schoonman, "Gas-to-Particle Conversion in the Particle Precipitation-Aided Chemical Vapor Deposition Process I. Synthesis of the Binary Compound Titanium Nitride," *Aerosol Science and Technology* 19, 549-561 (1993).

E.I. duPont de Nemours and Company, "Using Compacted Titanium Dioxide Pigment Particles in the Cooling Section of the Chloride Process for Making TiO$_2$," U.S. Patent, US5266108 (1993).

E.I. duPont de Nemours and Company, "Use of a Bimodal Distribution of Scrubs in a Process for Cooling a Hot Gaseous Suspension," U.S. Patent, US5372639 (1994).

FLUENT 5, Fluent Incorporated, Lebanon, New Hampshire (1998).

FLUENT 5, "FLUENT User's Guide," 1-4, Fluent Incorporated, Lebanon, New Hampshire (1998).

Foster, B.L., "3-D Rendering and Analysis of a Horizontal Zinc Selenide Reactor via Computational Fluid Dynamics," M.S. Thesis, Department of Mechanical Engineering, Oklahoma State University, Stillwater, Oklahoma (July 1999).

Freitas, R.A., Nanoscience, Landes Bioscience, Georgetown, Texas (1998).

Incropera, F.P., and D.P. DeWitt, Introduction to Heat Transfer, John Wiley and Sons, New York, (1996).

Jang, H.D., and J. Jeong, "The Effects of Temperature on Particle Size in the Gas Phase Production of TiO$_2$," *Aerosol Science and Technology* 23, 553-560 (1995).

Jang, H.D., S.K. Kim, and S.H. Young, "Modeling on Formation of Ultrafine Titanium Dioxide Particles by Gas Phase Reaction," *Journal of Aerosol Science* 26, S563-S564 (1995).

Kim, S.S., and Y.J. Kim, "Experimental Studies on Particle Deposition by Thermophoresis and Inertial Impaction from Particulate High-Temperature Gas Flow," *Particular Phenomena and Multiphase Transport* 4, 11-22 (1988).

Kobata, A., K. Kusakabe, and S. Morooka, "Growth and Transformation of TiO$_2$ Crystallites in an Aerosol Reactor," *AIChE Journal* 37, 347-359 (1991).

Kodas, T.T., and S.K. Friedlander, "Design of Tubular Flow Reactors for Monodisperse Aerosol Production," *AIChE Journal* 34, 551-557 (1988).

Kronos Titan GmbH, "Device for the Cooling of Hot Gaseous Solids Suspensions," U.S. Patent, US4569387 (1986).

Kronos Titan GmbH, "Process for the Production of Coarse, Scrubbing Aggregates of Titanium Dioxide Particles by Oxidation of Titanium Tetrachloride in the Vapor Phase and Use of Said Aggregates for the Prevention of Deposit in the Same Production Process," U.S. Patent, US4784841 (1988).

Kronos (USA) Inc., "Process for the Production of Titanium Dioxide," U.S. Patent, US5196181 (1993).

Lide, D.R., editor, CRC Handbook of Chemistry and Physics, Vol. 78, CRC Press, Boca Raton, Florida (1997).

Magnussen, B.F., B.H. Hjertager, "On Mathematical Models of Turbulent Combustion with Special Emphasis on Soot Formation and Combustion," *16th International Symposium on Combustion* (1976).

Montecatini Edison S.p.A., "Apparatus for the Combustion of Titanium Tetrachloride with Oxygen for the Production of Titanium Dioxide Pigment," U.S. Patent, US3676060 (1972).

Montecatini Edison S.p.A., "Process for the Combustion of Titanium Tetrachloride with Oxygen for the Production of Titanium Dioxide," U.S. Patent, US3552920 (1971).

Montecatini Edison S.p.A., "Process for Producing Pigment-Quality Titanium Dioxide," U.S. Patent, US3764667 (1973).

Montassier, N., D. Boulaud, F. Stratmann, and H. Fissan, "Comparison Between Experimental Study and Theoretical Model of Thermophoretic Particle Deposition in Laminar Tube Flow," *Journal of Aerosol Science* 21, S85-S88 (1990).

Nami Z., O. Misman, A. Erbil, G.S. May, "Computer Simulation Study of the MOCVD Growth of Titanium Dioxide Films," *Journal of Crystal Growth* 171, 154-165 (1997).

Okuyama, K., R. Ushio, Y. Kousaka, J.H. Seinfield, and R.C. Flagan, "Evaluation of Fine Particle Formation by CVD in a Laminar-Flow Reactor," *International Chemical Engineering* 32, 750-758 (1992).

Pittsburgh Plate Glass Company, "Process for Preparing Titanium Dioxide," U.S. Patent, US3356456 (1967).

Powell, Q.H., G.P. Fotou, T.T. Kodas, and B.M. Anderson, "Synthesis of Alumina- and Alumia/Silica Coated Titania Particles in an Aerosol Flow Reactor," *Chemistry of Materials* 9, 685-693 (1997).

Powell, R., Chemical Process Review Number 18 – Titanium Dioxide and Titanium Tetrachloride, Noyes Publications, Park Ridge, New Jersey (1968).

Pratsinis, S. E., H. Bai, P. Biswas, M. Frenklach, and S. V. R. Mastrangelo, "Kinetics of $TiCl_4$ Oxidation," *Journal of the American Ceramic Society* 73, 2158-2162 (1990).

Pratsinis, S. E., T. T. Kodas, M. P. Dudokovic, and S. K. Friedlander, "Aerosol Reactor Design: Effect of Reactor Geometry on Powder Production and Vapor Deposition," *Powder Technology* 47, 17-23 (1986).

Pratsinis, S. E. and P. T. Spicer, "Competition Between Gas Phase and Surface Oxidation of $TiCl_4$ During Synthesis of TiO_2 Particles," *Chemical Engineering Science* 53, 1861-1868 (1998).

Quest Consultants, "Quest Consultants Thermodynamic Properties Page," Norman, Oklahoma (1996).

Seto, T., M. Shimada, and K. Okayuma, "Evaluation of Sintering of Nanometer-Sized Titania Using Aerosol Method," *Aerosol Science and Technology* 23, 183-200 (1995).

Shay, C.D., "Design and Optimization of a High Temperature Reactor for the Production of Group II-VI Compounds via Computer Models and Statistical Experimentation," M.S. Thesis, Department of Chemical Engineering, Oklahoma State University, Stillwater, Oklahoma (December 1998).

Stovall, T.K., J.A. Crabtree, D.K. Felde, G. Farquharson, and J.E. Park, "Effects of Particle Inlet Blockages on High-Velocity Flow Through a Thin Rectangular Duct: Experimental and Analytical Results," *Transactions of the ASME – Journal of Heat Transfer* 119, 440-450 (1997).

Subcommittee on Military Smokes and Obscurants, National Research Council, "Toxicity of Military Smokes and Obscurants," Vol. 2, National Academy Press, Washington, D.C. (1999).

Suyama, Y., K. Ito, and A. Kato, "Mechanism of Rutile Formation in Vapor Phase Oxidation of $TiCl_4$ by Oxygen," *Journal of Inorganic and Nuclear Chemistry* 37, 1883-1888 (1975).

Titangesellschaft mbH, "Process for the Manufacture of Fine Particle Size Titanium Dioxide by Reacting Titanium Tetrachloride with Oxygen," U.S. Patent, US3647377 (1972).

Tioxide Group Ltd., "Process for the Oxidation of a Metal Halide in the Vapor Phase," U.S. Patent, US4013782 (1977).

Warneck, H.J., M. Schäfer, J. Prüss, and M. Weidenbach, "A Concept to Simulate an Industrial Size Tube Reactor with Fast Complex Kinetics and Absorption of Two Gases on the Basis of CFD Modeling," *Chemical Engineering Science* 54, 2513-2519 (1999).

APPENDIX A

THERMODYNAMIC PROPERTIES, PHYSICAL PROPERTIES, AND CALCULATION TECHNIQUES USED IN FLUENT

To obtain solutions for the mass, energy, and momentum balances in FLUENT computational fluid dynamics (CFD) software, the program must first be supplied with the appropriate properties for each molecule involved. FLUENT also requires the selection of a reaction and flow models, mixture properties, and acceptable numerical solver technique for all the balances.

To approximate the physical properties of TiO_2 monomer, individual molecules are treated as a single "grain" of solid with constant value for density, taken from the ASPEN database (1999). The heat capacity value is taken from the same source, as it was the only source available. For all other values, the particle is still treated as a gas.

The tables of densities below are tabulated for pressures of 1 atm. and 2.9 atm. The first value is for the operating pressure of the Cabot and Montecatini reactors; the second is for the Kronos reactor. Specific heat (table A-3) is independent of operating pressure.

Temp. (K)	298	400	500	750	1000	1500	2000	2500	3000	4000
Cl_2	2.91	2.2	1.7	1.13	0.85	0.57	0.43	0.35	0.28	0.21
CO	1.15	0.84	0.67	0.45	0.34	0.22	0.17	0.14	0.11	0.08
CO_2	1.8	1.36	1.06	0.7	0.53	0.35	0.26	0.22	0.18	0.13
O_2	1.31	0.96	0.77	0.51	0.38	0.26	0.19	0.16	0.13	0.1
$TiCl_4$	8.35	5.88	4.74	3.04	2.28	1.52	1.14	0.95	0.76	0.57
TiO_2	Constant: 4250									

Source: Quest Consultants (1996) except TiO_2, Aspen Technology (1999)

Table A-1: Density Values @ 1 atm. Used as Input in Simulations (kg/m^3)

Temp. (K)	298	400	500	750	1000	1500	2000	2500	3000	4000
Cl_2	8.28	6.31	4.96	3.33	2.48	1.63	1.21	0.99	0.85	0.64
CO	5.24	3.87	3.08	2.07	1.54	1.01	0.75	0.62	0.53	0.4
CO_2	2.22	1.6	1.28	0.85	0.63	0.41	0.31	0.25	0.22	0.16
O_2	3.74	2.78	2.24	1.47	1.12	0.74	0.54	0.45	0.38	0.29
$TiCl_4$	29.4	18.4	13.85	8.92	6.64	4.36	3.23	2.66	2.28	1.71
TiO_2	Constant: 4250									

Source: Quest Consultants (1996) except TiO_2, Aspen Technology (1999)

Table A-2: Density Values @ 2.9 atm. Used as Input in Simulations (kg/m^3)

Temp. (K)	298	400	500	750	1000	1500	2000	2500	3000	4000
Cl_2	484	499.9	510.8	523.4	529.9	604.3	896.7	1570.7	2789.9	7518.4
CO	1043.8	1049.8	1065.4	1126.6	1185	1122	535.4	-915.2	-3570.1	-13858.3
CO_2	849.1	940.8	1015.9	1150.1	1235.5	1404	1812.6	2753.6	198.89	11693.2
H_2O	1947.5	1951.6	1986.9	2122.9	2285.7	2594	2784.7	2597.8	1991.7	-1185.5
O_2	919.7	945.1	973.6	1044.9	1091.2	983	399.1	-910.1	-3194.3	-11686.2
$TiCl_4$	517.1	533.9	546.4	559	569.2	663.9	1073.5	2022.8	3741.8	10409.1
TiO_2	Constant: 905									

Source: Quest Consultants (1996) except TiO_2, Aspen Technology (1999)

Table A-3: Specific Heat Values Used as Input in Simulations (J/kg-K)

Viscosity and thermal conductivity for each component were calculated through kinetic theory, where kinetic theory specifically means the Chapman-Engksog method for viscosity Bird et al. (1960):

$$\mu = 2.6693 \times 10^{-5} \frac{\sqrt{MT}}{\sigma^2 \Omega_\mu} \tag{A-1}$$

where σ is the characteristic length of each molecule, A and B, and Ω is a dimensionless function of temperature and the energy parameter (ε/k) for the molecule. The value of σ and ε/k (the Lennard-Jones parameters), where k is Boltzmann's constant, for each molecule was obtained from the following correlations from Bird et al. (1960)

$$\varepsilon / k = 0.77T_c \qquad \sigma = 2.44(\frac{T_c}{P_c})^{1/3} \qquad\qquad \text{(A-2,A-3)}$$

$$\varepsilon / k = 1.92T_m \qquad \sigma = 1.222v_{m,sol.}^{1/3} \qquad\qquad \text{(A4,A-5)}$$

	T_c (K)	p_c (atm)	ε/κ (K)	σ (Å)
$O_2^{(1)}$	154.59	49.77	119.03	3.5601
$TiCl_4^{(2)}$	638	45.99	491.26	5.8629
$H_2O^{(1)}$	647.14	217.72	498.3	3.5082
$CO^{(1)}$	132.91	34.53	102.34	3.8239
$CO_2^{(1)}$	304.14	72.79	234.19	3.93
$Cl_2^{(1)}$	416.9	78.87	321.01	4.2504

	T_m (K)	v_m (cm^3/mol)	ε/κ (K)	σ (Å)
$TiO_2^{(3)}$	2113	20.487	4057	3.3437

Sources: 1 – 78th CRC Handbook of Chem. and Phys. (1997), 2 – Quest Consultants (1996), 3 – Subcommittee on Military Smokes and Obscurants (1999)

Table A-4: Lennard-Jones Parameters

Kinetic theory for thermal conductivity simply calculates k through an empirical relationship with viscosity and specific heat values:

$$k = \frac{15}{4}\frac{R}{M}\mu\left[\frac{4}{15}\frac{c_pM}{R} + \frac{1}{3}\right] \qquad\qquad \text{(A-6)}$$

For the Cabot reactor, FLUENT could not come to a solution using kinetic theory; the iterations consistently diverged. To get around this, constant values were calculated for μ and k of each component using kinetic theory, and those value entered into FLUENT. The table below shows those values.

	Temp. (K)	μ (kg/m-s)	k (J/kmol-k)
O_2	400	2.859E-05	0.0270212
$TiCl_4$	400	1.896E-05	0.0101217
CO	298	2.041E-05	0.0212999
CO_2	3500	7.242E-05	0.5870549
Cl_2	2500	6.204E-05	0.0974465

Table A-5: Viscosity and Thermal Conductivity Used in Cabot Reactor Simulations

	MW (kg/kgmol)	$H°$ (J/kg·mol)	$S°$ (J/kg·mol)	Ref. T
CO [1]	44.00995	-3.93E+08	213715.9	298.15
CO_2 [1]	28.01055	-1.11E+08	197531.6	298.15
Cl_2 [1]	70.9	2816.454	222988	298.15
O_2 [1]	32	0	205026.9	298.15
H_2O [1]	18.01534	-2.42E+08	188696.4	298.15
TiO_2 [2,3]	79.9	2397000	54332	298.15
$TiCl_4$ [2,4]	189.7	2.49E+07	49322	298.15

Sources: 1- FLUENT database (1998), 2- Kerr-Mcgee plant data, 3-Aspen Technology (1999), 4- Quest Consultants (1996)

Table A-6: Molecular Weight and Standard State Enthalpies and Entropies Used in Simulations

Additionally, FLUENT requires specification of mixture properties. "Mixture" in this case implies all substances present in the reactor, reactive or not.

Property	Calculation Method
Reaction Model	Finite Rate / Eddy Dissipation
Density (ρ)	Volume Weighted Mixing Law
Specific Heat (C_p)	Mixing Law
Thermal Conductivity (k)	Mass Weighted Mixing Law
Viscosity (μ)	Mass Weighted Mixing Law
Mass Diffusivity (D)	Constant Dilute Approximation

Table A-7: Mixture Property Calculations Used in Simulations

The reaction model in the table applies to both the combustion and $TiCl_4$ oxidation reactions. Fluent uses the reaction rate equation:

95

$$R_{i'} = M_{i'} \sum_{k=1}^{N_r} \hat{R}_{i',k} \tag{A-7}$$

The finite rate component of the overall rate is calculated as follows:

$$\hat{R}_{i',k} = k_{f,k} \prod_{j'=1}^{N} [C_j]^{\eta'_{j',k}} \tag{A-8}$$

FLUENT has the option of including third body efficiencies and backward reaction in this equation, but neither is required in this work. (The subscript f denotes forward reaction.) The Arrhenius rate constant k is calculated from the same form as equation 2-3.

Reaction	Pre-exponential Factor (A)	Activation Energy (E) kJ/mol	Temp. Exponent (β)
$TiCl_4 + O_2 \rightarrow TiO_2 + 2Cl_2$ [1]	8.26×10^4	8.88×10^7	0
$CO + \frac{1}{2}O_2 \rightarrow CO_2$ [2]	2.239×10^{12}	1.7×10^8	0

Source: 1 - Pratsinis (1992), 2 – FLUENT (1998)

Table A-8: Arrhenius Constants

The second component of the overall rate is the turbulence effect, calculated from the eddy-dissipation model:

$$R_{i',k} = \upsilon'_{i',k} k M_{i'} A\rho \frac{\varepsilon}{k} \frac{m_R}{\upsilon'_{R,k} M_R} \tag{A-9}$$

$$R_{i',k} = \upsilon'_{i',k} M_{i'} AB\rho \frac{\varepsilon}{k} \frac{\sum_P m_P}{\sum_{j'}^{N} \upsilon''_{j',k} M_{j'}} \tag{A-10}$$

This is also referred to as the Magnussen and Hjertager model (Magnussen and Hjertager 1976). The reaction rate is calculated from the equation of A-3 and A-4 with the smaller value. m_R and m_p represent the mass fractions of a particular reactant and any product, respectively. The ε/k factor is the inverse of the turbulent eddy time scale from the k-

epsilon turbulence model, and A and B are empirical constants equal to 4.0 and 0.5, respectively. In the finite rate/eddy dissipation reaction model, FLUENT calculates both components, and uses the slower rate as the reaction rate.

The mixing law calculations performed for C_p, k, and μ takes the form

$$\Phi = \sum_{i'} m_{i'} \Phi_{i'} \qquad (A-11)$$

where Φ is the mixture property. The volume-weighted form of the mixing law for density is

$$\rho = \frac{1}{\sum_{i'} \frac{m_{i'}}{\rho_{i'}}} \qquad (A-12)$$

In early runs, multicomponent binary diffusion coefficients were used for the mass flux equations, which were calculated with the Chapman-Engskog equation for diffusivity (Bird et al. 1960):

$$D_{AB} = 0.0018583 \frac{\sqrt{T^3 (\frac{1}{M_A} + \frac{1}{M_B})}}{p \sigma_{AB}^2 \Omega_{D,AB}} \qquad (A-13)$$

σ_{AB} and ε_{AB} are calculated from the arithmetic and geometric mean of the value for each molecule, respectively. Preliminary runs were performed for each reactor studied, utilizing a constant dilute approximation for the diffusion coefficient of all species.

Reactor	Area-Weighted Average Temperature	Operating Pressure
Cabot	1113 K	1 atm
Kronos	1067 K	2.9 atm
Montecatini	1876 K	1 atm

Table A-9: Average Reactor Temperature from Trial Runs

The following tables of diffusion coefficients were obtained for each set of conditions.

	O_2	$TiCl_4$	TiO_2	CO	CO_2
$TiCl_4$	0.6902				
TiO_2	1.0339	0.2701602			
CO	1.7572	0.7026795	1.035		
CO_2	1.4252	0.5173573	0.7184	1.4399	
Cl_2	1.1684	0.3867824	0.5322	1.1616	0.8946

Table A-10: D_{AB} (cm^{2}s^{-1}) @ 1113 K, 1 atm

	O_2	$TiCl_4$	TiO_2	H_2O	CO_2
$TiCl_4$	0.2223				
TiO_2	0.329	0.0854498			
H_2O	0.6083	0.2380853	0.2978		
CO_2	0.4605	0.1663926	0.2305	0.4811	
Cl_2	0.3764	0.1241583	0.1672	0.3996	0.2881

Table A-11: D_{AB} (cm^{2}s^{-1}) @ 1067 K, 2.9 atm

	O_2	$TiCl_4$	TiO_2	CO	CO_2
$TiCl_4$	1.676				
TiO_2	2.7134	0.7536373			
CO	4.1691	1.7020325	2.6983		
CO_2	3.4048	1.2751016	1.966	3.3414	
Cl_2	2.8199	0.9646221	1.4783	2.7849	2.1808

Table A-12: D_{AB} (cm^{2}s^{-1}) @ 1876 K, 1 atm

Use of multicomponent diffusion coefficients, however, resulted in convergence issues within FLUENT. Oscillating, non-converging residuals were obtained for species concentrations and k and ε values. As all coefficients obtained are within an order of

magnitude of each other for each reactor, a constant dilute approximation was used based on average multicomponent values for each case.

Reactor	D_{AB} (Const. Dilute Approx.)
Cabot	0.91557
Kronos	0.29836
Montecatini	2.09908

Table A-13: D_{AB} for each case (cm^2s^{-1})

FLUENT uses the constant dilute approximation form of the binary diffusion coefficient in the mass flux calculation:

$$J_{i',i} = -\rho D_{i',m} \frac{\partial m_{i'}}{\partial x_i}$$

(A-14)

(For Laminar Flow)

$$J_{i',i} = -(\rho D_{i',m} + \frac{\mu_t}{Sc_t}) \frac{\partial m_{i'}}{\partial x_i}$$

(A-15)

(For Turbulent Flow)

Where $Sc = \mu_t/\rho D_t$, and is the turbulent Schmidt number. Both the turbulent and laminar cases are encountered through the course of this work.

In all cases involving turbulent flow in this work, FLUENT was configured to calculate turbulent viscosity via the Standard k-ε Model. The values of k and ε are calculated via the following differential equations:

$$\rho \frac{Dk}{Dt} = \frac{\partial}{\partial x_i} \left[\left(\mu + \frac{\mu_t}{\sigma_k} \right) \frac{\partial k}{\partial x_i} \right] + G_k + G_b - \rho\varepsilon - Y_M$$

(A-16)

99

$$\rho \frac{D\varepsilon}{Dt} = \frac{\partial}{\partial x_i}\left[\left(\mu + \frac{\mu_t}{\sigma_\varepsilon}\right)\frac{\partial \varepsilon}{\partial x_i}\right] + C_{1\varepsilon}\frac{\varepsilon}{k}(G_k + C_{3\varepsilon}G_b) - C_{2\varepsilon}\rho\frac{\varepsilon^2}{k} \qquad \text{(A-17)}$$

The G terms represent energy generation from velocity gradients (G_k) and buoyancy (G_b), and Y_M represents the contribution from fluctuations in compressible turbulence. The C terms are constants, and σ_k and σ_ε are turbulent Prandtl numbers for k and ε. The final turbulent viscosity calculation is:

$$\mu_t = \rho C_\mu \frac{k^2}{\varepsilon} \qquad \text{(A-18)}$$

APPENDIX B

ADDITIONAL FLUENT OUTPUT OF INTEREST

Kronos Reactor
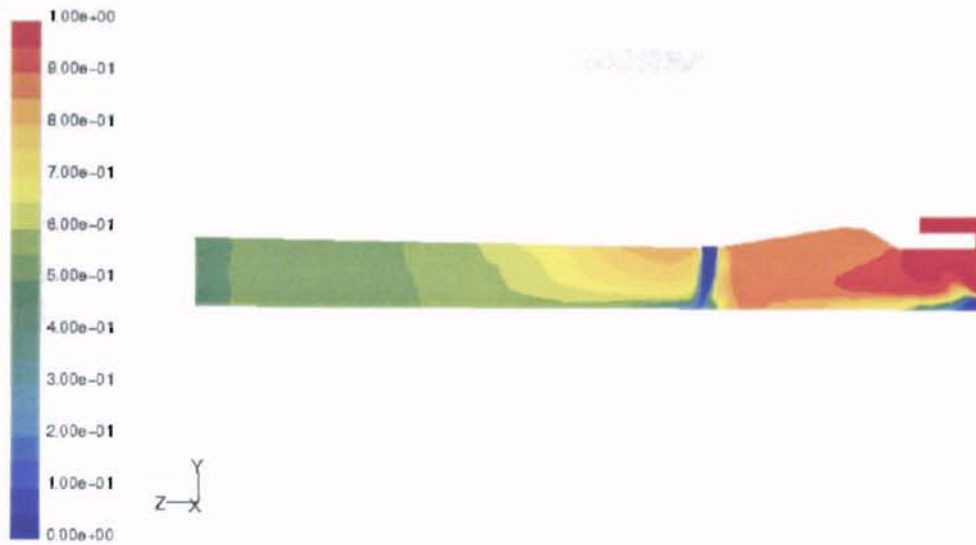
Figure B-1: O_2 Mole Fraction Contours for 2 Symmetric Inlets
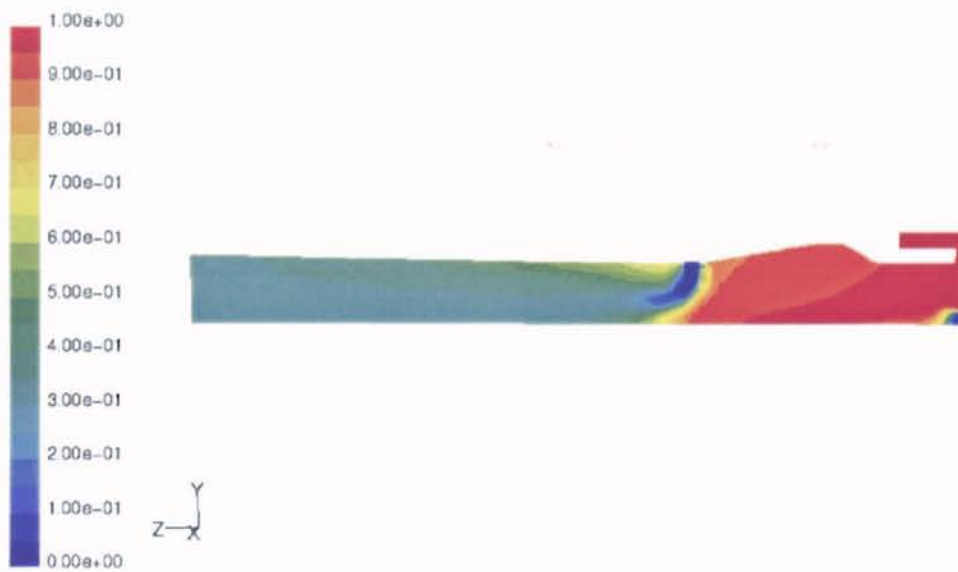
Figure B-2: O_2 Mole Fraction Contours for 4 Symmetric Inlets

Figure B-3: O$_2$ Mole Fraction Contours for 8 Symmetric Inlets
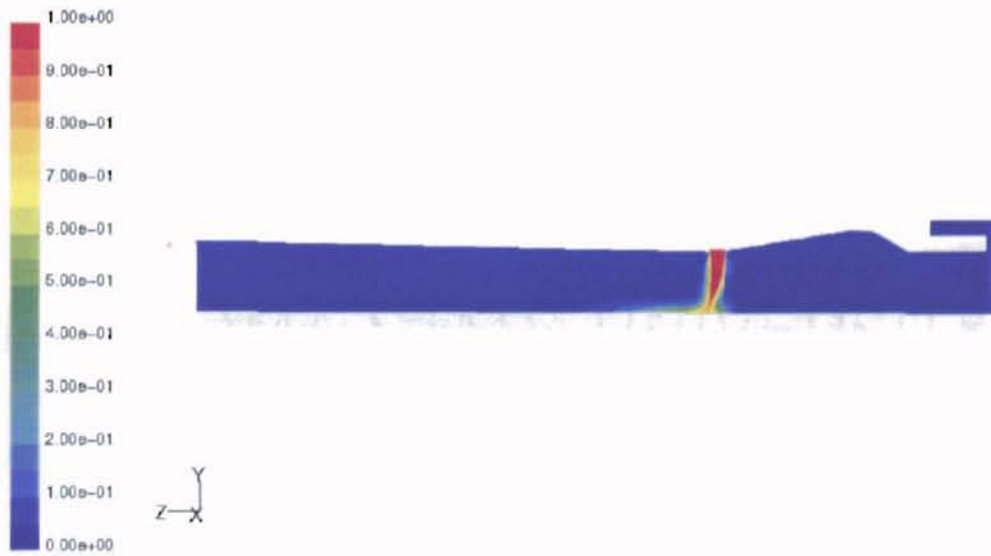
Figure B-4: TiCl$_4$ Mole Fraction Contours for 2 Symmetric Inlets
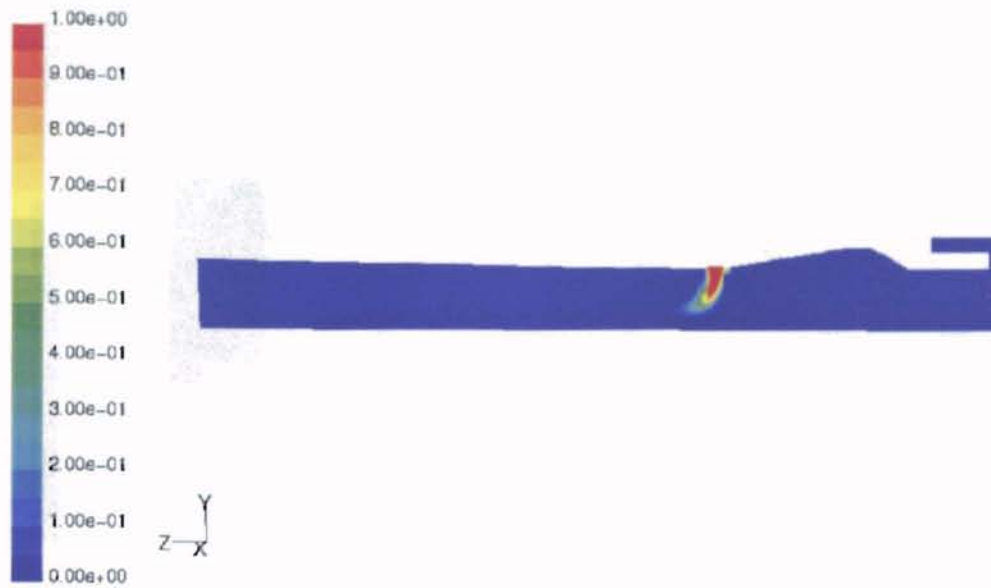
Figure B-5: TiCl$_4$ Mole Fraction Contours for 4 Symmetric Inlets
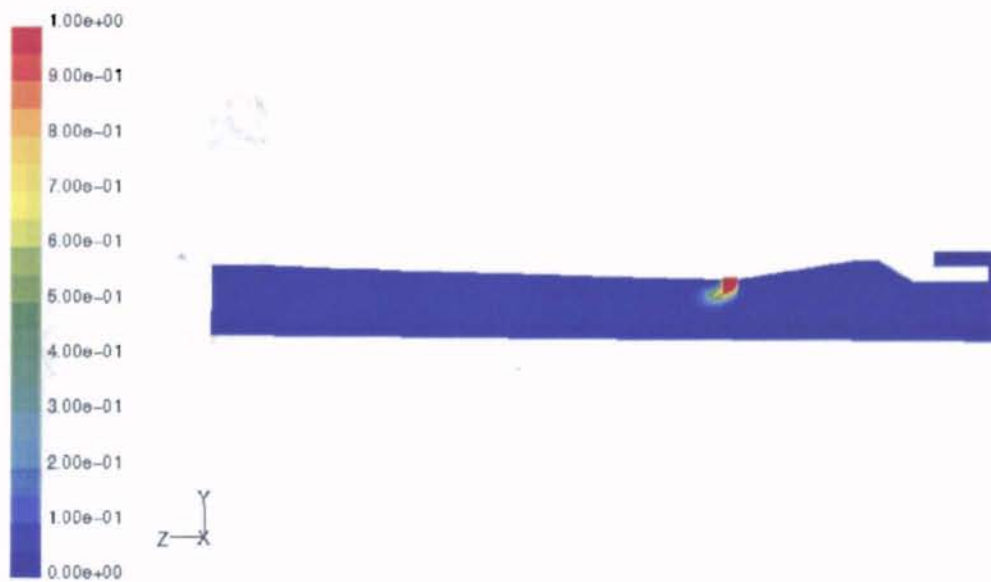
Figure B-6: TiCl$_4$ Mole Fraction Contours for 8 Symmetric Inlets
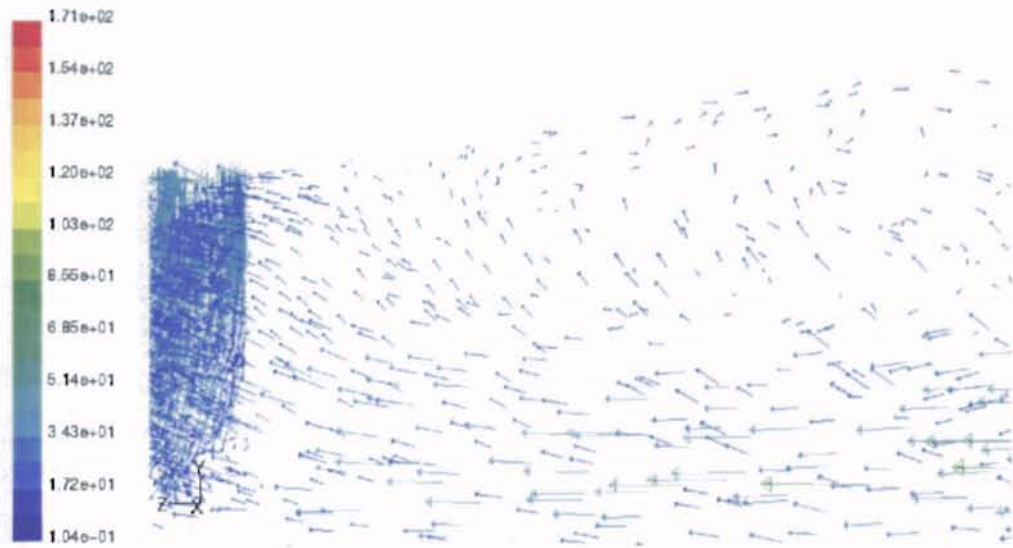
Figure B-7: Velocity Vectors In the Preheat Chamber for 2 Symmetric Inlets
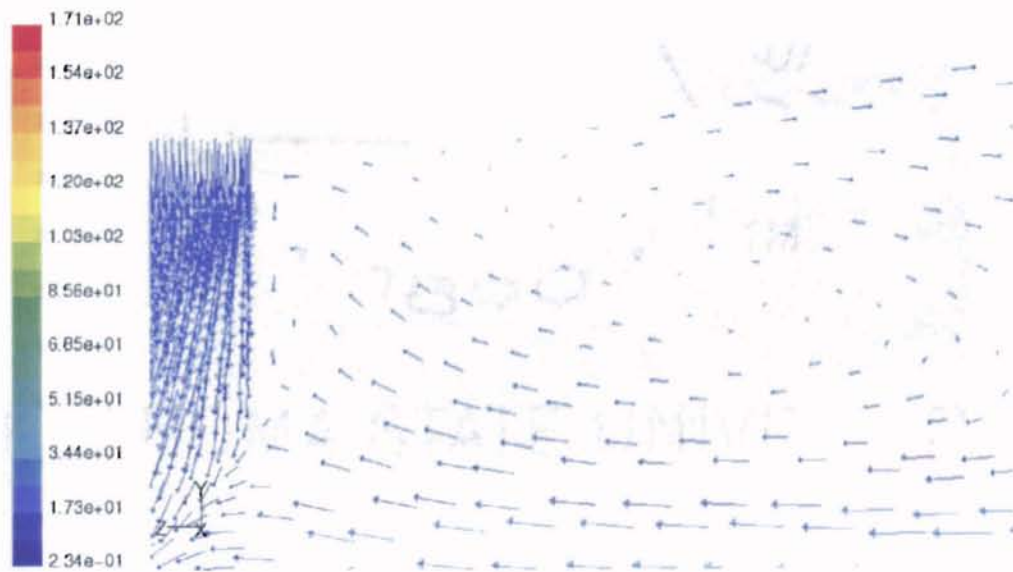
Figure B-8: Velocity Vectors In the Preheat Chamber for 4 Symmetric Inlets
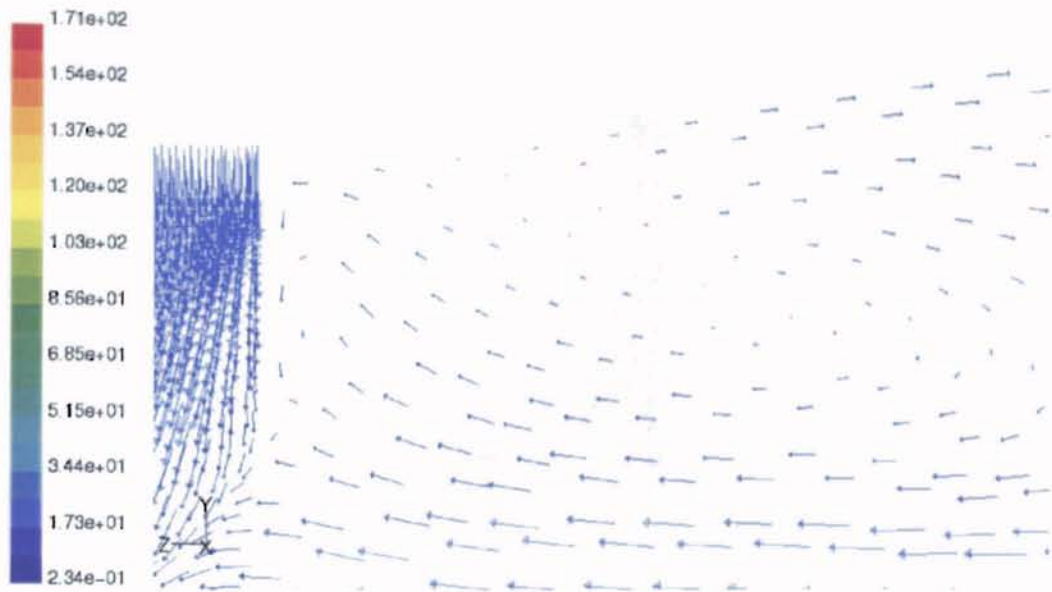
Figure B-9: Velocity Vectors In the Preheat Chamber for 8 Symmetric Inlets
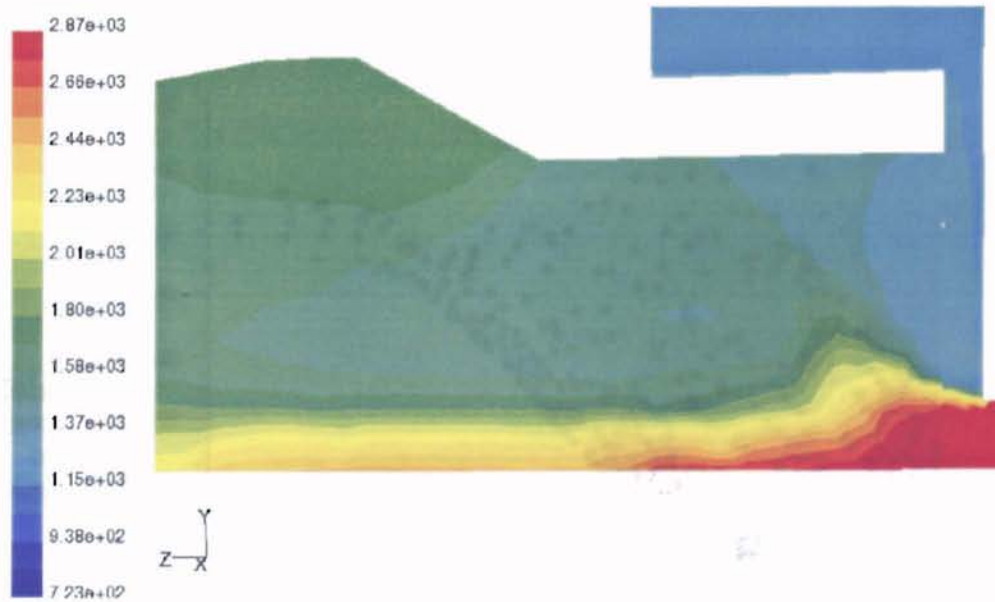
Figure B-10: Temperature Contours About the Toluene Burner (2 Inlet Case)
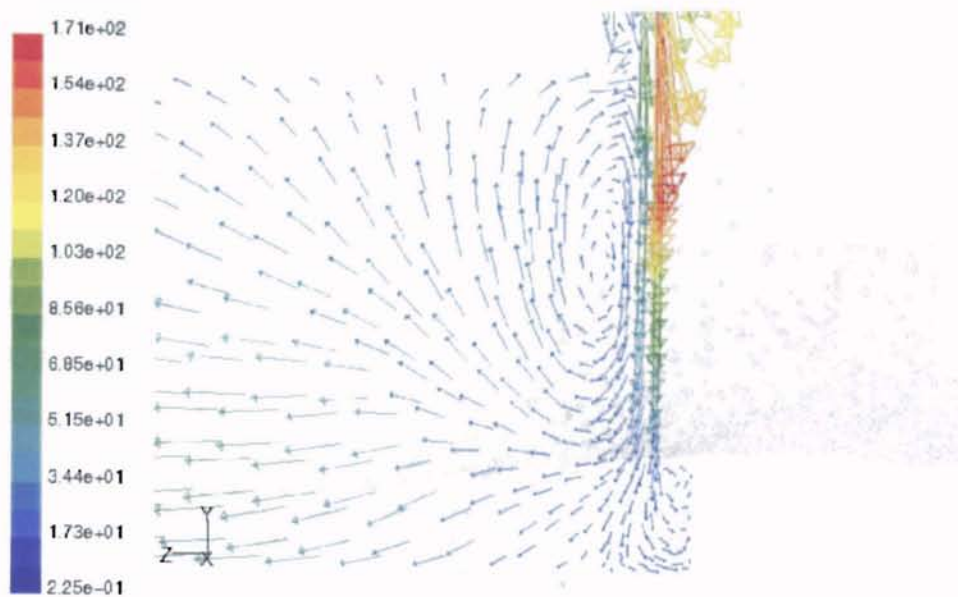
Figure B-11: Velocity Vectors Around the O_2 Annulus, Showing Recirculation
(2 Inlet Case)
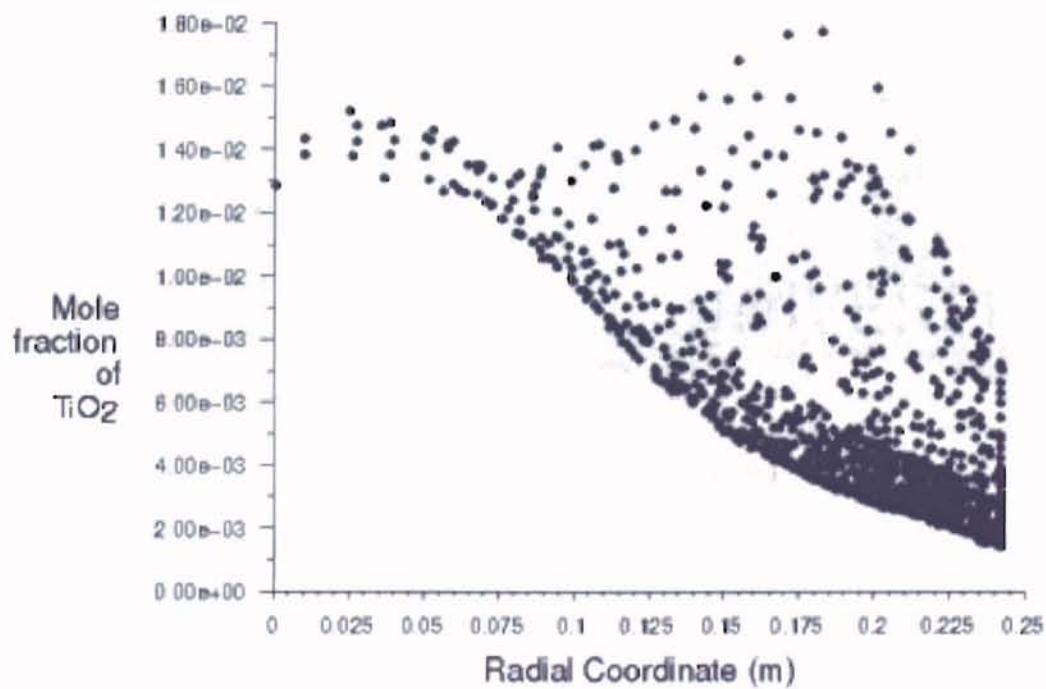
Figure B-12: TiO_2 Mole Fraction vs. Radial Coordinate at the Upstream End of the $TiCl_4$
spool for 2 Symmetric Inlets
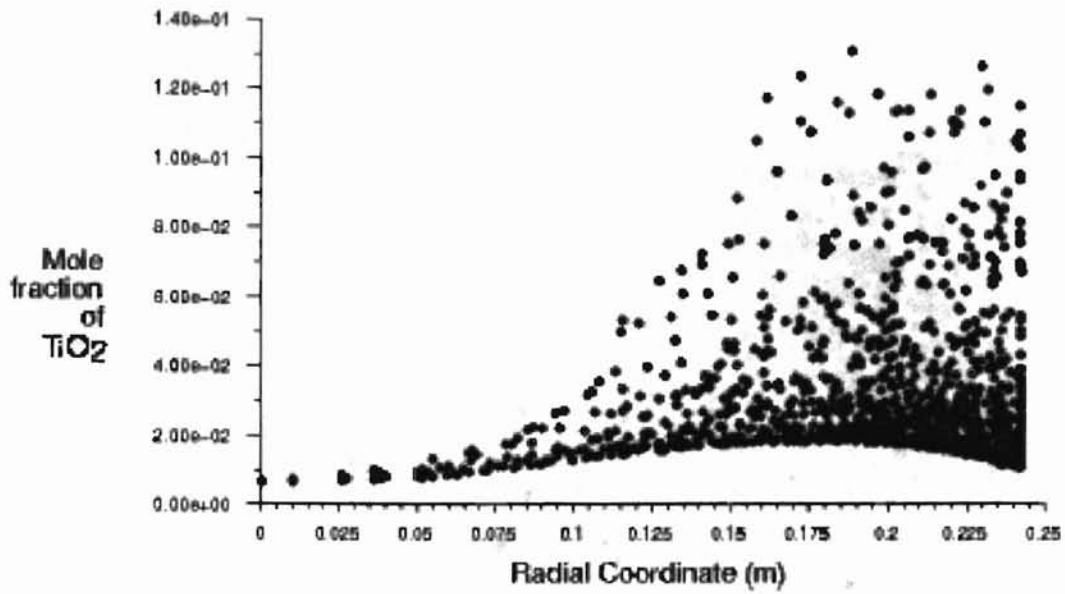
Figure B-13: TiO$_2$ Mole Fraction vs. Radial Coordinate at the Upstream End of the TiCl$_4$ spool for 4 Symmetric Inlets
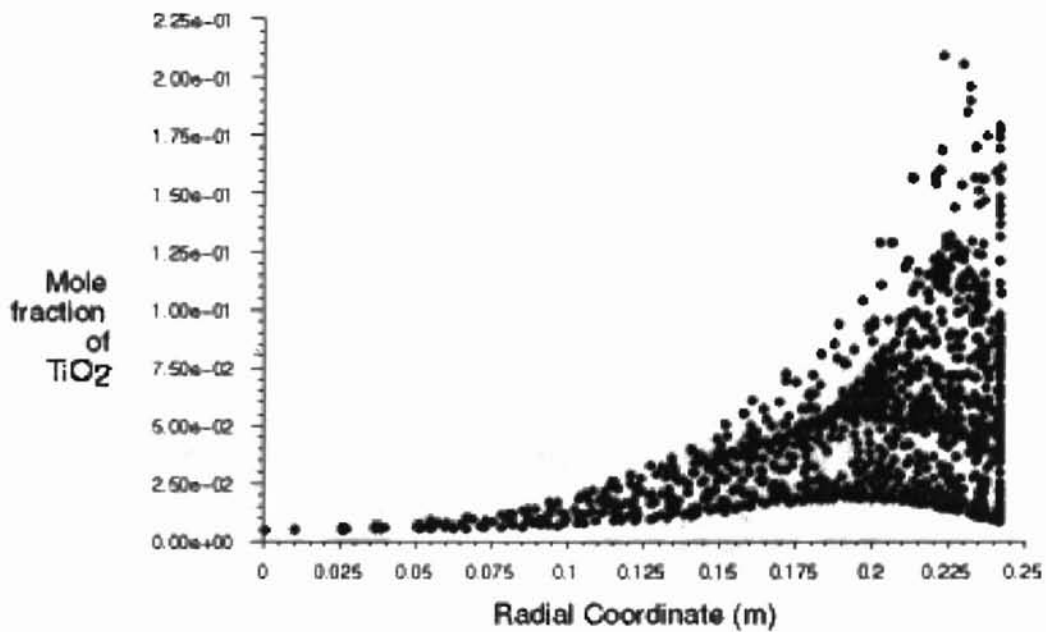
Figure B-14: TiO$_2$ Mole Fraction vs. Radial Coordinate at the Upstream End of the TiCl$_4$ spool for 4 Symmetric Inlets
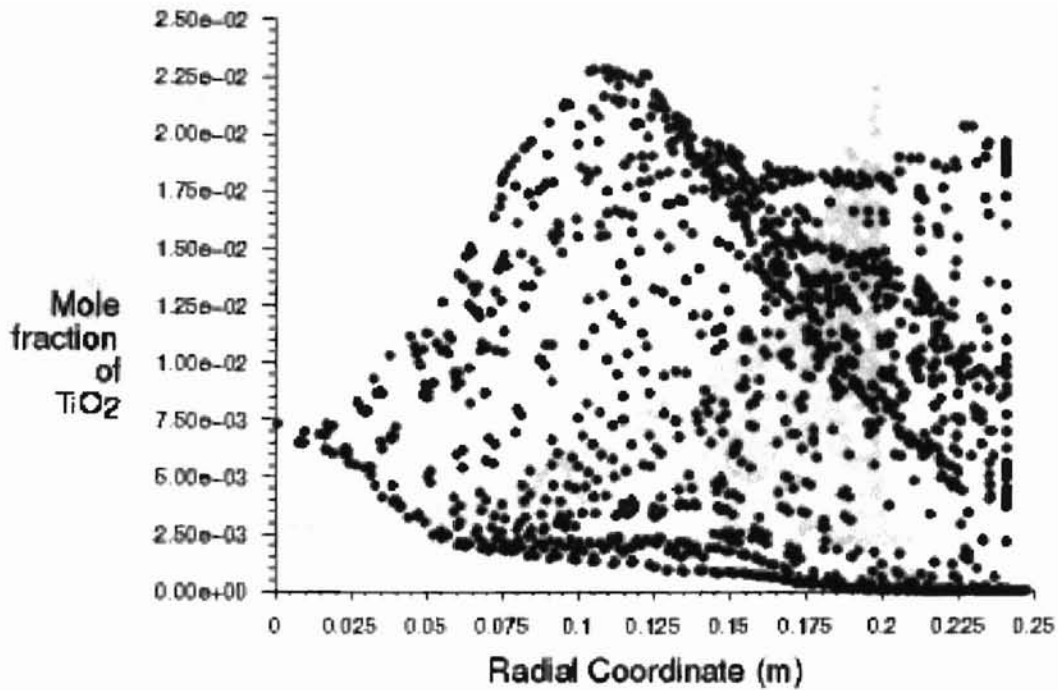
Figure B-15: TiO$_2$ Mole Fraction vs. Radial Coordinate at the Downstream End of the TiCl$_4$ spool for 2 Symmetric Inlets
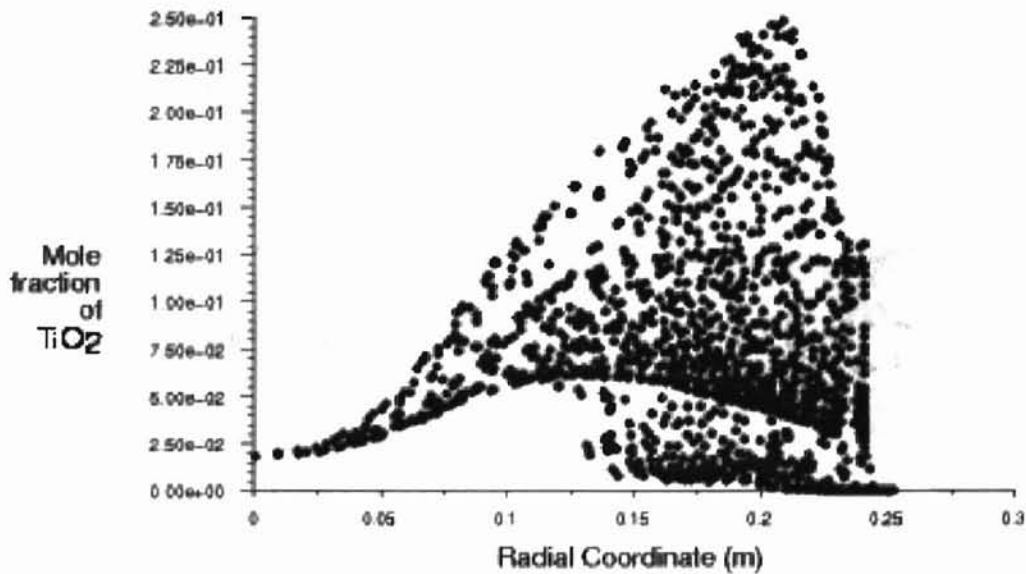
Figure B-16: TiO$_2$ Mole Fraction vs. Radial Coordinate at the Downstream End of the TiCl$_4$ spool for 4 Symmetric Inlets
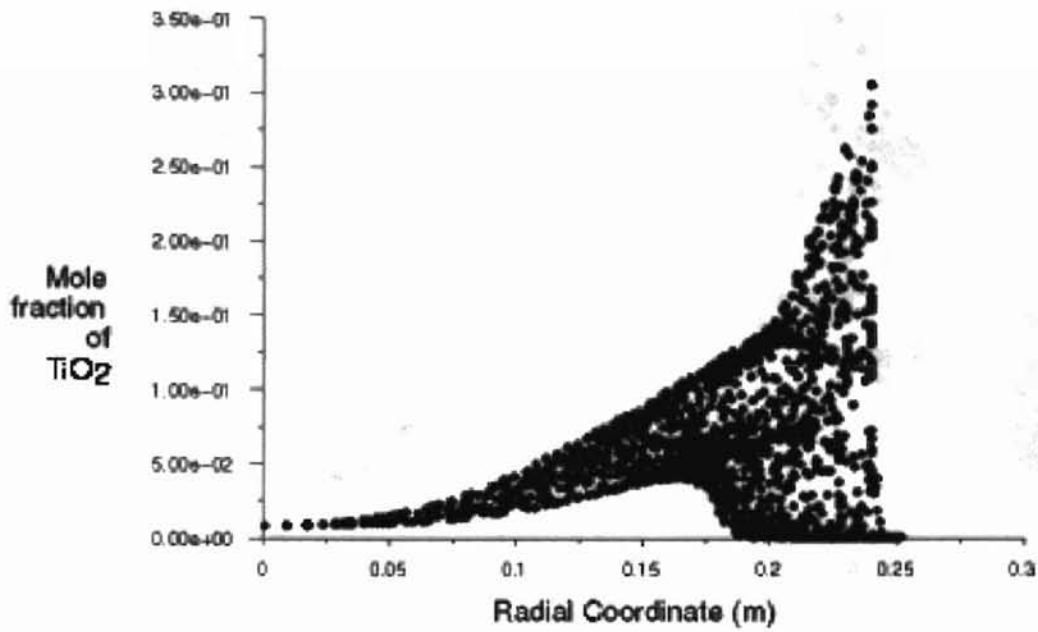
Figure B-17: TiO$_2$ Mole Fraction vs. Radial Coordinate at the Downstream End of the TiCl$_4$ spool for 8 Symmetric Inlets
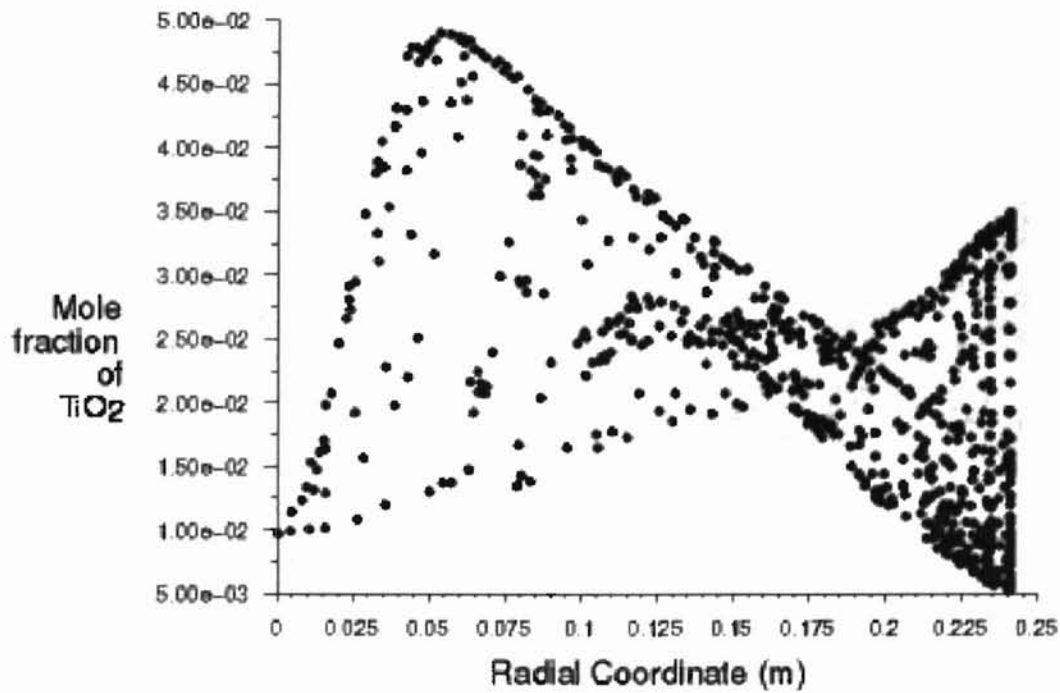
Figure B-18: TiO$_2$ Mole Fraction vs. Radial Coordinate 50 mm Downstream from the TiCl$_4$ spool for 2 Symmetric Inlets
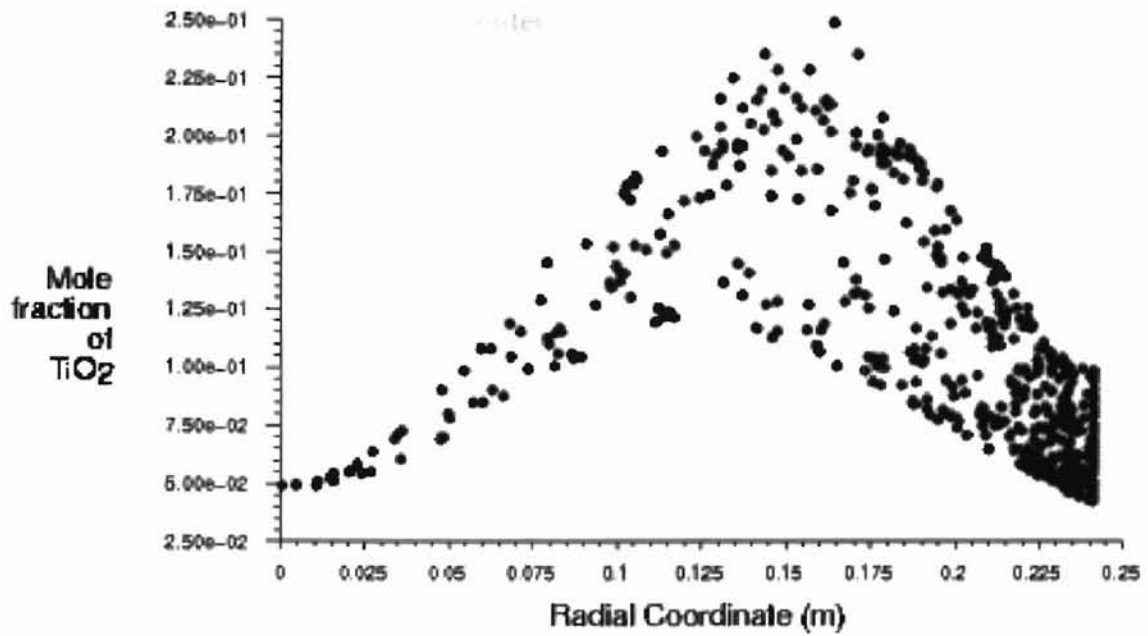
Figure B-19: TiO$_2$ Mole Fraction vs. Radial Coordinate 50 mm Downstream from the TiCl$_4$ spool for 4 Symmetric Inlets
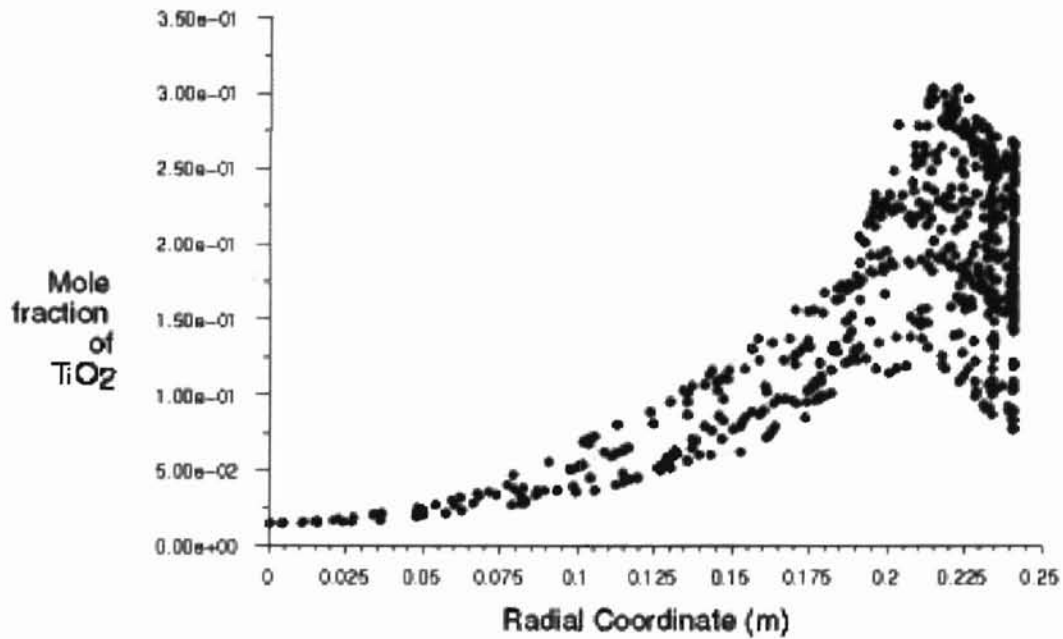
Figure B-20: TiO$_2$ Mole Fraction vs. Radial Coordinate 50 mm Downstream from the TiCl$_4$ spool for 8 Symmetric Inlets
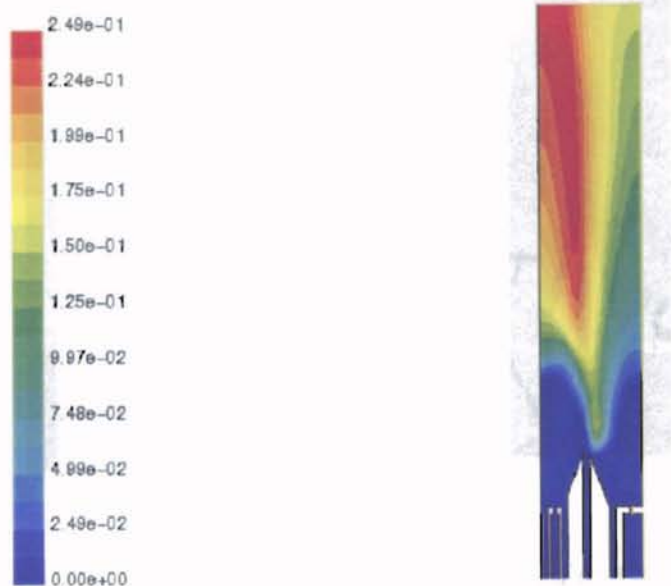
Figure B-21: TiO$_2$ Mole Fraction Contours for θ=20°
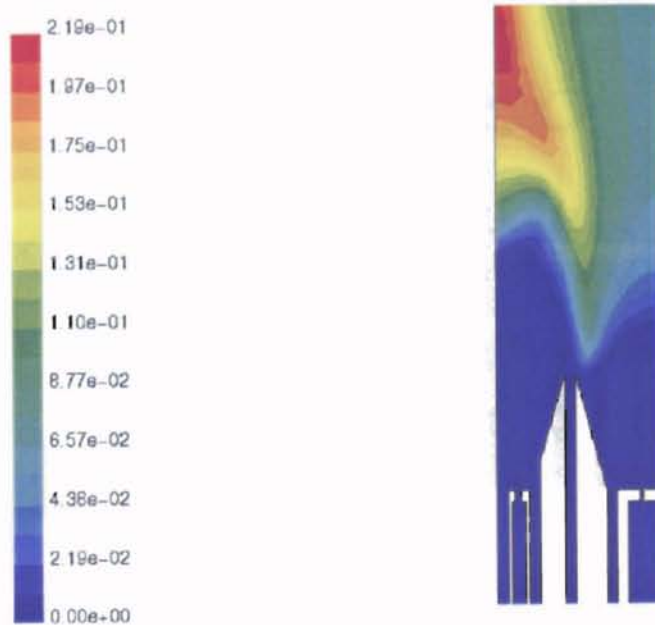
Figure B-22: TiO$_2$ Mole Fraction Contours for θ=16°
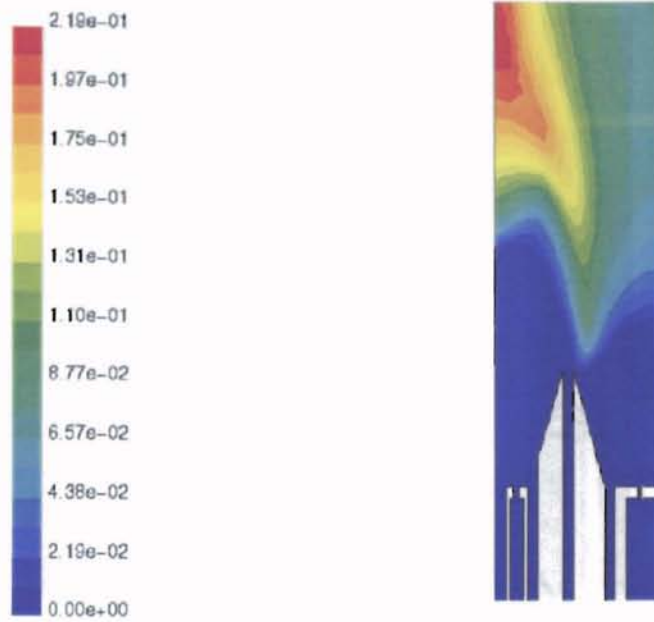
Figure B-23: TiO$_2$ Mole Fraction Contours for θ=12°

Figure B-24: TiO$_2$ Mole Fraction Contours for θ=8°
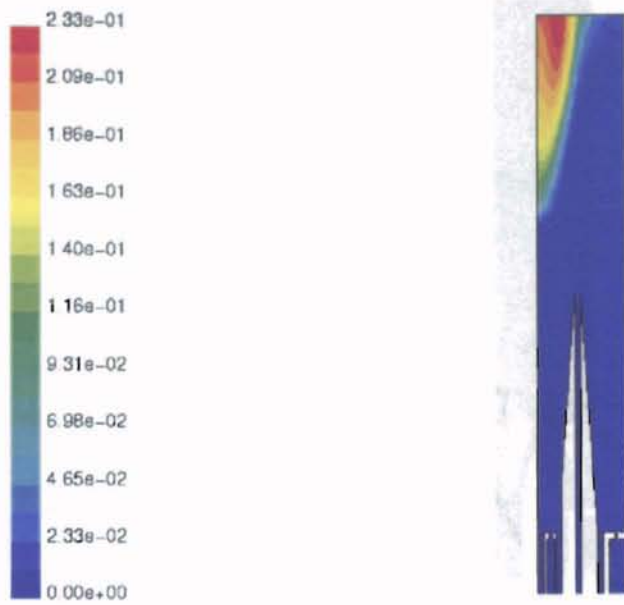
Figure B-25: TiO$_2$ Mole Fraction Contours for θ=4°
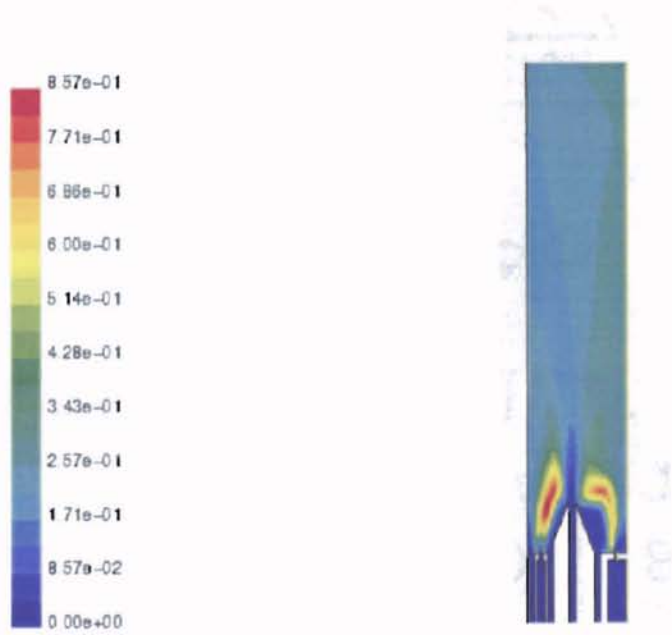
Figure B-26: CO$_2$ Mole Fraction Contours for θ=20°
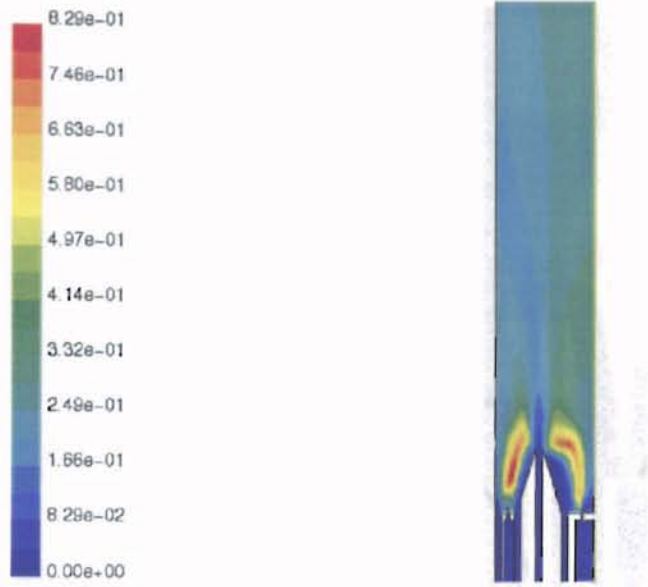
Figure B-27: CO_2 Mole Fraction Contours for $\theta=16°$
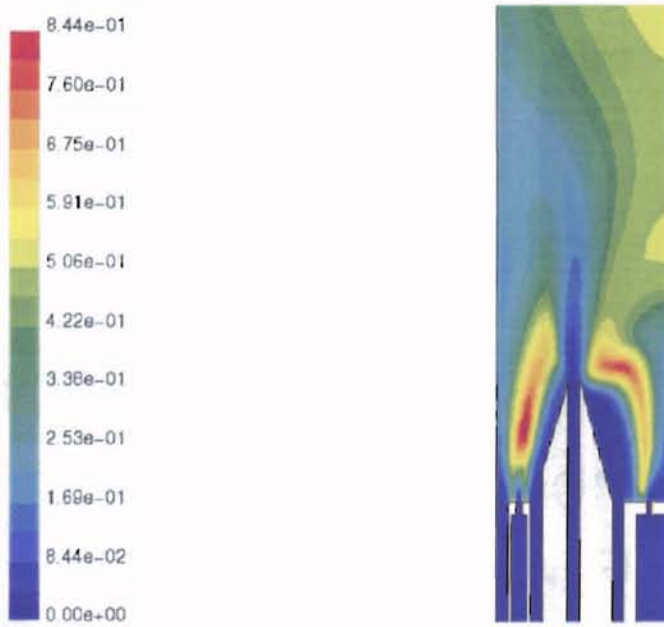
Figure B-28: CO_2 Mole Fraction Contours for $\theta=12°$
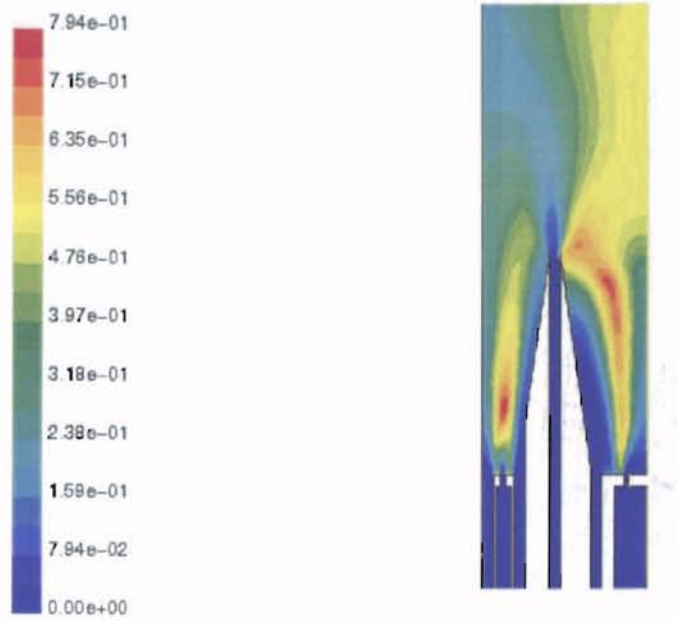
Figure B-29: CO_2 Mole Fraction Contours for $\theta=8°$
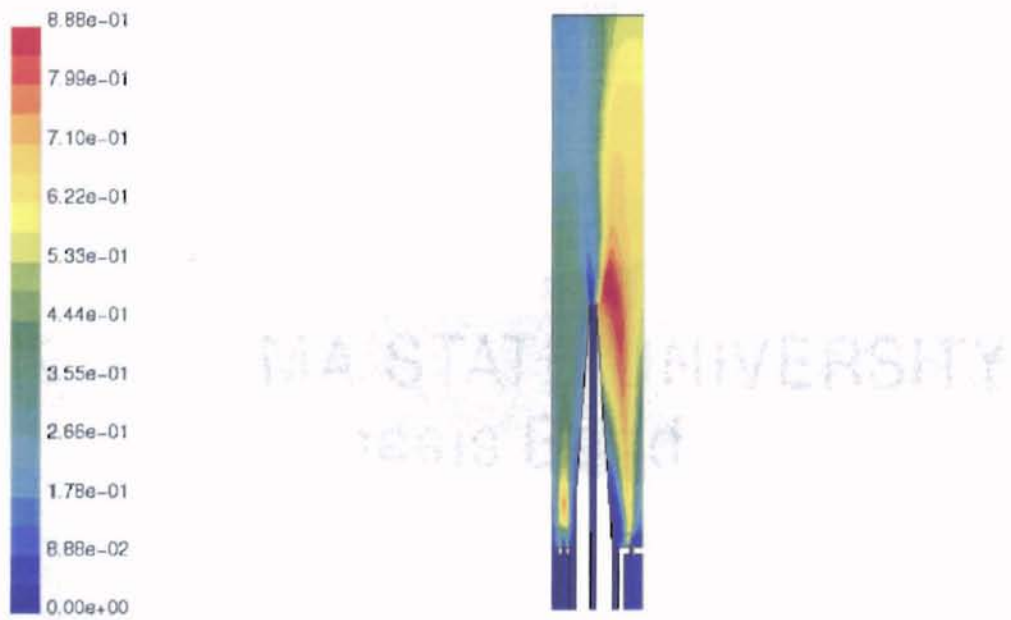
Figure B-30: CO_2 Mole Fraction Contours for $\theta=4°$
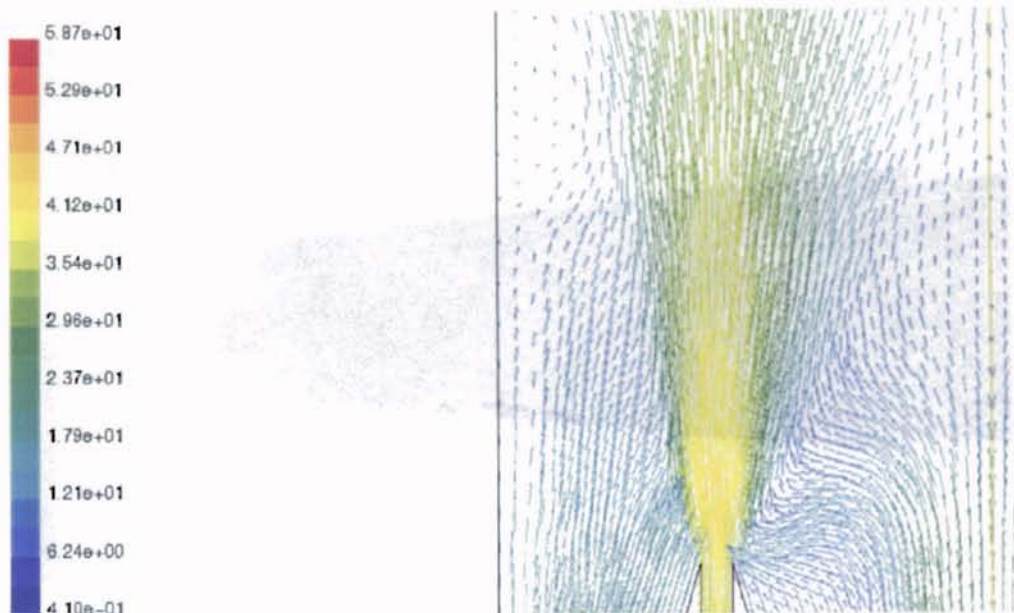
Figure B-31: Velocity Vectors Around TiCl$_4$ Inlet for $\theta = 12°$

Cabot Reactor
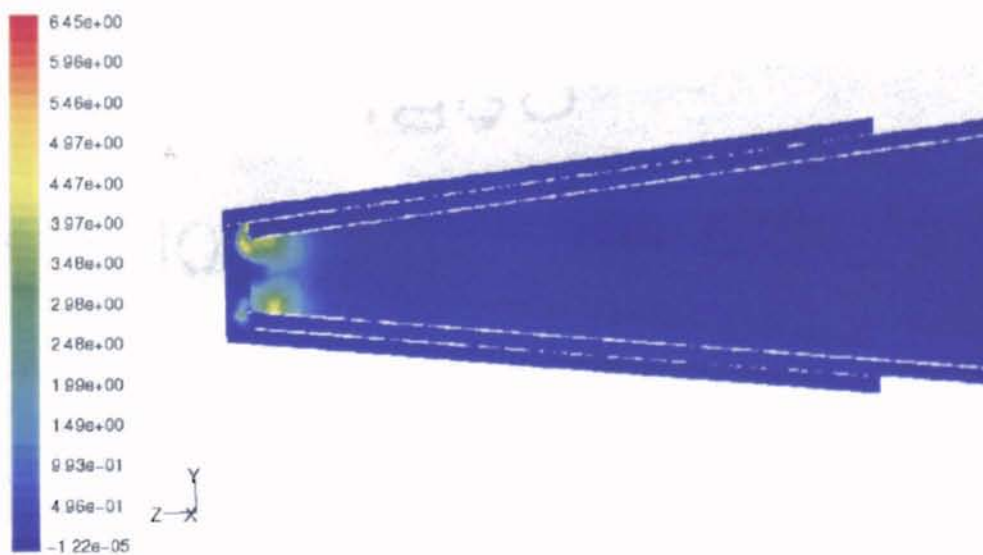
Figure B-32: TiCl$_4$ Oxidation Rate Contour for 0.1x Example TiO$_2$ Production Rate(kmol/s)

116
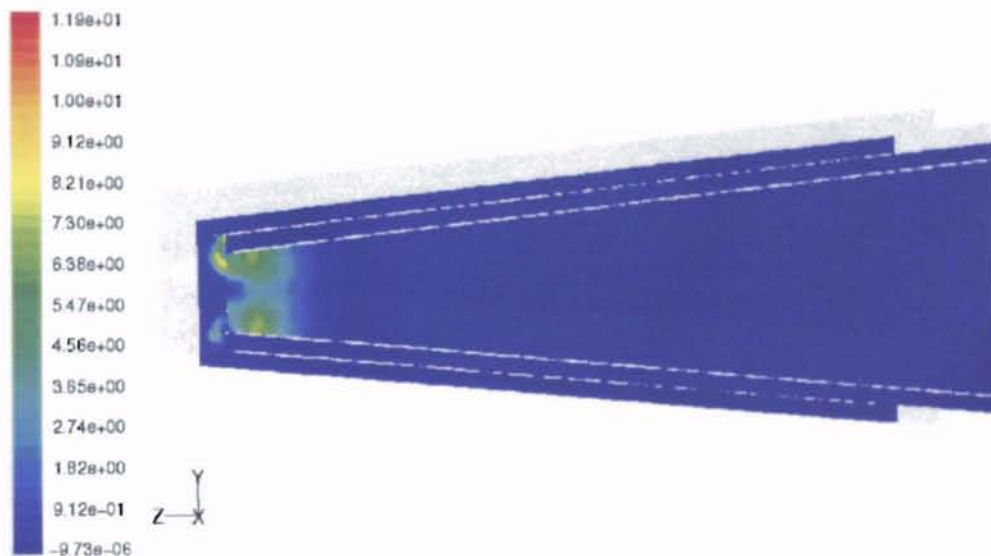
Figure B-33: TiCl$_4$ Oxidation Rate Contour for 0.2x Example TiO$_2$ Production Rate (kmol/s)
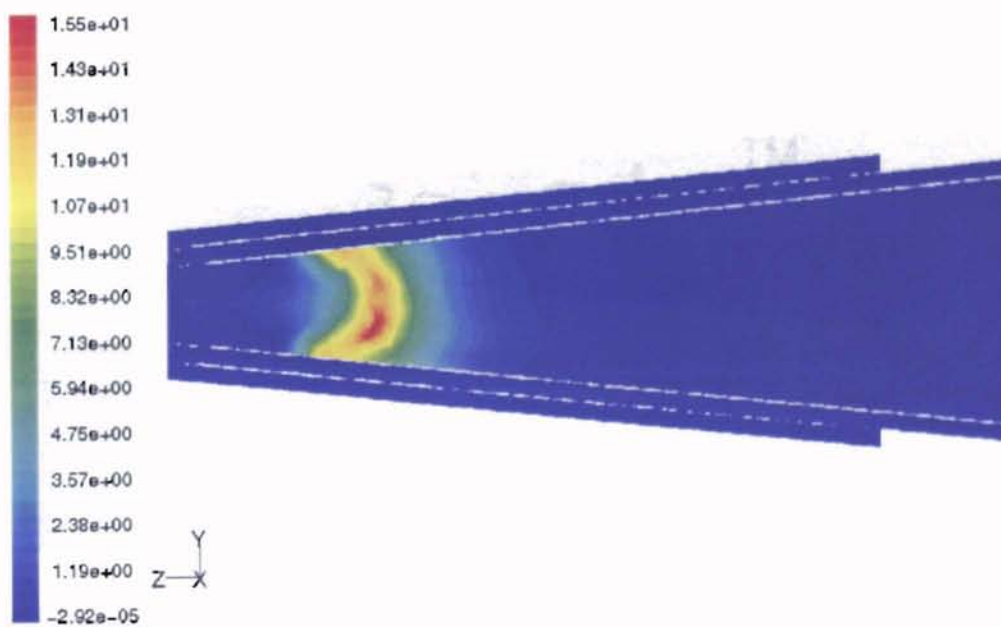
Figure B-34: TiCl$_4$ Oxidation Rate Contour for Example TiO$_2$ Production Rate (kmol/s)

117
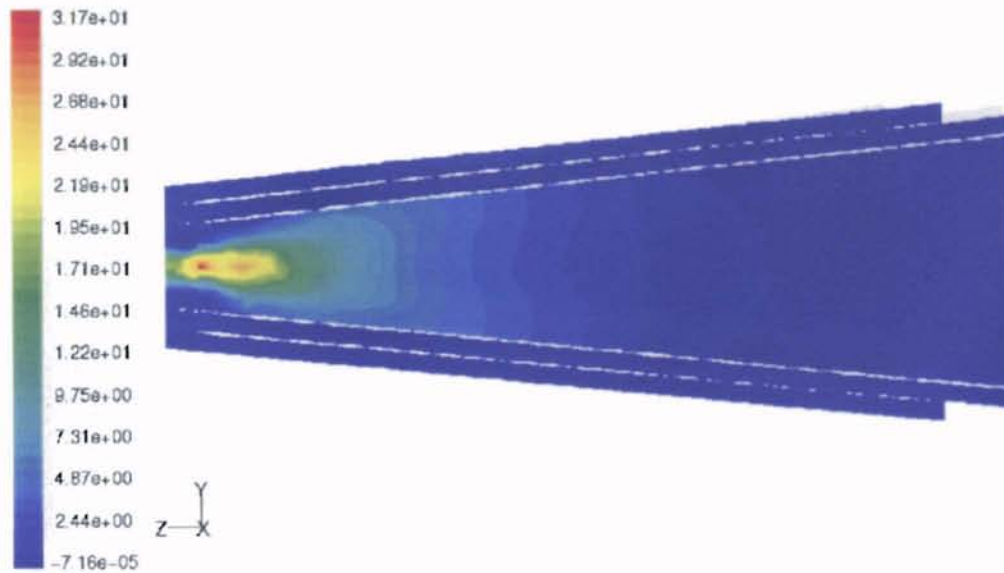
Figure B-35: TiCl$_4$ Oxidation Rate Contour for 3x Example TiO$_2$ Production Rate (kmol/s)
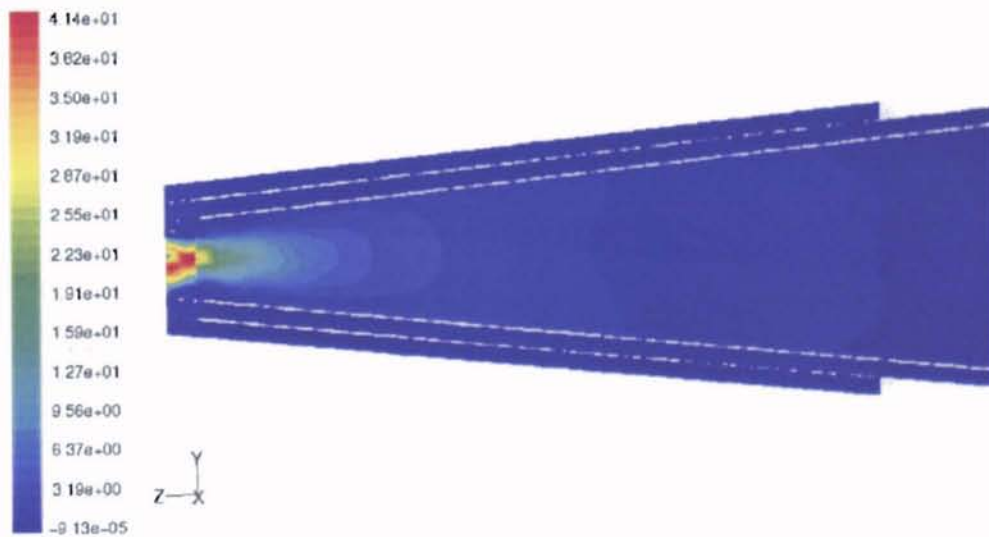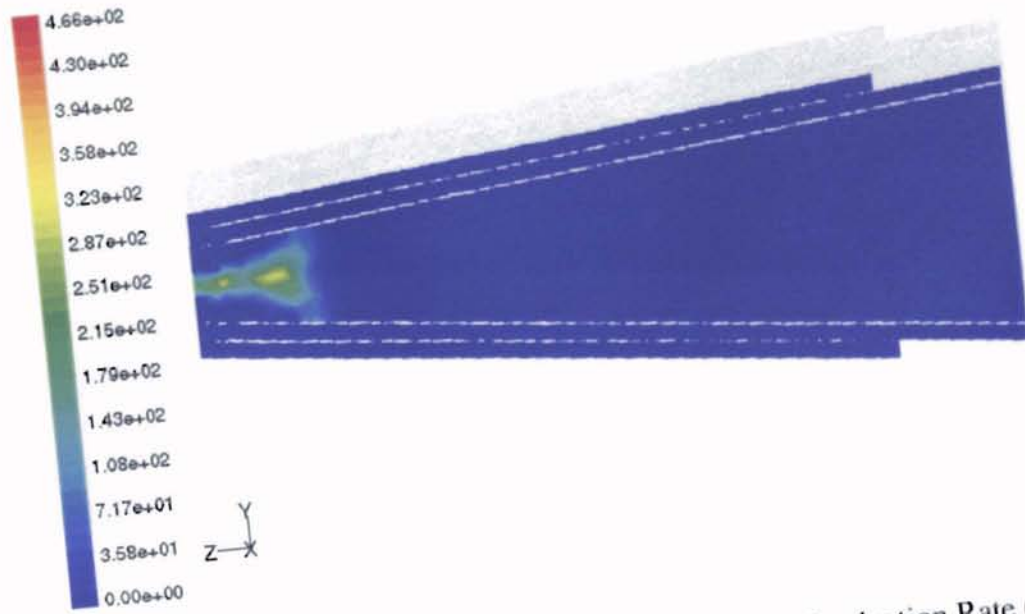

Figure B-36: TiCl$_4$ Oxidation Rate Contour for 3x Example TiO$_2$ Production Rate (kmol/s)
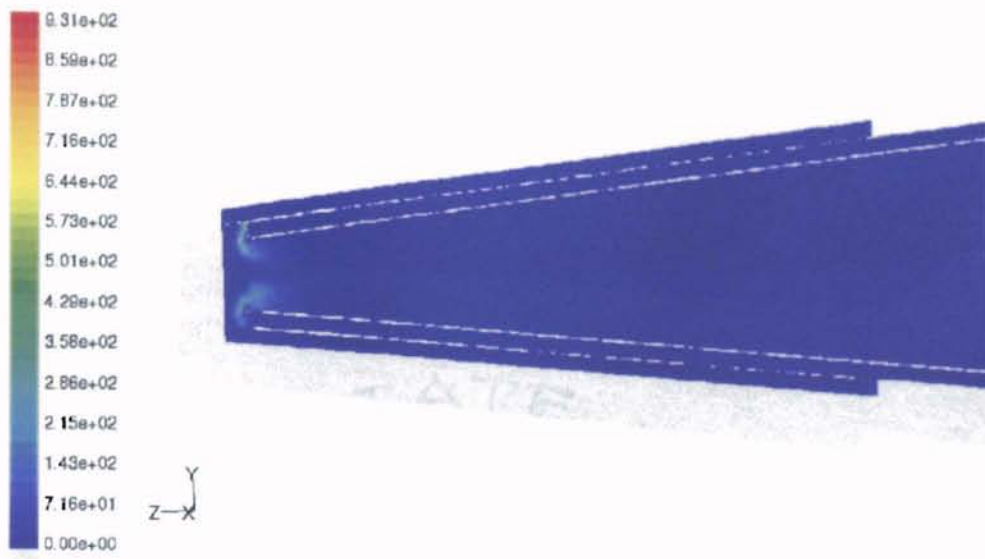
Figure B-37: CO Combustion Rate Contour for 0.1x Example TiO$_2$ Production Rate (kmol/s)
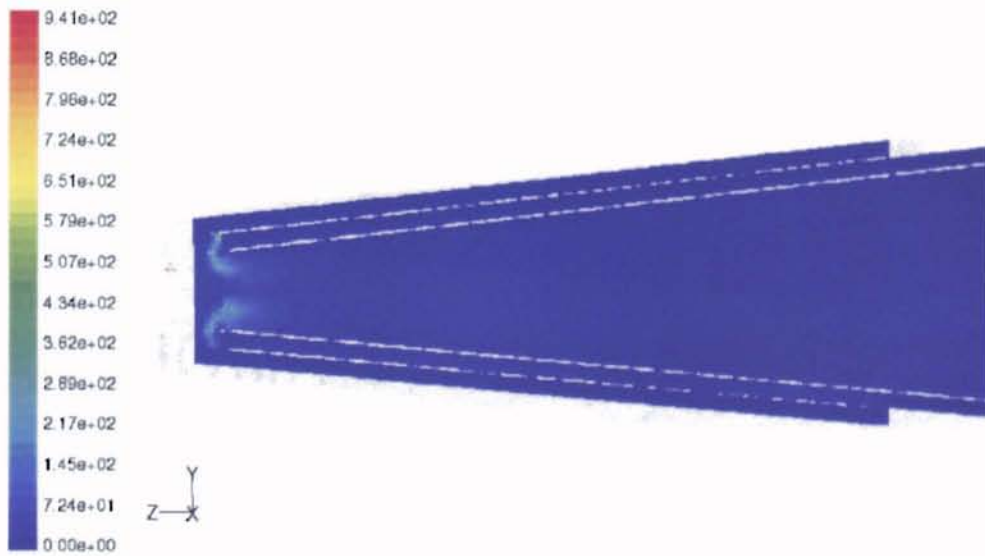
Figure B-38: CO Combustion Rate Contour for 0.2x Example TiO$_2$ Production Rate (kmol/s)

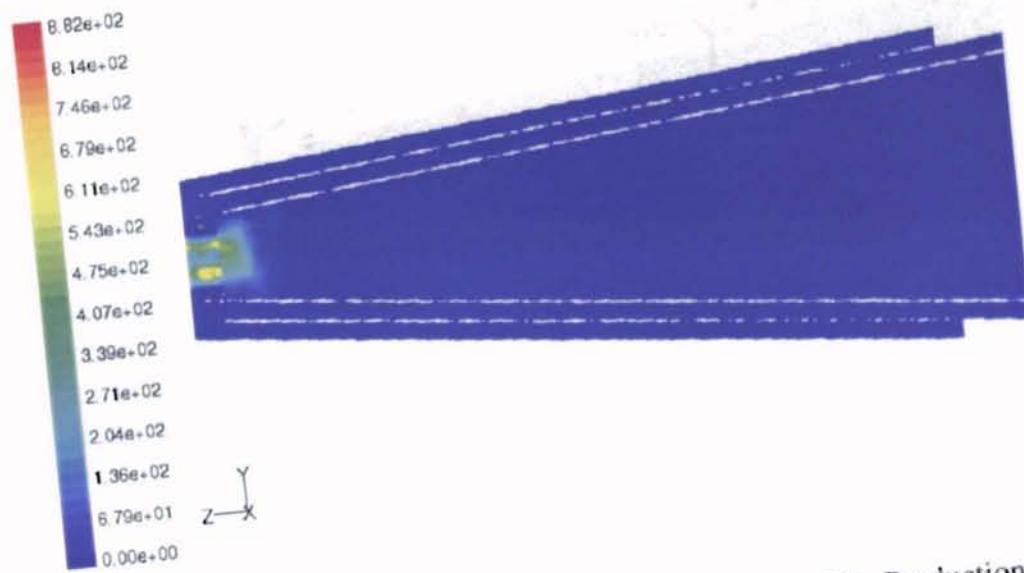Figure B-39: CO Combustion Rate Contour for Example TiO_2 Production Rate (kmol/s)

Figure B-40: CO Combustion Rate Contour for 2x Example TiO_2 Production Rate (kmol/s)

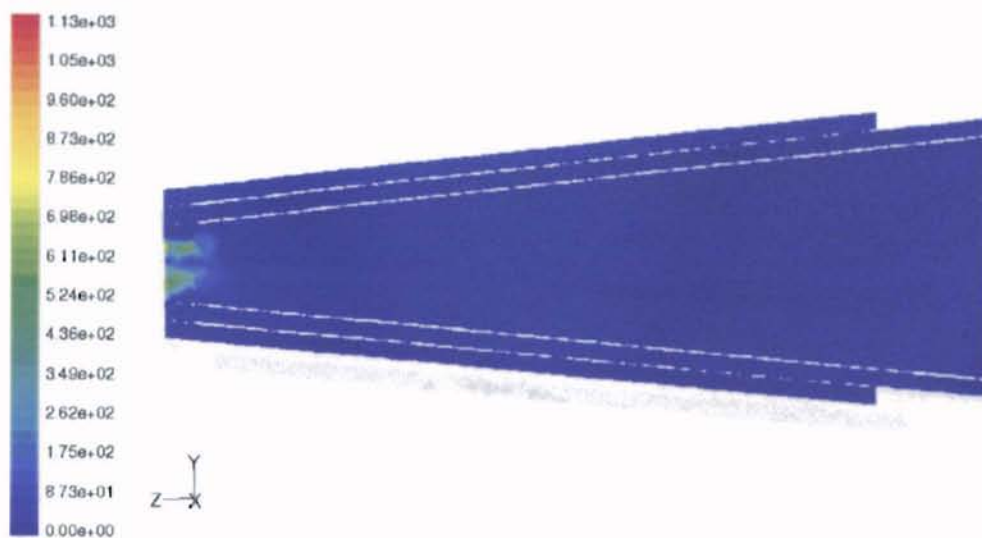Figure B-41: CO Combustion Rate Contour for 3x Example TiO$_2$ Production Rate (kmol/s)

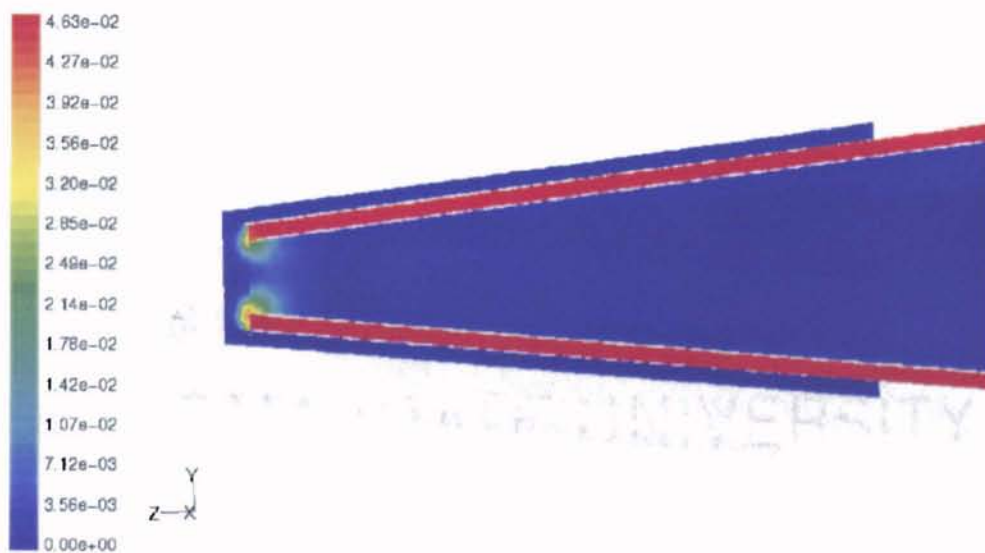Figure B-42: TiCl$_4$ Mole Fraction Contour for 0.1x Example TiO$_2$ Production Rate
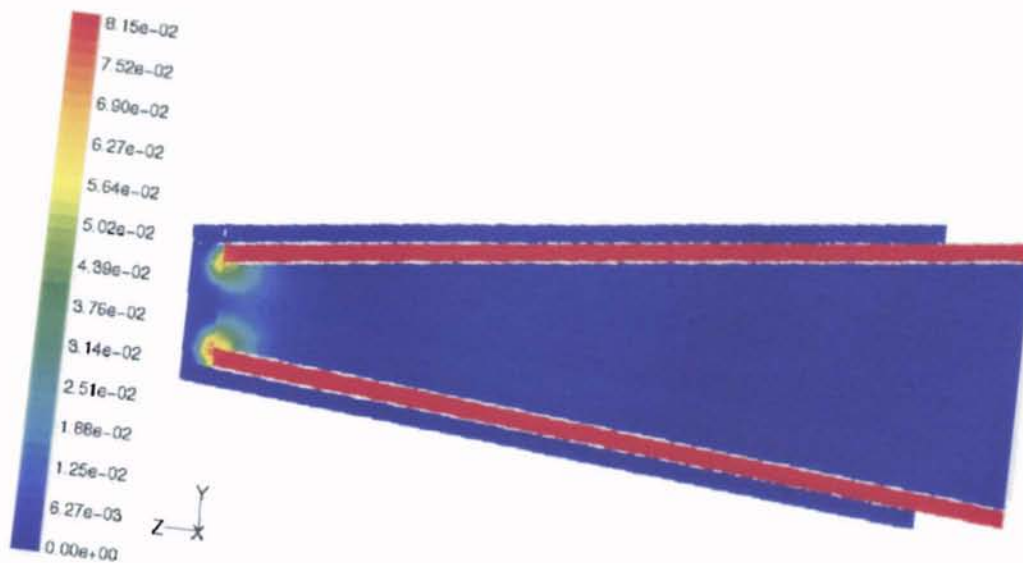
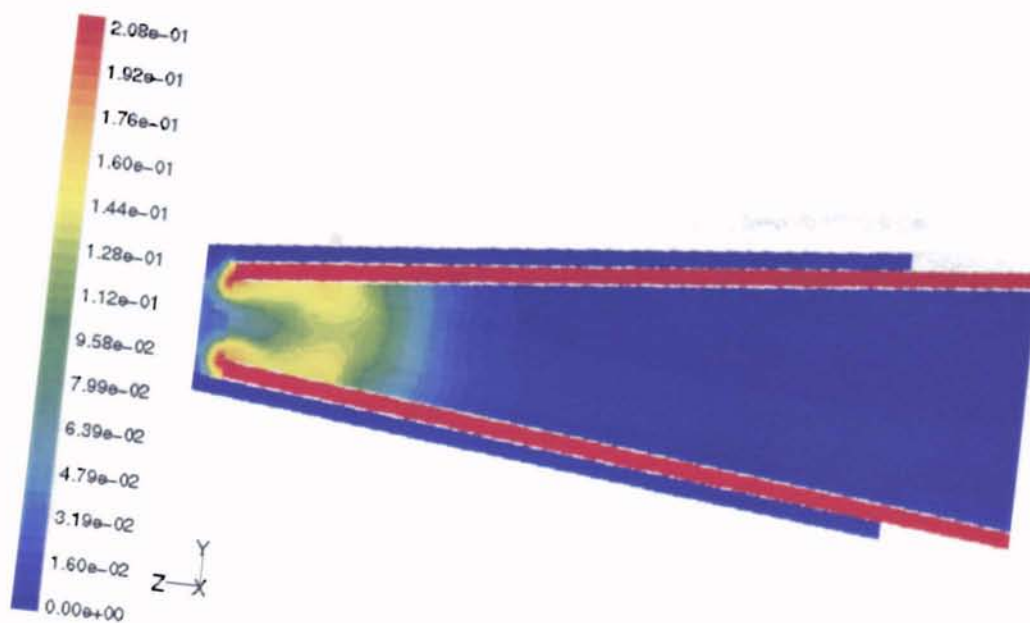Figure B-43: TiCl$_4$ Mole Fraction Contour for 0.2x Example TiO$_2$ Production Rate

Figure B-44: TiCl$_4$ Mole Fraction Contour for Example TiO$_2$ Production Rate

122
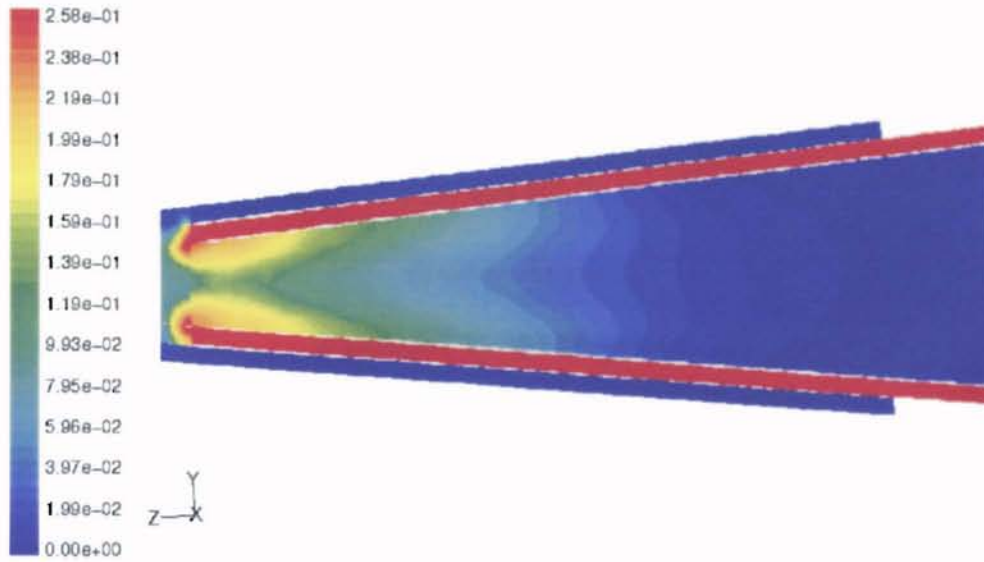
Figure B-45: TiCl$_4$ Mole Fraction Contour for 2x Example TiO$_2$ Production Rate
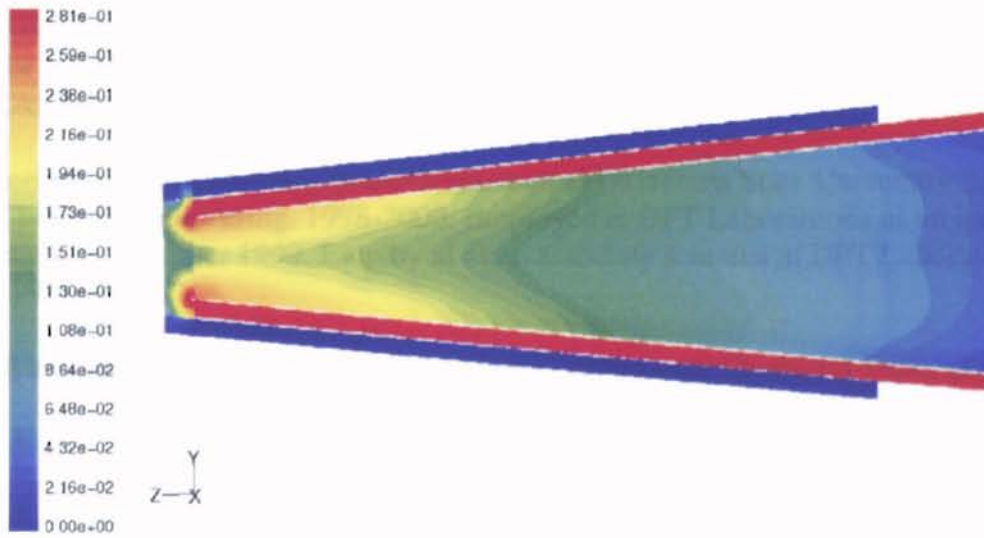

Figure B-46: TiCl$_4$ Mole Fraction Contour for 3x Example TiO$_2$ Production Rate

VITA

Brant L. Aggus

Candidate for the Degree of

Master of Science

Thesis: ANALYSIS OF REACTORS FOR THE PRODUCTION OF TITANIUM DIOXIDE THROUGH COMPUTATIONAL FLUID DYNAMICS

Major Field: Chemical Engineering

Biographical:

Education: Received Bachelor of Science degree in Chemistry from the University of Arkansas in Fayetteville, Arkansas in August 1996. Completed the requirements for the Master of Science degree with a major in Chemical Engineering at Oklahoma State University in December 2000.

Experience: Employed as a research assistant at Oklahoma State University School of Chemical Engineering, 1998-2000. Employed at DPT Laboratories as an intern engineer, summer 1999. Employed as an associate scientist at DPT Laboratories, 1996-1998.

Professional Membership: Alpha Chi Sigma Professional Chemistry Fraternity.